



Review

Light, Water, and Melatonin: The Synergistic Regulation of Phase Separation in Dementia

Doris Loh ¹ and Russel J. Reiter ^{2,*}

¹ Independent Researcher, Marble Falls, TX 78654, USA

² Department of Cell Systems and Anatomy, UT Health San Antonio, San Antonio, TX 78229, USA

* Correspondence: reiter@uthscsa.edu

Abstract: The swift rise in acceptance of molecular principles defining phase separation by a broad array of scientific disciplines is shadowed by increasing discoveries linking phase separation to pathological aggregations associated with numerous neurodegenerative disorders, including Alzheimer's disease, that contribute to dementia. Phase separation is powered by multivalent macromolecular interactions. Importantly, the release of water molecules from protein hydration shells into bulk creates entropic gains that promote phase separation and the subsequent generation of insoluble cytotoxic aggregates that drive healthy brain cells into diseased states. Higher viscosity in interfacial waters and limited hydration in interiors of biomolecular condensates facilitate phase separation. Light, water, and melatonin constitute an ancient synergy that ensures adequate protein hydration to prevent aberrant phase separation. The 670 nm visible red wavelength found in sunlight and employed in photobiomodulation reduces interfacial and mitochondrial matrix viscosity to enhance ATP production via increasing ATP synthase motor efficiency. Melatonin is a potent antioxidant that lowers viscosity to increase ATP by scavenging excess reactive oxygen species and free radicals. Reduced viscosity by light and melatonin elevates the availability of free water molecules that allow melatonin to adopt favorable conformations that enhance intrinsic features, including binding interactions with adenosine that reinforces the adenosine moiety effect of ATP responsible for preventing water removal that causes hydrophobic collapse and aggregation in phase separation. Precise recalibration of interspecies melatonin dosages that account for differences in metabolic rates and bioavailability will ensure the efficacious reinstatement of the once-powerful ancient synergy between light, water, and melatonin in a modern world.



Citation: Loh, D.; Reiter, R.J. Light, Water, and Melatonin: The Synergistic Regulation of Phase Separation in Dementia. *Int. J. Mol. Sci.* **2023**, *24*, 5835. <https://doi.org/10.3390/ijms24065835>

Academic Editor: Mariagiovanna Cantone

Received: 16 February 2023

Accepted: 17 March 2023

Published: 19 March 2023



Copyright: © 2023 by the authors. Licensee MDPI, Basel, Switzerland. This article is an open access article distributed under the terms and conditions of the Creative Commons Attribution (CC BY) license (<https://creativecommons.org/licenses/by/4.0/>).

Keywords: melatonin; dementia; amyloid- β ; ATP; adenosine; phase separation; infrared light; hydrogen bonds; viscosity; bioavailability

1. Introduction

Dementia is a neurodegenerative condition marked by varying levels of cognitive impairment [1], currently affecting approximately 46.8 million people around the world. It is estimated that 10 million people will develop dementia each year, and without approved pharmaceutical intervention to effectively target underlying causes [2–4], by the year 2050, healthcare spending attributable to dementia is projected to become a significant drain on resources representing 11–17% of total global healthcare spending [5]. Alzheimer's disease (AD) is one of the most common causes of dementia [6,7] followed by vascular dementia (VaD) [8,9]. Together with Lewy body dementias [10] and frontotemporal dementia (FTD) [11], these major neurodegenerative disorders account for approximately 90% of all dementia cases [12]. Dysregulated aggregation of biomolecular condensates formed as a result of multivalent macromolecule interactions may underlie the common molecular mechanisms responsible for the development of all AD and non-AD dementia (nADD) [13–15].

An Alzheimer's biomarker study performed within a defined population over a period of 15.7 years (maximum) found the absolute remaining lifetime risk for incident dementia to be significantly associated with elevated amyloid accumulation (hazard ratio 2.11; 95% CI 1.43–2.79). Even though 87% of the 4984 participants were diagnosed as cognitively unimpaired at enrollment, higher amyloid accumulation was a significant biomarker correlated with accelerated dementia progression [16]. Vascular risks are generally associated with the progression of VaD [8,9]. However, midlife hypertension and late-life amyloid- β (A β) deposition were found to be independently associated with increased dementia risk in 298 participants aged 45–64 in a study that spanned 30 years. The study was unable to identify evidence of synergy between vascular risk and A β deposition on a multiplicative scale in subjects with dementia, implying that unique molecular pathways may be involved in the development of dementia [17].

2. Aberrant Phase Separation Is the Fundamental Molecular Driver behind Dementia

In 2017, Banani et al. defined intracellular biomolecular condensates as cytosolic and nuclear micron-scale compartments not bound by membranes and formed via phase separation driven by multivalent macromolecular interactions [18]. These membrane-less organelles (MLOs) are responsible for strategic cellular organization in response to changing environments including endogenous and exogenous stress [14,19–21]. MLOs are ubiquitously utilized not only by all eukaryotes, but also bacteria [22], and viruses which are now recognized as master architects of biomolecular condensates, using phase separation to form viral replication “factories” [23,24]. The disruption of phase separation in key cellular processes results in diseases including neurodegenerative disorders and cancer [25–29].

The forces that drive phase separation encompass simple density transitions in single-component fluid systems [30] to changes in macromolecule saturation levels in binary mixtures achieved via manipulating in vitro macromolecule expression levels, interaction energies, and inclusion of hydrotropes/surfactants [31–34]. Spontaneous or driven phase-separated biomolecular condensates are usually nonstoichiometric assemblies of multiple proteins and nucleic acids [35]. These multivalent macromolecules engage in site-specific interactions that conform to the “stickers-and-spacers” architecture [35–37], forming reversible crosslinks that may involve hydrogen bonds [38–40], ionic strength [41], cation- π , and π - π interactions [42] that fine-tune percolation thresholds that may further define phase separation processes [43–46].

The significant discovery by Kar et al. that fused in sarcoma (FUS) and other phase-separating RNA-binding proteins in the FET family, namely EWSR1 and TAF15, form reversible clusters of varying sizes in subsaturated solutions where phase separation was not observed [47], highlights the relevance of percolation without phase separation in phase transitions in vivo. The aggregation of FUS, EWSR1, and TAF15 are associated with neurological disorders and the three FET family RNA-binding proteins are widely expressed in most cell types [48,49]. Thus, the detection of FUS percolation clusters formed in subsaturated solutions and clusters that are coupled to phase separation in supersaturated solutions [47] offers additional insight in the aggregation of macromolecules in vivo where saturation concentration that can initiate phase separation has been questioned [50]. In this review, in order to accurately capture the concept that phase separation can be coupled to percolation as well as other phase transitions in vivo including the conversion to fibrillar solids [51,52], the term phase separation is employed in lieu of the more popular nomenclature of liquid–liquid phase separation (LLPS) which restrictively implies only viscous liquids are present in the coexisting phases [53].

2.1. Phase Separation of α -Synuclein into Amyloid Fibrils in Dementia

In 1992, Hardy and Higgins proposed that the deposition of amyloid fibrils in AD is the direct cause of cell loss, vascular damage, and dementia [54]. Continued research indicated that the AD disease process may be the result of the dyshomeostasis between the production

and clearance of amyloid β -peptides ($A\beta$) [55,56]. The nomenclature committee of the International Society of Amyloidosis (ISA) defines *in vivo* amyloid fibrils as extracellular protein fibril deposits associated with 36 human amyloid proteins. Intracellular aggregates such as tau and α -synuclein (α -syn), which are present in all synucleinopathies and are the major component of Lewy bodies associated with Lewy body dementia and Parkinson's disease (PD) [57,58], are excluded from this list [59,60]. However, the hallmark feature of amyloid fibrils is the self-association of soluble amyloid monomeric fibers into insoluble cross- β sheets [61–63], and both α -syn [64–66] and tau [67–69] have been reported to self-assemble into cross- β sheet structures.

Encoded by the *SNCA* gene on chromosome 4 [70], α -synuclein (α Syn) comprises 140 amino acids [71] with intrinsically disordered regions prone to fibrillization [72]. The aberrant self-assembly of physiological, soluble α Syn monomers into neurotoxic protein aggregates implicated in PD and other synucleinopathies [73,74] is now attributed to phase separation where macromolecular interactions trigger the irreversible liquid-to-solid transition into amyloid hydrogels containing oligomeric intermediates and cross- β -sheet fibrils [75–79]. The documentation of the conformational evolution of α Syn phase transitions has been successfully captured by solution and solid-state magic-angle spinning (MAS) nuclear magnetic resonance (NMR) spectroscopies [51], and the study and analysis of the material components as well as intermolecular interactions of protein molecules within α Syn condensates during phase separations were performed employing fluorescence recovery after photobleaching (FRAP) and Förster resonance energy transfer (FRET) techniques [80]. Since phase separation is an early event in α Syn aggregation, modulating phase separation and/or interfering with liquid-to-solid phase transitions during α Syn amyloid phase transitions become attractive molecular targets [81].

Phase transitions from soluble monomeric to insoluble β -sheet fibrils observed *in vivo* employing C-direct detection NMR in combination with structural bioinformatics further supports the concept of phase separation as the common molecular pathway underlying not only AD, but also VaD [82]. Among the 36 amyloid proteins recognized by the ISA in 2018 [59], medin (AMed) is the most common amyloid found in the human body [83,84]—being an internal component of milk fat globule-EGF factor 8 (MFG-E8), also known as lactadherin—that is now associated with vascular $A\beta$ in cerebral amyloid angiopathy (CAA) pathology [85].

Present in blood vessels of most adults over the age of 50, medin is cleaved from lactadherin to form insoluble amyloid aggregates [86,87] that co-localize with vascular $A\beta$ deposits [88] to cause cerebrovascular dysfunction in aging mice and human subjects with VaD [89,90]. Cerebral arteriole medin is regarded as a novel biomarker for AD and VaD [91]. Even though the glycoprotein lactadherin has multiple, important physiological functions [92] including phagocytosis [93], angiogenesis [94], and mucosal repair [95], medin aggregates alter cellular homeostasis, causing microvascular endothelial dysfunction by inducing permeability via the formation of pores in lipid membranes that result in upregulated ionic current flow [96,97], a mechanism not dissimilar to how $A\beta$ peptides form calcium ion channels in lipid bilayer membranes [98,99]. However, the conditions that trigger the cleavage of medin from lactadherin causing medin to self-assemble into pathogenic, insoluble fibrils remain unclear [82,83].

The self-recognizing aggregation of amyloid proteins is not limited to homotypic enrichment in one protein, but often also involves heterotypic interactions in condensates containing up to hundreds of proteins [100,101], and the outcome of amyloid aggregation is modified by these associated heterotypic interactions [102]. Aberrant phase separation resulting in delayed disassembly of stress granules (SGs) causes the formation of non-dynamic SGs that entrap and immobilize TAR DNA-binding protein 43 (TDP-43), rendering the protein insoluble in FTD pathogenesis [15]. Increasing understanding that phase-separating RNA-binding proteins such as FUS [47,103] and those that associate with tau [104] play important modulatory roles in the heterotypic interactions that can promote

or suppress amyloid aggregation [102,105–107], warrants exploration of specific conditions that may trigger aberrant phase separation in RNA-binding proteins.

2.2. The Underappreciated Role of Hydrogen Bonds and Protein Hydration in Phase Separation in Dementia

Dementia-related neurodegenerative disorders are often associated with gene mutations that may cause the dysregulation of RNA-binding proteins responsible for the aggregation of pathological amyloid fibrils during phase separation [108]. The mechanisms reported mostly involve dysregulation in the low-complexity domains of proteins such as TDP-43 and FUS [103,105,109–111]. Low-complexity domains (LCDs) are generally regarded as universally disordered; however, LCDs can also adopt stable, structured conformations [112]. Therefore, aberrant phase separation observed in LCDs may involve other factors in addition to the dysregulation of intrinsically disordered regions that are essential in the promotion of phase separation. Intrinsically disordered proteins (IDPs) usually serve as necessary scaffolds that facilitate phase separation of biomolecular condensates [18,113–115] which can be tuned by controlling enthalpy, minimizing entropic costs in phase separation [116–118].

Intrinsically, phase separation is entropically unfavorable and driven predominantly by enthalpically favored protein interactions [119–121]. In addition to energetically favorable multivalent protein–protein interactions that offset entropic costs, variations in ions and salt concentration, pH, and temperature can result in thermodynamic changes in entropy–enthalpy compensation that regulate phase separation [122–124]. Phase separation in proteins such as Ddx4 [125] and hnRNPA1 [126] exhibiting upper critical solution temperature (UCST) cannot take place above a critical temperature at which the system remains homogeneous, whereas proteins exhibiting lower critical solution temperature (LCST) cannot phase separate below a critical temperature at which the system remains homogeneous [127]. Therefore, increasing temperatures can either stabilize or destabilize biomolecular condensates formed by phase separation [128], and variations in salt concentration and pH levels can further promote or disrupt phase separation [122].

Stress granules (SGs) are phase-separated membraneless organelles that are formed under endogenous and exogenous stress conditions; and persistent formation of stress granules may lead to fibrillization associated with neurodegenerative disorders [126,129]. Adjusting pH levels in solutions tunes both UCSTs and LCSTs that trigger phase separation [130,131]. Alterations in tightly controlled cytosolic pH not only affect the survival of yeast and other organisms, but also determine the material properties of phase-separated stress granule-like condensates that regulate stress responses [132,133]. A reduction in pH in yeast generates reversible condensates that dissolve upon restoration of neutral pH; whereas phase-separated condensates induced by heat in yeast can only be reversed with the help of chaperones [134]. Similarly, in lipid membranes, both pH and salt can increase or decrease critical temperatures that trigger phase separation [124].

In vitro elevation of salt concentrations produces either a dehydrating, salting-out (kosmotropic) effect that induces phase separation [135,136], or a hydrating, salting-in (chaotropic) effect that inhibits phase separation [137–139]. Classic interpretations of the Hofmeister effect where kosmotropic anions that remove water molecules from a protein's hydration shell to reduce protein solubility, increasing potential for aggregation via electrostatic and hydrophobic interactions [140], and chaotropic anions that exhibit the opposite effect of increasing protein solubility, functioning as a hydrotrope preventing phase separation and aggregation [141,142] may not fully account for other relevant conditions including the reversal of the Hofmeister effects in anions and cations [143], or the effect of pH on the aggregation of proteins relative to their isoelectric points (pI) [138].

At its pI of 4.7 pH, α -syn formed highly ordered, fibrillar structures even at low salt concentrations compared to other conditions due to favorable intermolecular energy interactions that compensated for the lack of salting-out effects in a low-salt environment [144]. The hydrophobic, hydrogen-bonded, B-rich amyloid cores in α -syn are intrinsically disor-

dered and participate in dynamic intermolecular energy interactions during fibril assembly and maturation [145–147]. As such, protein hydration exerts a distinct effect on the pathological aggregation of amyloid fibrils in dementia, as the hottest mutational spots are often located in residues that form protective hydrogen bonds but have lost their native protecting functions resulting in protein misfolding [148].

2.3. Hydration Water Activates Amyloid Aggregation and Regulates Oligomer Toxicity

The role of water hydrogen bond networks that hydrate protein surfaces in biomolecular systems is known to be active and dynamic [149–152], but its role in intracellular phase separation is often less understood. Hydrophilic residues are more hydrated than hydrophobic residues. Thus, entropy and enthalpy become the two fundamental thermodynamic driving forces in phase separation that provide the requisite energetically favorable decrease in free energy. Lum, Chandler, and Weeks postulated that the price for minimizing broken hydrogen bonds within interfacial hydration water compared to bulk is an increased enthalpic cost that scales with the surface area of the hydrophobic solute [153]. Therefore, the removal of hydration water into bulk (entropic) leads to increased protein concentration that facilitates enthalpically favored protein–protein interactions resulting in condensate formation [154,155].

In other words, desolvation or the release of water molecules from protein hydration shells into bulk water [156–158] create entropic gains that promote phase separation and fibril aggregation [136,159,160]. Tau proteins that phase separate from salting-out effects via increased salt concentration become dehydrated and mature into irreversible, canonical tau fibrils, whereas tau proteins in reversible condensates formed via electrostatically driven phase separation remain hydrated and do not mature into pathogenic fibrils with restricted water accessibility and increased micro-viscosity [135]. Mutational hotspots with structural defects that affect protein interactions in monomeric states can be regions with an immense propensity to aggregate if the exclusion or removal of water in those regions confer a high thermodynamic benefit [148].

In 1959, Walter Kauzmann proposed that hydrophobicity in protein hydration shells drives protein folding where protein hydration accumulates hydrophobic free energy and removing the water molecule from the hydration shell can supply the free energy required to drive protein folding [161]. This hypothesis remained largely controversial [162,163] until support from experimental evidence on protein hydration shells was published. When the original clathrate water hydration shell used by Kauzmann in 1959 was replaced by a dynamic one formed by van der Waals (vdW) attraction [164], it became clear that the structural differences between water molecules in hydration shells and bulk [165] contributed to changes in free energy produced in vdW attraction interactions that favored protein folding [166,167]. Furthermore, the fact that the addition of salt can tune the hydrophobic effect by breaking hydrogen bonds in hydration shells [168] and rearrange the hydrogen-bonding environment in interfacial waters [169], provides additional support for the role of dehydration in the formation of pathogenic amyloid fibrils.

Highly sensitive femtosecond time-resolved fluorescence spectroscopy revealed the presence of dynamically distinct, confined interfacial hydration water molecules with severely restrained mobility compared to bulk water [170]. The removal of these confined water molecules in the intrinsically disordered amyloidogenic NAC domain of α -syn changes the rate of intramolecular backbone reconfiguration to facilitate the formation of cytotoxic oligomers [171] via intermolecular associations involving chain desolvation, indicating the entropically favored removal of confined water molecules into bulk water [170]. Early studies found the aggregation of protofilaments from A β 16–22 peptides was due to the hydrophobic collapse of protofilaments caused by water molecules being released [172,173]. Similarly, the aggregation propensity of A β 1–40 was significantly elevated via escalating salt concentrations to enhance salting-out effects, with the implication of heightened protein–protein interaction energy and diminished hydrogen-bond strength [174,175]. Out of 3.45 hydrogen bonds formed by a water molecule, only 2.41 are

considered “strong” hydrogen bonds. Per the hydrophobic effect, the ability to form hydrogen bonds directly affects the stability of protein where net stabilization at 1–2 kcal/mol can be provided by each intramolecular hydrogen bond [176].

Limited hydration in the interior of MLOs fosters a favorable environment for liquid-to-solid phase transitions observed in amyloidogenic aggregates that are often preceded by liquid-to-liquid phase separation [79,177]. During α -syn nucleation, limited hydration lowers the desolvation barrier and intermolecular hydrogen bond barrier. Thus, the simple removal of confined water molecules in the hydrophobic amyloid NAC domain in α -syn can easily breach high desolvation barriers that normally prevent aggregation of amyloid fibrils [178–180]. Furthermore, the level of protein hydration determines whether homogeneous or heterogeneous nucleation is selected as the primary aggregation mechanism, which further defines the type of amyloid polymorph generated as well as the cytotoxicity of the α -syn oligomers formed [178]. Unfortunately, reduced hydration may be an inevitable phenomenon associated with aging in the human brain.

During normal aging, even though total protein content in the normal aging brain can decline by 5–15% between the ages of 30 and 90 years, water-soluble protein content actually increases by 16–48%, providing a viable explanation for observations of significantly decreased water content in normal aging brain cells [181,182]. The fact that confined and “bridging” interfacial water molecules have limited mobility and exceptionally slow hydrogen-bond rearrangement compared to bulk water, respectively, [170,183] highlights the importance of the binding dynamics of interfacial hydration water around residues located in IDPs prone to phase separation under conditions of limited mobility and hydration [184,185]. Atomistic MD simulations revealed that during the growth of $A\beta_{9-40}$ fibrils, the collective movement of confined interfacial water with reduced mobility provides the entropic energy for pathogenic fibril formation via the removal of 60–85 water molecules that concurrently supplies a dry binding interface between filament and monomer [186]. Consequently, the ability to manipulate the relative thermodynamics of hydrogen bonds [187] in interfacial water compared to bulk becomes an extremely attractive proposition in the regulation of protein aggregation in dementia.

2.4. The Synergistic Regulation of Hydrogen Bonds by Light, Water, and Melatonin

The International Union of Pure and Applied Chemistry (IUPAC) defined a hydrogen bond as “an attractive interaction between a hydrogen atom from a molecule or a molecular fragment X–H in which X is more electronegative than H, and an atom or a group of atoms in the same or a different molecule, in which there is evidence of bond formation” [188]. Although hydrogen bonding can affect important physicochemical properties including density, refractive index, and conductivity [189], due to a limitation of scope, this review is solely focused on the relevant associations between hydrogen bonds and viscosity [190,191] in the context of protein hydration in phase separation in dementia.

Interfacial water can exhibit viscosity 106 times higher than bulk water [192], and the breaking and forming of hydrogen bonds in water [193] can affect viscosity of interfacial water. Viscosity is measured in units of centipoises (cPs) [194], and viscosity can accurately indicate flow resistance in water and other solvents. Viscosity in interfacial water is increased by hydrophilicity and reduced by hydrophobicity, implying the strength of the hydrogen bond is critical to maintaining the integrity of the viscous phase in interfacial water [192]. Low-level microwaves, and other electric and electromagnetic fields (EMF) can restructure hydrogen bonding [195,196] where weakened or broken hydrogen bonds decrease viscosity [197,198] and the formation of stronger hydrogen bonds increases absolute viscosity [199]. Light is a form of electromagnetic radiation (EMR) [200], and plants are exposed to an entire spectrum of EMR from sunlight. However, plants only absorb visible light but reflect infrared light.

During canopy photosynthesis, visible light from the sun is absorbed and utilized while a directly proportional amount of infrared is reflected [201–203]. A tight, linear correlation exists between canopy photosynthesis and correspondingly reflected NIR in all

types of plants examined, including well-watered crops, wetland vegetation, grasslands, and savannas, with different functions, structure, capacity, and even, soil conditions [204]. Surprisingly, or not, a higher level of greenness or presence of vegetation is associated with reduced risk for AD (20%, odds ratio 0.80; 95% CI, 0.75–0.85) and non-AD dementia (11%, odds ratio, 0.89; 95% CI, 0.82–0.96) [205]. However, subjects with dementia treated with UVB irradiation did not exhibit any of the greenness effect even though plants are exposed to both spectrums in sunlight [206].

Similarly, photobiomodulation employing visible red light (670 nm), non-visible near infrared (NIR, 800–1090 nm), and even far infrared (FIR, 3–25 μm) show encouraging results in the attenuation of symptoms associated with dementia including a reduction in A β deposition, size and number of plaque and fibril formation, clearance of misfolded proteins, increased ATP production and reduced ROS production, improved executive and cognitive functions, processing speed, memory performance, mood, energy, and sleep [207–217] (Table 1). The proposal that red and near-infrared wavelengths may promote melatonin synthesis in mitochondria via the pathway involving nitric oxide and enhanced activity of soluble adenylyl cyclase further bolsters the synergistic relationship between light and melatonin [218,219].

Table 1. A sample collection of popular wavelengths employed in photobiomodulation, starting from visible 670 nm to non-visible near- and far-infrared wavelengths, and their effects on various symptoms associated with dementia in animals and humans.

Wavelength	Model/Cell Line/Device	Duration/Intensity	Results	Ref.
670 nm	APP/PS1 AD transgenic mice/transcranial LED	90 s (4 Joule/cm ²)/day \times 20 over 4 wks	Attenuated cerebellar cortex A β deposition, fibril formation.	[207]
670 nm	K3 tau, APP/PS1 AD transgenic mice/transcranial LED	90 s (4 Joule/cm ²)/day \times 20 over 4 wks	Neocortex and hippocampus of K3 and APP/PS1 mice showed reduction in tau/fibril formation and size/number of A β , respectively.	[208]
670 nm	C57BL/6, transgenic 2576 mice/transcranial LED	90 s (4 Joule/cm ²)/day \times 20 over 4 wks	All mice showed reduced A β oligomer binding at CNS synapses.	[209]
670 nm	h tau, 3xTgAD mice/transcranial LED	90 s (4 Joule/cm ²)/day \times 20 over 4 wks	Reduced toxic tau oligomers, improved memory deficits, upregulated clearance of misfolded proteins in both models	[210]
808 nm	A β -treated microglia cells from health mice/diode laser	5 min (9 Joule/cm ²)	Exceeded control cell ATP production after 24 h by 155%, suppressed ROS production promoting neuronal survival.	[211]
810 nm	8 patients diagnosed with dementia/transcranial+transnasal LED	20 min (pulsed at 40 Hz at 50% duty cycle), 3 times/wk for 12 consecutive wks	Significant score improvements in ADAS-cog (13.8%) NPI-FS (61.4%) compared to baseline ¹ .	[212]
1060–1080 nm	11 patients with dementia/transcranial LED helmet	6 min (1100 LEDs pulsed at 10 Hz at 50% duty cycle)/day \times 28 consecutive days	Improved executive functioning in clock drawing, immediate recall, praxis memory, visual attention, and task switching.	[213]
1060–1080 nm	60 patients with mild to moderate dementia/transcranial LED helmet	2 \times 6 min (23.1 mW/cm ²)/day \times 8 consecutive weeks	Improved cognitive functions, auditory and verbal learning, processing speed, mood, energy, and sleep.	[214]
1060 nm	27 healthy participants aged 45+/transcranial LED helmet	2 \times 6 min (12 mW/cm ²)/day \times 28 minimum	Significant improvements in motor function, memory performance, and processing speed.	[215]
1040–1090 nm	APP/PS1 AD double-transgenic mice/LED irradiation	6 min (15 mW/cm ²)/day \times 55 with a 28-day suspension after day 40	Improvement in memory, spatial learning ability, and modest plaque reduction; suspension period indicated treatment effects were transient.	[216]
500 nm/ 800 nm/ 3–25 μm	APP/PS1 AD double-transgenic mice/LED irradiation	60 min (0.13 mW/cm ²)/day \times 45	FIR (3–25 μm) enhanced A β phagocytosis via increased ATP production and attenuated cognitive dysfunction compared to other wavelengths tested.	[217]

¹ ADAS-cog Alzheimer's Disease Assessment Scale-cognitive; NPI-FS: Neuropsychiatric Inventory frequency severity.

The ability to increase adenosine triphosphate (ATP) production in mitochondria is one of the most widely accepted mechanisms behind the effectiveness of photobiomodulation in dementia and other health challenges [211,217,220–222]. The fact that both infrared light and melatonin increase ATP production, and the adenosine moiety of ATP which is structurally similar to melatonin is capable of solubilizing protein aggregation point to the existence of a most unexpected, dynamic relationship between NIR light and melatonin that is inextricably connected to the regulation of hydrogen bonds, viscosity, protein hydration, and protein aggregation (Figure 1). The following section will present what is currently known about molecular mechanisms that drive the synergistic relationships between light, water, and melatonin in the regulation of phase separation of pathological aggregates in dementia. In subsequent discussions, the term light refers to red and near-infrared wavelengths unless otherwise indicated.

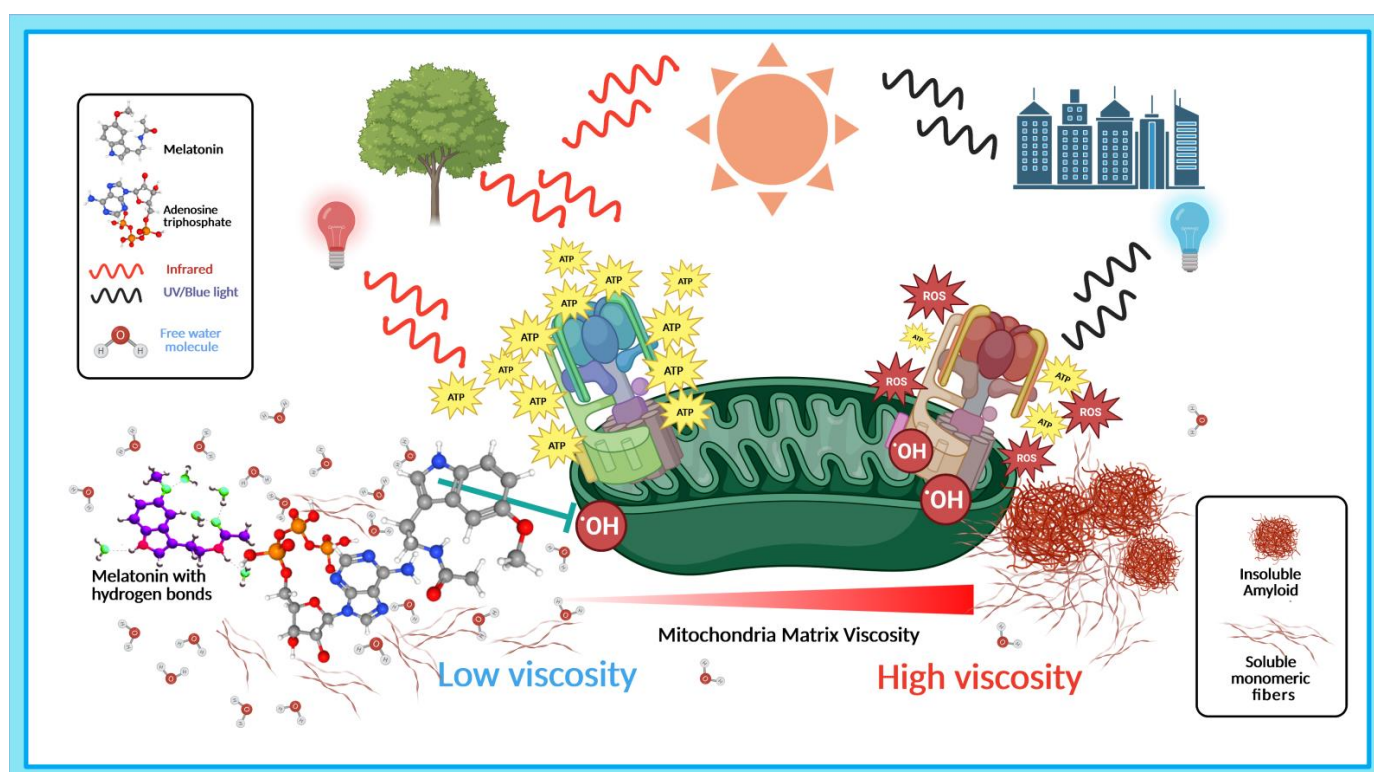


Figure 1. Visible 670 nm red light reduces viscosity in mitochondria interfacial water to increase free water molecules and enhance ATP synthase ability to generate more adenosine triphosphate (ATP). Reactive oxygen species (ROS) increase viscosity and lower ATP synthase efficiency to inhibit ATP production. Melatonin lowers viscosity by scavenging hydroxyl radical ($\bullet\text{OH}$) and ROS. Increased free water molecules from lower viscosity form stronger hydrogen bonds with melatonin to enhance its intrinsic features that include binding interactions with the adenosine moiety of ATP, inhibiting water removal from protein hydration shells that facilitate amyloid fibril aggregation and solubilizing aggregates formed as the result of aberrant phase separation.

3. Light, Water, and Melatonin: Ancient Synergies in a Modern World

The synergistic relationship between melatonin, water, and light may have originated billions of years ago when primitive unicellular organisms depended on this effective and precise synergy to modulate phase separation to control protein aggregation and associated biological effects. The efficacy of this synergy also provides a credible explanation for the immensely successful and rapid distribution of melatonin via horizontal gene transfer [223]. The discovery of the serotonin N-acetyltransferase (*SNAT*) gene responsible for the synthesis of essential melatonin substrate N-acetylserotonin (NAS) in archaea [224,225] firmly establishes the quintessential role played by melatonin in early primitive organisms that

use phase separation as the fundamental driver for relevant biochemical and biophysical processes to support metabolism, replication, and survival [226–232].

Melatonin (N-acetyl-5-methoxytryptamine) was first isolated from bovine pineal gland in 1958 [233]. Since then, revelations from the study of melatonin led to a continuously expanding list of appellations that aim to describe its impressive yet often pleiotropic and contradictory behaviors. Melatonin is known as a hormone, an antioxidant, an anticancer agent, an antiviral, an autocoid, a chronobiotic, a hypnotic, an anxiolytic, a glycolytic, a sleep aid, a universal panacea, a biological modifier, and even a Higgs boson [234]. These nomenclatures are excellent illustrations of some of the broad-based metabolic effects achieved by melatonin as it regulates fundamental phase separation processes in living organisms. The role of melatonin in the regulation of phase separation in the context of neurodegenerative disorders, cancer multidrug resistance, and viral phase separation are clearly defined in several in-depth reviews [230,235,236]. Due to a limitation of scope, the reader may review these extensive discussions for a better understanding of molecular mechanisms employed by melatonin in the regulation of phase separation under different biological contexts. This review will focus on the presentation of known, relevant molecular mechanisms that facilitate and enhance the synergistic relationship between light, water, and melatonin in the regulation of phase separation in dementia.

3.1. Light, Water, and Melatonin: Viscous Relationships with Hydrogen Bonds

Water molecules confined in interfacial hydration water exhibit severely restrained mobility compared to bulk water [170]. The mobility of these water molecules is reduced by interfacial viscosities as high as 106 times that of bulk [192,237]. However, the viscosity of water constrained in extremely narrow spaces such as the interior of carbon nanotubes increases and decreases with increased and decreased diameters, respectively [238,239]. In carbon nanotubes with diameters below 20 Å, water stops behaving like bulk water with different boiling points, self-diffusion coefficient, and viscosity [238,240–242]. Even the mobility of water molecules in ultra-confined spaces is enhanced by reduced viscosity [239,243] which is facilitated by a reduction in hydrogen bonds.

In general, viscosity is increased by stronger intermolecular interactions that form more hydrogen bonds in water molecules [238]. During phase separation, the variation in internal micro-viscosity between tau droplets formed via homotypic and heterotypic associations can be as much as a 7-fold increase [244]. Systematic reductions in droplet micro-viscosity during biological aging may imply continuously evolving intermolecular interactions that shift droplet equilibrium, modifying aggregation potential that favor pathological outcomes [14,245,246]. Therefore, novel properties such as enhanced solubility, diffusion, and electron transfer in specially treated water molecules with lower viscosity and reduced/broken hydrogen bonds [247] may have distinctive effects on the modulation of aberrant protein aggregation in dementia.

Hydrogen bonds (HBs) can be reduced/broken by hot electron transfer when plain, deionized bulk water is allowed to flow through gold nanoparticles under resonant illumination. The water—known as plasmon-activated water (PAW)—created by this method exhibits features conspicuously different from bulk even at room temperature [247]. The reduced intermolecular hydrogen bonds in water molecules not only decrease viscosity, but also impart a higher degree of freedom in interaction that allows the formation of stronger intermolecular hydrogen bonding with hydrophilic solutes while enhancing the solubility of hydrophobic solutes [247,248]. Essentially, the elevated interactions with other molecules via increased free water molecules in PAW enhance the intrinsic activities of these molecules. Melatonin is known to dissolve poorly in water [249]; however, melatonin is able to form stronger hydrogen bonds in PAW resulting in enhancement of solubility between ~120% [248] to ~150% [250].

3.1.1. PAW Modulates Melatonin Hydrogen Bonding and Conformation

Melatonin has five distinct hydrogen bonding sites for water, forming up to five hydrogen bonds with water molecules simultaneously at varying strengths. Two of these hydrogen molecules from two water molecules can even reside indefinitely when they are coordinated with the O of the amide group due to the high degree of stability between the H-bond as indicated by Helmholtz free energy [251,252]. For melatonin, water can either be a H-bond donor or acceptor, depending on the site it is attached to. However, even one single water molecule attached to melatonin can change its conformational preference by modulating the relative energies of the conformations and the heights of the barriers that separate conformations, where strong H-bonds can produce substantial electronic frequency shifts. Furthermore, the relative abundance of the conformations can also be regulated by H-bonds, implying that preferential binding between specific sites and water molecules can produce conformational clusters with populations as high as 10 times over other species [252]. In bulk water, melatonin forms the strongest H-bond with its carbonyl O group, stabilizing its tendency to self-aggregate resulting in low solubility [253].

Melatonin prepared in PAW compared to bulk deionized water exhibited enhanced clearance of hydroxyl radical at 11.9% vs. 6.69%, respectively; its antiviral potency against dengue virus in infected human hepatocarcinoma cells is also enhanced, reducing infectivity by 14.7% vs. 20.6% in bulk [250]. Male Wistar rats subjected to chronic sleep deprivation (CSD) using the disc-on-water methodology [254] and treated with 10 mg/kg melatonin via intraperitoneal (IP) injection dissolved in PAW exhibited significantly better results in all parameters detected, including hepatic function and metabolic activity, than control (no treatment), CSD only, and CSD + melatonin dissolved in bulk deionized water groups [250]. It is plausible that when melatonin is dissolved in PAW, the intrinsic anti-inflammatory properties of PAW may also be responsible for molecular mechanisms that support/enhance melatonin's antiviral and antioxidative features. Indeed, APP/PS1 transgenic AD mice treated with PAW showed improved memory function and reduced amyloid burden, potentially via anti-inflammatory and anti-oxidative effects, compared to age-matched wild-type controls [255,256]. There is no doubt that the anti-oxidative properties of PAW enhance melatonin's intrinsic activities. However, the molecular mechanism involved is an unexpected, viscous one.

3.1.2. Reactive Oxygen Species Increase Viscosity

Hydrophilicity enhances viscosity in interfacial water at values up to ~106 times that of bulk due to an increase in ordering and hydrogen-bond dynamics [192]. The negative polarity of reactive oxygen species (ROS) is able to increase hydrophilicity and elevate viscosity. When the oxygen atom of one of the most reactive ROS hydroxyl radical ($\bullet\text{OH}$) becomes highly negative and acts as a hydrogen bond acceptor, it can lower the reaction barrier stabilizing $\bullet\text{OH}$ bonding to water during the polar transition state. Thus, water and viscosity of water can modulate and stabilize the highly reactive $\bullet\text{OH}$ [257]. In bulk water, $\bullet\text{OH}$ forms three stable hydrogen bonds and a weaker hemibond with surrounding water molecules comprising its solvation shell [258].

In mitochondria, $\bullet\text{OH}$ is derived from superoxide radicals produced as a result of a one-electron reduction of oxygen (O_2) from electron leakage during mitochondrial electron transport [259,260]. Simply stated, the presence of excess, unneutralized ROS can significantly elevate viscosity in these essential energy-producing organelles, negatively impacting mitochondrial functions and ATP production associated with pathological $\text{A}\beta$ aggregation [261]. Hydrogen peroxide (H_2O_2)—a ubiquitous ROS with classical intracellular signaling functions at lower physiological levels [262]—is also produced in mitochondria from electrons leaked during mitochondrial electron transport activities [259]. Similar to $\bullet\text{OH}$, H_2O_2 accumulation can increase matrix viscosity in mitochondria [263,264]. Furthermore, an NIR emissive fluorescent probe with a large Stokes shift detected significantly elevated viscosity and H_2O_2 levels in brain mitochondria of APP/PS1 transgenic AD mice compared to normal BALB/c mice [265].

3.1.3. Reduction in Viscosity and Hydrogen Bonds Enhance Melatonin ROS Scavenging

Melatonin is known for its ability to scavenge $\bullet\text{OH}$ and other free radicals [266–270] where one molecule of melatonin can scavenge two $\bullet\text{OH}$ radicals to produce the stable cyclic 3-hydroxymelatonin (3-OHM) metabolite [266]. However, the addition of only one water molecule that provides an H-bonding relay pathway significantly lowered the energy barrier in the tautomerization step to enhance the scavenging potential by melatonin [271]. The fact that melatonin prepared in PAW exhibit 78% increased effectiveness in $\bullet\text{OH}$ scavenging compared to bulk (11.9% vs. 6.69%) [250] implies that melatonin may adopt more favorable conformations that enhance its intrinsic activities as a result of stronger H-bonds formed in water with reduced viscosity and H-bonds compared to bulk.

In the context of aberrant protein aggregation in dementia, the signature reduction in viscosity and H-bonds in PAW inadvertently accentuates an unconventional but relevant perspective on the viscous relationships between light, melatonin, and ROS that surprisingly, or not, converge on the synthesis of ATP in mitochondria. In response to conditions that reduce ATP, budding yeast conserves energy by increasing cytosolic viscosity to slow cellular processes by reducing protein diffusion rates. Additionally, increased viscosity modulates phase separation, impeding the formation of stress granules and inducing aberrant phase separation to form aggregates that were not present in cells that could not elevate viscosity [272].

3.2. Light, Melatonin, and Viscosity in the Elevation of ATP Synthesis

Mitochondrial matrix exists mostly as interfacial water due to the density of proteins, and matrix water exhibits similar restrained mobility as interfacial water. Consequently, matrix water is significantly more viscous than cytoplasm [273]. The viscosity of the mitochondrial matrix is correlated with the respiratory state of the organelle that can affect not only signal transduction, but also how mitochondrial networks are organized. The abnormal elevation of viscosity in mitochondria results in dysregulation in metabolite diffusion that can cause aberrant phase separation resulting in malignancies associated with fatty liver, diabetes, atherosclerosis, accelerated aging, cancer, AD, and other neurodegenerative disorders. Therefore, the accurate detection and determination of mitochondrial viscosity can facilitate the understanding of molecular mechanisms behind various diseases associated with mitochondrial dysfunctions [265,274–294]. A fluorescent probe that can detect mitochondrial viscosity fluctuations was used for the first time in the successful, early diagnosis of liver and kidney injury in animal models [295], while other probes are employed to effectively distinguish normal cells from cancerous cells with distinct, elevated viscosity [296–299].

In HeLa cells, the average viscosity of mitochondria is determined to be ~ 62.8 cP [300], in stark contrast to the 2.04 ± 0.49 cP obtained for HeLa nucleoplasm viscosity which is already higher than that in HeLa cytoplasm [301]. Furthermore, treatment with pharmaceuticals, such as monensin and nystatin, can further drive matrix viscosity up to 90.5 and 109 cP, respectively [300,302]. Mitochondria of HeLa cells under oxidative stress generate a tremendous amount of ROS [303]. Therefore, ROS such as $\bullet\text{OH}$, which is naturally produced during mitochondrial respiration, and excess oxidative stress, can potentially increase matrix viscosity from its hydrogen-bonding interactions with water molecules. Dual-targeting fluorescent probes are developed to easily identify viscosity changes in mitochondria in the presence of specific free radical species [304]. Mechanistically, increased viscosity in the matrix can result in the lower production of ATP catalyzed by the ATP synthase.

3.2.1. Efficiency of ATP Synthase Is Modulated by Viscosity

The mitochondrial ATP synthase (F_0F_1) is a rotary motor enzyme with a proton-driven F_0 motor that is embedded in the inner mitochondrial membrane and is connected to the ATP-driven F_1 motor that protrudes into the mitochondrial matrix [305–307]. The higher viscosity of the medium can slow down the rotation of the F_1 motor to reduce ATP

synthesis not only in mitochondria [308] but also chloroplasts [309]. While ATPase turnover rates are more effective when detected by probes designed with lower viscous drag [310], viscous drag can dramatically slow the rate of rotation to 3% of the enzyme turnover rate in *Escherichia coli* [311].

Nonetheless, 100% efficiency of the F_1 rotor can theoretically be achieved if the 120° power strokes rotate at a constant angular velocity [312]. However, power stroke and dwell duration are easily modified by viscosity. Viscous loads applied to the ATP F_1 motor of *E. coli* can cause the increase in the duration of the 120° power stroke that is correlated to a 20-fold increase in the length of the dwell. Thus, the power stroke velocity is limited by the viscous load on the motor, and consequently, increases in transition time are the direct result of increases in viscosity and not from inhibition of the ATPase by other means [313]. A deeper analysis of viscosity sensitivity showed that viscous drag on rotations of the γ -subunit in the F_1 motor [314] can cause variations of more than 5000-fold by using a variety of rotation probes [315].

3.2.2. The 670 nm Wavelength Elevates ATP Production in Mitochondria

The benefits of photobiomodulation employing the 670 nm wavelength for dementia and other neurodegenerative disorders are extensively documented (Table 1). Even though improved ATP production and reduced ROS production are associated with the use of 670 nm irradiation, the exact mechanism responsible for these effects remains controversial. Experimental works employing 670 nm report the reduction in inflammation via increased expression of cytochrome C oxidase (COX) in an age-related macular degeneration mouse model [316]; increased COX expression and ATPase activities in Wistar rats exposed to suppressive effects of fluorescent light [317]; significantly elevated ATP production in aging mouse retina via increased COX expression [318]; and the restoration of neuronal ATP and prevention of apoptosis induced by potassium cyanide—an irreversible inhibitor of COX [319]. Therefore, benefits from photobiomodulation, especially the enhancement of ATP production and mitochondrial function, are generally believed to be associated with the involvement of COX via increased COX expression and activities.

COX, or complex IV [320], is the fourth enzyme that catalyzes the transfer of electrons from ferricytochrome C to oxygen in the mitochondrial electron-transport complexes, and COX is highly susceptible to inactivation by oxidative damage induced by ROS including $\bullet\text{OH}$ and 4-hydroxynonenal (HNE), a major lipid peroxidation product [321–325]. Even though COX is viewed as the primary photoacceptor, molecular mechanism that elucidates the association of irradiation by 710–790 nm and 650–680 nm wavelengths with reduced and oxidized states of COX, respectively, remain elusive [326]. Furthermore, experimental work that combined nanoindentation and 670 nm laser irradiation to modulate viscosities of interfacial water supports the proposal that lower viscosity in mitochondria is the real driver behind photobiomodulation propelling enhanced ATP synthesis, and not increased COX expression and activities [327–329]. However, if reduced viscosity from light irradiation is responsible for increased ATP synthesis via increased power stroke velocity producing more efficient F_1 motor rotations, then this proposal should be inclusive of COX involvement also.

3.2.3. Viscosity Modulates COX Activities in Mitochondria

In 1987, the main activity of COX—the oxidation of ferricytochrome C by COX—was demonstrated to be viscosity-dependent at both high and low ionic strengths [330]. While laser flash photolysis revealed a dramatic decrease in the rate of intramolecular electron transfer (IET) between the heme and molybdenum centers of chicken liver sulfite oxidase when solution viscosity was increased [331]. The evidence supporting the enhancement of ATP synthesis via light irradiation is solid [332,333], and it is also not unreasonable to propose that the reduction in mitochondrial matrix viscosity by light or ROS scavenging can increase ATP production, and increased ATP is associated with clearance of pathogenic aggregates from aberrant phase separation.

Thus, the ability to clear A β aggregation by the antioxidant epigallocatechin-3-gallate (EGCG) may be the result of upregulated COX activities and ATP production from reduced ROS and matrix viscosity [334,335]. In human neuroblastoma (SH-EP) cells, 670 nm irradiation dramatically elevated ATP levels by 20% which was subsequently diminished after irradiation-associated clearance of A β 42 aggregation. Both 670 nm irradiation and EGCG were independently able to reduce A β 42 aggregation at the expense of ATP consumption compared to controls. However, the combined, complementary treatment produced even better results in the clearance of amyloid aggregates compared to controls [334].

3.3. Melatonin Prevents and Disaggregates Aberrant Protein Aggregation in Dementia via Association with ATP

Melatonin, a mitochondria-targeted molecule [336] that is known for being a potent ROS scavenger [266–271], promotes ATP synthesis via the elevation of COX expression and activities. Melatonin administered to aged rats at 10 mg/kg per day in drinking water prevented the 30% age-related decline in COX activity while abolishing concomitant elevation of H₂O₂ in brain mitochondria of aged rats compared to controls [337]. Melatonin administered orally at 10 mg/kg/day for 17 weeks to male Zucker diabetic fatty (ZDF) rats restored the 25% decline in renal mitochondrial COX activity and attenuated other mitochondrial dysfunctions including diminished ATP production compared to lean controls [338]. Melatonin administered in drinking water at the same amount to ZDF rats reversed the 76% decline in brown adipose tissue mitochondria COX activity by 35% while increasing COX activity by a staggering 31% in normal, lean controls [339].

3.3.1. Melatonin Elevates ATP Production via Modulation of COX and Viscosity

Even though cyanide (CN[−])—a highly cytotoxic molecule that inhibits COX to suppress mitochondrial respiration and ATP production, and elevates ROS by modulating antioxidant defense—is proposed to be a novel mammalian gasotransmitter that can stimulate COX activity and enhance cellular bioenergetics at low endogenous nanomolar levels, at levels beyond 10 μ M, CN[−] remains exceedingly toxic [340–345]. As a result, sophisticated dual-response sensors and probes are used to detect fluctuations in mitochondria viscosity in the presence of varying levels of cyanide in living cells [278,346].

Not unexpectedly, the *in vitro* study of rat brain mitochondria treated with 5 μ M potassium cyanide revealed that 50% inhibition of COX activity was nearly entirely counteracted by treatment with 100 μ M melatonin in a dose-dependent manner compared to control; while COX activity in rat liver mitochondria under same treatment conditions achieved 30% higher efficiency than control. However, at 100 μ M cyanide exposure, even 5 mM of melatonin was unable to reverse the 100% inactivation of COX [347]. *In vivo* administration of melatonin at 10 mg/kg (IP) significantly elevated COX activity in rat brain and liver mitochondria in a time-dependent manner while reversing COX activity inhibition and preventing mitochondrial damage and oxidative stress induced by ruthenium red treatment at 60 μ g/kg (IP) [348]. Ruthenium complexes can also increase viscosity and induce cell apoptosis via ROS-mediated mitochondrial pathways [349,350].

3.3.2. Fibril Disaggregation by Melatonin Is Dose-Dependent

Melatonin is intensively studied and extensively reviewed as a likely ideal therapeutic molecule for AD and other neurodegenerative disorders [351–355]. A novel understanding of melatonin regulation of biomolecular condensate phase separation in neurodegenerative disorders [230] provides additional relevant molecular mechanisms behind reported observation including the inhibition, destabilization, reduction, and delay of α -Syn and A β fibril aggregation. Melatonin not only increased survival rates in transgenic AD mice, but also reversed A β -induced synaptic disorder, memory deficit, neurodegeneration, as well as phosphorylation of tau in wild-type mice injected with A β peptides [356–366] (Table 2). However, inconsistent results were observed when there were discrepancies in dosage and timing/duration of administration [363].

Table 2. In vitro and in vivo studies that reveal important relationships between melatonin dosage, timing, and administration that produced different results for symptoms associated with dementia.

Melatonin Dosage/Duration	Study Design	Results	Ref.
25 μ M, 250 μ M, 2.5 mM	In vitro α -Synuclein peptide aggregation	Blocked α -Syn fibril formation and destabilized preformed fibrils in a dose- and time-dependent manner; increased viability of primary mixed neurons treated with α -Syn to ~97% in a time-dependent manner.	[356]
10 mg/kg (IP) \times 5/day for 2 days, then \times 2/day for 5 days	Arsenite-induced oxidative injury in substantia nigra of adult male rats	Attenuated arsenite-induced α -Syn aggregation, lipid peroxidation, and glutathione depletion.	[357]
100 μ M melatonin	A β peptides (1-40) and (1-42) β -sheet/fibril formation	Progressive reduction in A β 1-40 β -sheet structures to 24% after 24 h incubation; immediate reduction in A β 1-42 β -sheet structures from 89% to 65%, decreasing to 59% after 4 h.	[358]
Melatonin dissolved in 2 mM ammonium acetate	A β peptide (1-40) β -sheet/fibril formation	Inhibited β -sheet formation by targeting hydrophobic A β -peptide segment (29-40) intermolecular activities.	[359]
1 mM melatonin	A β 1-40 peptide, profibrillogenic apoE4/apoE	Melatonin alone delayed fibril formation from 24 h up to 72 h. Combined with either apoE4 or apoE3, inhibition remained effective at termination of experiment.	[360]
2 mg/mL in drinking water starting at age 4 months until euthanasia	Transgenic Tg2576 AD mice, terminated at 4 months 1 wk or 15.5 months	The brains of animals treated with melatonin terminated at 15.5 months exhibited dramatic decline in oligomeric A β 40 together with a significant increase in soluble monomeric A β 40, and a decreasing trend in A β 42 compared to untreated mice at same age. Melatonin prolonged survival rates of 15.5-month mice to levels attained by non-transgenic mice.	[361]
2 mg/mL in drinking water starting at age 4 months until euthanasia at 15.5 months	Transgenic Tg2576 AD mice	Increased survival in treated mice (3 deaths/41 survivals) compared to untreated (13 deaths/31 survivals).	[362]
0.5 mg/mL in drinking water starting at age 4 months	Transgenic Tg2576 AD mice	Striking reductions in A β levels in brain tissues of treated mice at 8, 9.5, 11, and 15.5 months.	[362]
16 μ g/mL in drinking water starting at age 14 months	Transgenic Tg2576 AD mice	Melatonin treatment failed to reduce brain A β levels or even oxidative damage.	[363]
40-ppm (<i>w/w</i>) in pelleted minimal basal diet	Male B6C3F1 mice aged 6, 12, and 27 months	Significant reduction in A β in brain cortex tissues: 57% in A β 40 and 73% in A β 42; increased melatonin levels in cerebral cortex in all 3 treated age groups (12 > 6 > 27 mos) compared to untreated.	[364]
10 mg/kg (IP) daily for 3 weeks	Male wild-type C57BL/6N mice (8 wks old) injected with A β 1-42 peptide	Melatonin treatment reversed A β 1-42-induced synaptic disorder, memory deficit, and prevented A β 1-42-induced apoptosis, neurodegeneration, and tau phosphorylation.	[365]
10 mg/kg in drinking water from day 7 after tauopathy induction to day 28 at termination	4-month-old C57BL/6J mice injected with human tau mutation P301L (AAV-hTau)	Increased ROS and tau hyperphosphorylation starting at day 7 precedes cognitive decline; melatonin-treated animals showed reduced memory impairment, tau hyperphosphorylation, ROS, and neuroinflammation.	[366]
10 μ mol/L	Ex vivo brain slices from 3-month-old SD rats exposed to okadaic acid to induce tau hyperphosphorylation	Melatonin reduced tau hyperphosphorylation and ROS to control levels in OA-treated brain slices.	[366]
100 μ M–5000 μ M	Aggregation/disaggregation of repeat domain Tau (K18wt)	Pre-formed tau fibril disaggregation was dose-dependent: 14% with 100 μ M, 54% with 5000 μ M.	[367]
200–5000 μ M	Aggregation/Disaggregation full-length tau (hTau40wt)	Tau treated with 200 μ M melatonin showed no change in morphology compared to controls; 5000 μ M melatonin treatment did not prevent aggregation but disaggregated tau fibrils into broken filaments.	[368]

Similarly, in vitro studies on tau fibril aggregation and disaggregation in the presence of melatonin at varying strengths found disaggregation effects to be dose-dependent

where 100 μM led to 14% disaggregation while 5000 μM disaggregated ~54% of pre-formed repeat domain tau [367] (Table 2). However, 200 μM melatonin treatment in full-length tau aggregates failed to produce morphological changes, and 5000 μM treatment could not prevent aggregation but was able to disaggregate tau fibrils into small, broken filaments [368] (Table 2).

3.3.3. Melatonin Hydrogen Bonding May Modulate Salt Bridge Formation in Aggregates

The general consensus on the disaggregation mechanism employed by melatonin is the disruption of salt bridge formation or the reduction of hydrophobic interaction between proteins [358,359] (Table 2). Salt bridges formed between tau proteins can strengthen and stabilize the core of the paired helical filaments which enhances aggregation [367,369]. Both hydrogen bonds and salt bridges provide favorable free energy during protein–protein binding. Therefore, unfulfilled hydrogen bonds or isolated charges without forming salt bridges can destabilize binding due to the desolvation effect [370,371].

During A β oligomerization, the prerequisite expulsion of water molecules from protein hydration shells facilitates the formation of salt bridges [372]. In general, weaker hydrogen bonds are formed in interfacial regions due to the restrictive translational and rotational freedom constraints in interfacial regions. Consequently, more water molecules are required in interfacial regions for bridging hydrogen bond networks across protein interfaces [370]. When interacting with melatonin, water can act as both a H-bond donor to the amide carbonyl, methoxy oxygen, or indole π clouds and a H-bond acceptor from the amide NH and indole NH groups [252]. Therefore, the ability to form π hydrogen bonds [373] potentially allows melatonin to prevent the formation of salt bridges that impede intramolecular tau filament aggregation [374]. However, in vitro studies produced results that did not fully support in vivo and ex vivo work on melatonin and tau hyperphosphorylation [367,368] (Table 2).

3.3.4. Hyperphosphorylation Reduces Water Hydration during Fibril Aggregation

Hyperphosphorylation of tau is a reversible physiological process, but abnormal hyperphosphorylation in neurodegenerative disorders including AD is resistant to dephosphorylation and proteolysis [375–378]. It is believed that the cytotoxicity of A β is tau-dependent where tau and A β together drive healthy neurons into diseased states and that both A β and tau toxicity reinforce each other via a feedback loop [379–382]. The oligomerization of tau fibrils resulting in the formation of pathological tau aggregates is thermodynamically facilitated by hyperphosphorylation of tau proteins [383]. Hydrophobically driven phase separation which leads to the removal of water molecules from protein hydration shells is the predominant interaction that amplifies hydrophobic attractions that cause hyperphosphorylation of tau and fibrillization [135,384]. Recall tau proteins that phase separate due to salting-out effects mature into pathogenic, irreversible, canonical tau fibrils with restricted water accessibility and increased micro-viscosity [135] (see Section 2.3).

Furthermore, hyperphosphorylation can generate conformation changes critical for in vitro phase separation of full-length tau which precedes aggregation. Hyperphosphorylation shifts the equilibrium between soluble and phase-separated tau to favor the droplet state, enhancing maturation that initiates pathological aggregation [385]. Consequently, the ability to form hydrogen bonds to maintain protein solubility may determine the level of effectiveness of melatonin treatment in the prevention of tau hyperphosphorylation and subsequent phase separation events that ultimately result in the formation of pathological tau aggregates.

Therefore, in vitro work that showed dose-dependent disaggregation of pre-formed tau fibrils but the inability to prevent aggregation even at high concentrations of 5000 μM in contrast to in vivo and ex vivo work that reported a significant reduction in tau hyperphosphorylation even after the establishment of tauopathy (Table 2) may simply reflect the absence of ATP that can modulate hydrophobic interactions from hydrogen-bonding

activities. In the context of phase separation in dementia, ATP may be the quintessential lynchpin that brings light, water, and melatonin together in a dynamic and effective synergy. After all, the regulation of aberrant protein aggregation in dementia by light and melatonin is associated with molecular mechanisms including reduced viscosity, hydrogen bonding, protein hydration, and elevation of ATP synthesis (Figure 1).

3.4. Light, Water, and Melatonin: The Adenosine Moiety Effect of ATP

The ability of ATP to solubilize hydrophobic substances in aqueous solutions at neutral and elevated pH was first reported by Mandl and Neuberg in 1952 [386]. Several decades later, ATP was observed to behave as a hydrotrope, solubilizing and dissolving protein aggregates in *Xenopus* oocyte nucleoli, preventing the aggregation of synthetic A β ₄₂ peptides, and even dissolving preformed tau fibrils [387,388]. However, employing all-atom molecular dynamics (MD) simulations, Kurisaki et al. observed contradictory results where ATP actually did not have any effect on the dissociation of monomers or the decomposition of the A β ₄₂ oligomer. Instead, the hydrophobic adenosine moiety of ATP was reported to dissociate A β ₄₂ monomers via contacts with A β ₄₂ backbone atoms, potentially dissolving the A β ₄₂ oligomer by shifting thermal equilibrium from an on-pathway species to an off-pathway species [389].

These observations were further clarified by Mehringer et al. demonstrating via MD simulations that ATP did not exhibit classic features of a hydrotrope or displayed chaotropic salting-in effects. In fact, ATP can be considered a kosmotropic anion with salting-out effects as a result of the triphosphate moiety of ATP capable of lowering the solubility of organic compounds in water. The ability of ATP to prevent and dissolve aggregates formed by phase separation observed in earlier works [387,388] is facilitated mainly by the interaction of the aromatic adenosine moiety in ATP with intrinsically disordered proteins, while the highly charged phosphate moiety served to heighten the solubility of the hydrophobic adenosine in ATP [390]. This molecular mechanism clearly explains why AD transgenic mice exhibit significantly reduced ATP production and mitochondrial dysfunction [391]. The adenosine moiety prevents hydrophobic collapse and aggregation by increasing solubility that prevents water removal [173]. As a consequence, the presence of ATP is highly effective in the suppression of A β ₁₆₋₂₂ peptide aggregation [392].

Adenosine is a primordial metabolite [393] that is an integral component of ATP and RNA [394,395]. Not unexpectedly, both ATP and RNA modulate phase separation biphasically where low concentrations enhance phase separation but high concentrations inhibit droplet formation [387,396–399]. MD simulations demonstrate succinctly that the dissolution of FUS by ATP-Mg²⁺ is promoted by solubilization via the adenine moiety and the phosphate moiety served only to enhance the requisite hydration effect [400].

Mechanistically, the adenosine moiety may prevent amyloid fibril formation by interfering with A β peptide π - π stacking [401,402]. Interestingly, the indole ring of tested indole derivatives effectively inhibited the formation of amyloid fibrils in hen egg-white lysozyme induced by low pH and high temperatures via hydrophobic interactions that accelerated disaggregation and destabilized the amyloid fibrillar state [403,404]. Therefore, it is perhaps not an evolutionary coincidence that melatonin not only exhibits structural homology to the adenosine moiety of ATP [401] (Figure 2), but also binds to adenosine via a hydrogen bond [405–408]. Consequently, ATP and melatonin may have been used for billions of years by living organisms to efficiently regulate phase separation in proteins with a high propensity for aggregation [230,401,409].

Arguably, the absence of ATP, despite the ability of melatonin to disrupt salt bridge formation, may be the reason why *in vitro* works on melatonin and tau fibril aggregation reported distinctly different results in the inhibition of fibril formation that could not confirm *in vivo* and *ex vivo* observations even at high concentrations of 5000 μ M (Table 2).

Extracellular adenosine is derived from the degradation of ATP and adenosine monophosphate (AMP), whereas hydrolysis of AMP is the main source of intracellular adenosine [410,411]. It is estimated that extracellular adenosine can rise 1000-fold from the

low nanomolar range of ~20–300 nM to the low micromolar range as high as 30 μ M under conditions of high physical stress including extreme exercise and high altitude with low ambient oxygen [412]. Neurodegenerative diseases, inflammatory conditions, autoimmune diseases, cancer, diabetes, and cerebral ischaemia are pathological conditions associated with elevated extracellular adenosine [410,413–417].

Under optimal conditions, the high reserve/maximum capacity of melatonin synthesis in humans theoretically confers enhanced survival fitness as higher melatonin production allows rapid adaptation to unpredicted internal and external stressors [418]. Assuming that melatonin can be bound to adenosine at a 1:4 ratio [406–408], 6–20 nM plasma adenosine in venous blood collected from normal, healthy subjects [419] can theoretically bind to 1.5–5 nM of plasma melatonin. However, the lower range of 1.5 nM already reflects the highest 1.13 nM median level detected in nocturnal plasma melatonin concentration in children between the ages of 1–3 [420], and melatonin production begins to decline at the early age of 20–30 to approximately 0.12 nM after the age of 50 [421–423].

Furthermore, although there are contrary outcomes in some other reports, there may be conditions where endogenous production of melatonin is suppressed by constant exposure to 60 Hz magnetic field [424] and ambient light at night [425,426]. In addition to binding adenosine, melatonin can significantly elevate ATP production in mitochondria [347,348]. Therefore, the adenosine moiety effect of ATP in phase separation is directly affected by how much melatonin is available, and the dosage of melatonin becomes a critical moving target in the study of phase separation regulation in dementia.

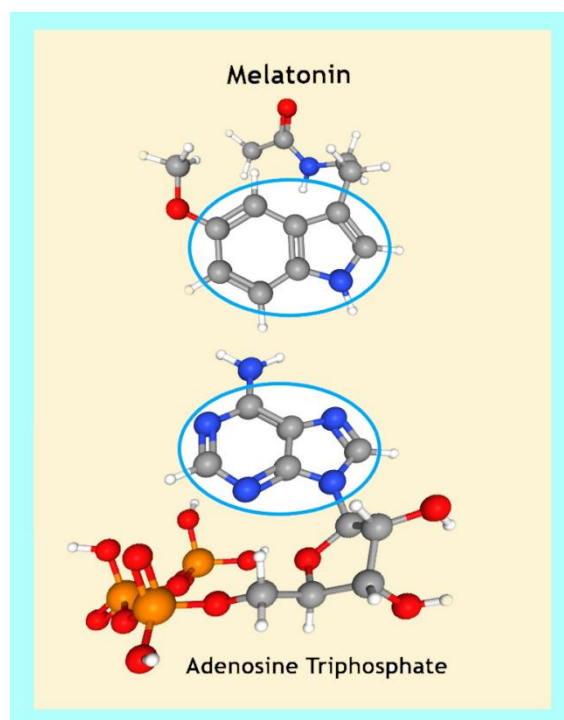


Figure 2. Homologous molecular structures between the electron-rich aromatic indole moiety in the melatonin molecule [427] and the adenosine moiety of ATP [428,429].

4. Of Mice and Men: Perfecting the Human Equivalent Dose for Melatonin in the Regulation of Phase Separation in Dementia

The *in vitro* and *in vivo* effects of melatonin in dementia is not only dose-dependent, but may also be time-, and perhaps even age-dependent (Table 2). Three experiments that tested the same strain of transgenic Tg2576 AD mice with 0.016, 0.5, and 2.0 mg/mL of melatonin added to the drinking water starting at various ages, produced not only different, but also contradictory results (Table 2). Tg2576 mice are leaner compared to wild types as they age [430–432]. Assuming an average weight of 22.5 g for each animal drinking 3 mL

of water per day [361,362], the approximate daily melatonin supplementation would have been 2.13, 66.66, and 266.66 mg/kg, respectively.

Tg2576 mice receiving ~2.13 mg/kg daily starting at age 14 months failed to show any benefit in the reduction in A β accumulation in the brain or oxidative stress levels [363]; whereas Tg2576 mice receiving ~66.66 mg/kg daily starting at age 4 months showed a significant reduction in A β levels in brain tissues, as well as lowered abnormal nitration of proteins [362]. Importantly, Tg2576 mice receiving ~266.66 mg/kg daily starting at age 4 months produced the most impressive results where the brains of mice terminated at 15.5 months not only exhibited a dramatic decline in oligomeric A β 40, but also a significant increase in soluble monomeric A β 40. A noticeable decreasing trend in A β 42 was observed in treated compared to untreated mice at the same age [361]. When Tg2576 mice from two separate experiments were administered ~266.66 mg/kg melatonin in drinking water daily starting at age 4 months until termination at 15.5 months, survival was significantly increased in treated compared to untreated mice [361,362]. Melatonin treatment at ~266.66 mg/kg daily in drinking water was able to reduce mortality in Tg2576 mice to levels observed in wild-type mice [361] (Table 2). Consequently, the effective translation of melatonin doses between animals and humans becomes the primary consideration when designing the dosage for clinical trials.

4.1. Aiming at Moving Targets in Allometric Scaling of Melatonin Interspecies Conversion

Animals have different metabolic rates. In general, larger animals have lower metabolic rates; therefore, the metabolic rate requires scaling in the conversion of interspecies doses. Allometry broadly describes the study of consequences between body and organ sizes [433,434]. The concept of interspecies allometric scaling was first presented in 1637 by Galileo Galilei [435]. Since that time, various allometric approaches have been proposed and used to determine the most efficacious human equivalent dose (HED) [436–450]. However, the identification of a definitive unified principle that effectively scales and optimizes different energy metabolism systems across animal species remains elusive and highly controversial [441,451–454].

In 1880, Rubner first proposed the body surface law that scales metabolic rate with body mass raised to the power of $\frac{2}{3}$ [455]. The seminal work by Kleiber in 1932 led to extensive empirical evidence that supports the metabolic rate in most animals and plants scales to the power of $\frac{3}{4}$ of body mass instead of $\frac{2}{3}$ [454,456]. To date, there is no consensus as to whether $\frac{2}{3}$ or $\frac{3}{4}$ power of body mass should be used as the basal metabolic rate scale in connection with the body mass to determine dose conversion. In general, the exponent of $\frac{2}{3}$ may be more applicable for pharmaceuticals that are eliminated via the kidneys, whereas the exponent of $\frac{3}{4}$ is more suitable for molecules such as melatonin that are cleared by metabolism or via combined metabolism and renal elimination [441,445]. However, once a correction factor (K_m)—a ratio that accounts for the interspecies difference between humans and animals obtained by dividing body weight by body surface area (BSA) [447,457]—is applied during the conversion of animal to human doses, where

$$\text{HED (mg/kg)} = \text{Animal dose (mg/kg)} \times (\text{animal } K_m / \text{human } K_m)$$

The results obtained are invariably higher than the $\frac{2}{3}$ metabolic scale exponent of 0.67 (assuming human $K_m = 37.9$).

For example, to calculate the HED for a 70 kg human, BSA 1.846, K_m 37.9, the metabolic rate exponents for a mouse weighing 0.02 kg, BSA 0.007 (M^2), K_m 2.857, and K_m ratio 13.265; and a rat weighing 0.15 kg, BSA 0.025 (M^2), K_m 6, and K_m ratio 6.317, after adjustments would be 0.683 and 0.700, respectively. For a mini pig weighing 40 kg, BSA 1.14 (M^2), K_m 35.088, and K_m ratio 1.08, the exponent for metabolic scaling for a 70 kg human becomes 0.863.

Thus, the accuracy of HED calculations during interspecies conversion is strictly dependent upon both body weight and BSA. The human BSA can be estimated via the formula $\text{BSA} = \frac{1}{6} (\text{Weight} \times \text{Height})^{0.5}$ [458], whereas specific animal BSA is often more difficult

to ascertain. Popular manuals containing instructions for interspecies HED conversions rely upon predetermined animal BSAs based upon a mathematical formula ($BSA = kW^{2/3}$) postulated by Meeh in 1879, where BSA is derived from a constant k and volume estimated from body mass that is scaled to the $2/3$ -power. For most small animals including mice, the mean constant k is accepted to be 9.83 [459,460]. However, empirical determination for Meeh constants in mice with different body compositions and shapes revealed a range from 9.822 (normal) to 8.288 (obese) [459]. Therefore, the difference in Meeh constants between measured and calculated values would be important considerations when using mice with altered body composition. Furthermore, modifications for cell porousness per fractal theory indicate that the scaling exponent can vary from 0.694 to 0.83 [450].

As such, the estimated HEDs in this review will be calculated employing metabolic rate scaling using body weight raised to the $3/4$ -power where

$$\text{HED (mg/kg)} = \text{animal dose (mg/kg)} \times (\text{WEIGHT[kg]}_{\text{animal}}/\text{WEIGHT[kg]}_{\text{human}})^{(1-0.75)}$$

Using this formula, the estimated HED for a rat weighing 0.2 kg with a 10 mg/kg melatonin dose will be 2.12 mg/kg and 2.4 mg/kg for a 100 kg and 60 kg human, respectively. Nevertheless, the often-large differential in interspecies bioavailability and pharmacokinetics that can be modulated by route of administration, dosage, solubility, and formulation must also be taken into account for the accurate determination of an efficacious HED during conversion/scaling processes.

4.2. The Many Faces of Bioavailability in the Interspecies Conversion of Melatonin

The bioavailability of a substance is generally accepted as a key pharmacokinetic parameter, expressed as a percentage, that describes the rate and extent the substance becomes available in the general circulation after being delivered from a pharmaceutical form. Absolute bioavailability is a percentage obtained by comparing extravascular administration to intravenous injection (IV) assumed to be 100% available, whereas relative bioavailability compares different routes or formulations without reference to an IV administration [461]. Early work found healthy male subjects who ingested a single 80 mg melatonin (gelatin capsules) displayed varying levels of peak serum melatonin and absorption levels (up to 25-fold difference) 60–150 min after ingestion. This peak level could be extended from ~1.5 h to 4–6 h when subjects were given one 80-mg capsule/h over a 3 h period [462]. Melatonin bioavailability in humans, absolute or relative, is delivery-, dose-, solubility-, and formulation-dependent.

4.2.1. Administration Routes Modulate Melatonin Bioavailability

The bioavailability of melatonin is affected by different routes of administration, where the mean bioavailability for 25 mg of melatonin delivered via intravesical, transdermal, rectal, and vaginal administration in healthy female volunteers were 3.6%, 10.0%, 36.0%, and 97.8%, respectively, compared to IV administration [463]. However, the determination of the bioavailability of oral melatonin may be complicated by melatonin metabolism. In humans, melatonin is mainly cleared by first-pass hepatic metabolism. When the clearance of an IV melatonin dose was combined with plasma concentrations of oral doses from previous data, the calculated oral bioavailability of melatonin was estimated to be 3–6% after a 2.5 mg dose, 3–76% after an 80 mg dose, but only 9% after a 100 mg dose [464].

In 2000, DeMuro and coworkers determined the absolute oral bioavailability of 2 and 4 mg melatonin doses (tablets) to be $14.3\% \pm 7\%$ and $15.9\% \pm 6\%$, respectively, compared to IV melatonin (2 mg) [465]. Fifteen years later, a systematic review of 22 studies identified from 392 records that tested oral or IV melatonin dosages between 0.3 and 100 mg found the bioavailability of melatonin to be approximately 15% with significant variability between individuals, where critically ill patients often displayed accelerated absorption but compromised elimination [466].

4.2.2. Melatonin Bioavailability Is Inversely Correlated to 6-Sulfatoxymelatonin

As such, the interpretation of bioavailability may not be straightforward considering the fact that absolute bioavailability of oral melatonin has also been reported at ~3% (10 mg gelatin capsule) albeit with considerable variability among the 12 tested healthy male subjects (20–40 yr old) [467]. Low absolute bioavailability in oral melatonin is often the prominent effect of first-pass hepatic metabolism which produces the major melatonin metabolite 6-sulfatoxymelatonin (6-OHMS). Consequently, low endogenous production of melatonin in the elderly is associated with a significant reduction of 6-OHMS in older test subjects compared to younger ones (82–21 years old) [421]. However, a small study sample found a significant inverse correlation between oral bioavailability and 6-OHMS, where lower oral bioavailability (10%, 12%) was correlated with high plasma 6-OHMS (31%, 14%). Conversely, high bioavailability (56%, 54%) was associated with lower 6-OHMS in plasma (4%, 3%) of healthy male subjects (21 to 32 years old) tested [468].

This inverse relationship was also observed in children admitted to an intensive care unit where septic patients who did not survive exhibited nocturnal melatonin levels that were significantly higher than survivors, but total 6-OHMS excretion was dramatically lower in nonsurvivors compared to survivors. Additionally, septic shock patients had higher nocturnal melatonin levels than non-septic patients [469]. Low plasma 6-OHMS is correlated with autism [470,471], and low 6-OHMS excretion level is associated with adults who were lean at birth but obese in adult life, and high excretion rates were associated with opposite observations [472]. Similarly, patients with unstable angina exhibited significantly lower 6-OHMS than healthy controls and no negative correlation with age was observed in coronary patients as opposed to healthy subjects [473]. Therefore, the interpretation of melatonin bioavailability becomes more meaningful when 6-OHMS levels are taken into consideration.

4.2.3. Animals Show Large Variations in Melatonin Bioavailability

In animals, melatonin bioavailability via different administration routes varies greatly with strain, species, and first pass metabolism after administration. Yeleswaram and coworkers determined the absolute bioavailability of melatonin for a 10 mg/kg oral dose compared to IV in male Sprague Dawley (SD) rats to be 53.5%, but more than 100% in dogs and monkeys. However, the oral bioavailability in dogs is dose-dependent, where 1 mg/kg resulted in only 16.9% bioavailability. IP injection of melatonin at 10 mg/kg in SD rats increased bioavailability to 74.0% compared to oral at 53.5%.

In rats, IV administration at half the dose (5 mg/kg) achieved 80% bioavailability via IP at 10 mg/kg [474]. Rats, regardless of strain and administration, metabolize melatonin completely. SD rats excreted 60–70% of radiolabeled melatonin via IV injection as the major metabolite 6-OHMS [475]; and male Wistar rats administered 12.5–250 µg melatonin via IP injection also showed concentration-dependent increases in plasma of melatonin and 6-hydroxymelatonin, which always maintained a constant ratio of 1% of plasma melatonin irrespective of dosage. However, the sulfate conjugate 6-OHMS reached at maximum, ~64-fold elevation of maximum plasma 6-hydroxymelatonin levels [476].

Similar to rats, female C57BL/6 mice (age 8–10 weeks) administered varying doses of melatonin at 31.25, 62.5, 125, 250, and 500 mg/kg showed no difference in the ability to clear and eliminate melatonin; and the concentration of melatonin in the liver and gastrointestinal tracts was higher than other vital organs by 5- to 10-fold, indicating that hepatic first-pass metabolism is also prominent in mice. However, the effect of melatonin in mice is also dose-dependent even at supra-pharmacological concentrations. After exposure to lethal radiation, mice administered 500 mg/kg had the highest survival rate (55%) compared to 250 and 125 mg/kg (40%) [477].

4.2.4. Solubility and Formulation Modulate Melatonin Bioavailability

The oral bioavailability of melatonin, at any dose, can be modulated by altering solubility. The oral bioavailability of melatonin in critically ill patients with sepsis was

greatly enhanced by the use of solvents, where melatonin dissolved in glycerol achieved a 5-fold increase in relative bioavailability over melatonin in capsules at the same doses (20 or 50 mg) [478]. Similarly, when compared to IV solution (62.5 mg/kg dissolved in water), absolute oral bioavailability in mice of an aqueous melatonin suspension at 250 mg/kg administered via gavage tube was 29%, whereas 250 mg/kg melatonin dissolved in a popular co-solvent polyethylene glycol 400 (PEG400) and administered in the same manner achieved absolute bioavailability of 98.5% [477]. However, PEGs are very hydrophilic molecular crowders that can amplify entropy gain from water-release, causing dehydration that drives phase separation [136]. Hence, the use of PEG as a solvent in applications for the regulation of phase separation must be carefully weighed.

Variations in formulation also affect melatonin bioavailability. In rabbits, intranasal delivery of melatonin encapsulated in starch microspheres achieved absolute bioavailability of 84.07%, whereas intranasal administration via solution produced much lower pharmacokinetics [479]. While intranasal melatonin administration in male Wistar rats via niosomes—bilayer vesicles of nonionic surfactant-based liposomes—achieved absolute bioavailability of 98.7% compared to IV melatonin solution [480]. Therefore, the successful conversion of an animal melatonin dose into an efficacious human equivalent requires equal considerations of metabolic rate scaling, bioavailability as determined by intrinsic differences between species, administration route, as well as solubility and formulation.

4.3. *Timing Is Everything in the Dosing of Melatonin for the Regulation of Phase Separation in Dementia*

The daily supra-pharmacological dose of 266.66 mg/kg administered in drinking water to transgenic Tg2576 mice from 4 months to 15.5 months not only prevented aggregation of amyloid fibrils but also prolonged survival compared to untreated mice [361,362]. This dose can be converted into a HED using metabolic scaling to the $\frac{3}{4}$ -power, with the assumption of mice and human body weight to be 0.0225 kg and 70 kg, respectively; and oral bioavailability of mice and humans to be 63.75% and 15%, respectively. 63.75% oral bioavailability is a conservative estimation of a 50% enhancement of solubility in water achieved by first dissolving melatonin in hydroxy methyl cyclodextrin before dilution in drinking water to the final concentration of 2 mg/mL [361]. Cyclodextrins (CDs) are small carbohydrates that enhance the solubility of molecules and drugs, resulting in higher bioavailability [481,482]. The HED obtained before the bioavailability adjustment is 2499 mg. Without solubility enhancement, the adjusted bioavailability HED dose is 4831 mg. After correcting for a 50% enhancement in bioavailability (calculated based on oral bioavailability data obtained by Choudhary et al. [477]), the final HED is a staggering dose of 10,621 mg.

Even though the toxicity of melatonin as defined by LD₅₀ has not been determined in human or rodents, where early studies failed to produce death in mice at 800 mg/kg [483], and acute oral toxicity that result in LD₅₀ in rats is reported at concentrations higher than 3200 mg/kg (in one single dose [484]) according to the latest Merck safety data sheet on melatonin (Regulation (EC) No. 1907/2006, revised 17 November 2021), without a convincing rationale for a high HED in the context of phase separation in dementia, this extreme supra-pharmacological HED may seem unjustified.

4.3.1. The Rationale for Frequent Division of Melatonin Doses

The Tg2576 mice drank ~3 mL of water containing a total of 6 mg melatonin in a 24 h period. Accordingly, total HED should also be administered in divided doses of 885 mg × 12. This hypothetical HED now resembles the HED used by Martin et al. to elevate ATP production via complex I and COX (complex IV) activities in the brain and liver mitochondria of rats [348].

Male Wistar rats with a body weight between 200–230 g were administered 10 mg/kg melatonin via IP injection. Respiratory complex activity enhancements were tissue- and time-dependent. Complex I activities in the liver achieved peak levels and returned close

to baseline at ~30 and ~180 min, respectively; whereas in the brain, peak activity levels were attained at ~60 min and returned to baseline at ~180 min. COX activities in both the liver and brain became significantly elevated at ~30 min, but reached a peak in the liver at ~100 min before declining close to baseline at 180 min, whereas brain activities quickly dropped to baseline soon after 120 min [348]. In other words, in the brain, complex I and COX reached peak activity levels at 60 and 30 min, respectively, before returning to baseline at ~120 min. Whereas in the liver, complex I and COX activities were both elevated at ~30. Complex I steadily declined to close to baseline at ~180 min, but COX activities remained elevated and reached a peak at ~100 min before declining close to baseline at ~180 min.

The difference in peak and duration of respiratory enzyme activities may reflect the effect of prominent first-pass hepatic metabolism where more melatonin is retained in the liver and gastrointestinal tracts than other vital organs such as the brain [475,477]. Regardless, bioavailability via IP in rats is ~74%, or 4.933-fold higher than oral bioavailability in humans. Therefore, assuming an average body weight of 0.215 kg and 70 kg for rats and humans, respectively, the total daily HED that can effectively maintain peak complex I and COX activity at a sustained level throughout a 24 h period in order to provide adequate ATP and adenosine that can prevent and solubilize aberrant phase separation and aggregation is 9755 mg, adjusted for differences in metabolic rate and bioavailability, assuming average intake of $812.90 \text{ mg} \times 12$ in a 24 h period. However, the amount quickly doubles to 19,509.60 mg if maximum complex I and COX activities were to be sustained in the brain over a 24 h period based on observations reported by Martin et al. [348].

At this point, the estimated daily total HED of 10,621 mg obtained from Tg2576 mice taking 266.6 mg/kg in drinking water becomes quite reasonable and theoretically justifiable. In addition, *in vitro* work found a strong correlation between ATP and melatonin concentration for disaggregation of fibrils [367,388], where 1 mM of ATP and melatonin both were able to dissolve 20% of aggregates, respectively; 4 mM and 5 mM of ATP and melatonin dissolved 50% and ~60% of aggregates, respectively (Figure 3). Therefore, the rationale supporting supra-pharmacological oral melatonin doses to maintain elevated ATP synthesis that prevents aberrant phase separation and aggregation warrants further investigation.

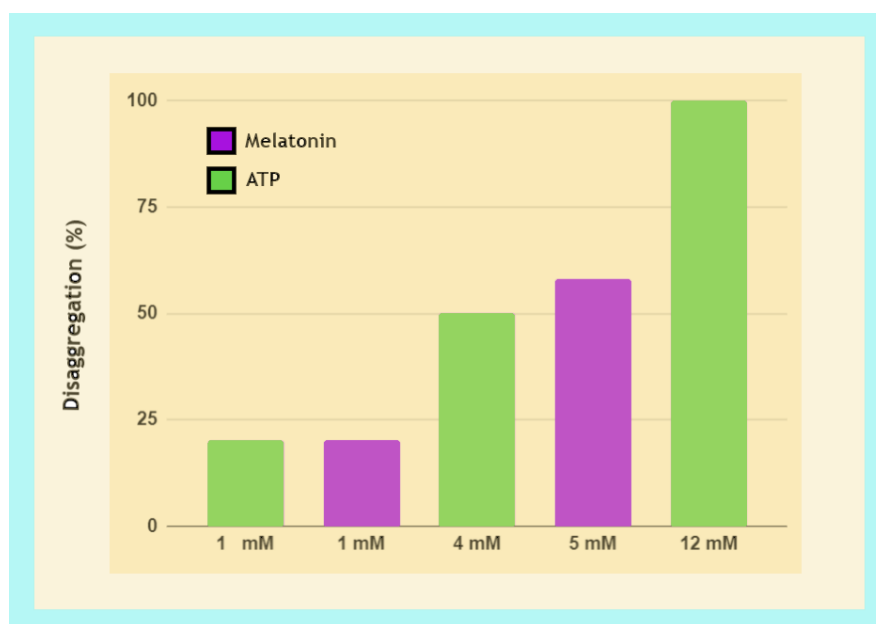


Figure 3. Comparison of disaggregation percentages obtained when different concentrations of melatonin and ATP were added to mediums containing repeat tau aggregates [367] and egg white aggregates [388], respectively.

4.3.2. The Calculation of HED Estimates Adjusted for Differences in Metabolic Rates, Bioavailability, and Formulation

A close examination and comparison of various HED estimates obtained from the different in vivo experiments discussed in Table 2 may provide clarification on melatonin doses required for the effective regulation of phase separation in dementia. Importantly, there is a difference in doses required to obtain similar results in healthy versus diseased, transgenic animal models.

Table 3 illustrates how (A) oral melatonin HED for a human weighing 70 kg is converted from animal doses by using metabolic rate scaled to $3/4$ power with body weight ($M_b^{3/4}$); (B) where HED (A) is further adjusted by interspecies bioavailability difference that takes into account both species differentials and administration routes; and (C) adjusts (A) to reflect enhancements via solubility/formulation as per study design. In the absence of data, where applicable, the average body weight of transgenic Tg2576 and wild-type mice is assumed to be 0.0225 kg and 0.025 kg, respectively. Daily food intake for mice [364] is assumed to be ~4.5 g [432]. The oral bioavailability of melatonin in humans and mice is assumed to be 15% [465,466] and 29% [477], respectively, in the conversion for values in column (B). Bioavailability enhancement via increased solubility is estimated at a conservative 50% increase based on data reported by Choudhary and coworkers [477]. Therefore, values in column (C) are obtained by multiplying (A) by 4.25.

Table 3. Calculations of three HEDs converted from animal doses using different adjustments that account for differences in (A) Metabolic rates by scaling to the $3/4$ -power; (B) Bioavailability; (C) Bioavailability that is enhanced by solubility and/or formulation.

Study Design/Total Daily Dose/Duration/Ref.	Results	(A) HED Daily Total (mg/kg) Scaled to $M_b^{3/4}$	(B) Dose (A) Adjusted by Bioavailability	(C) Dose (A) Adjusted by Enhanced Bioavailability
2 mg/mL in drinking water, Tg2576 AD mice/266.66 mg/kg/11.5 mos starting at 4 mos old/[361,362]	Striking reductions in A β aggregates at all ages during treatment; dramatic extension of survival of AD mice to levels similar to wild types.	2499 mg (35.7 mg/kg)	4831 mg (69 mg/kg)	10,621 mg (151.73 mg/kg)
0.5 mg/mL in drinking water, Tg2576 AD mice/66.66 mg/kg/11.5 mos starting at 4 mos old/[362]	Striking reductions in A β levels in brain tissues of treated mice at 8, 9.5, 11, and 15.5 months.	625 mg (8.928 mg/kg)	1208 mg (17.26 mg/kg)	2656 mg (37.94 mg/kg)
0.016 mg/mL in drinking water, Tg2576 AD mice/2.13 mg/kg/10 wks starting at age 14 mos old/[363]	Failed to reduce brain A β levels, unable to reverse oxidative damage.	19.96 mg (0.285 mg/kg)	38.58 mg (0.55 mg/kg)	84.83 mg (1.21 mg/kg)
10 mg/kg in drinking water, healthy, normal C57BL/6J mice/14 days after tauopathy initiation/[366]	Reduced memory impairment, tau hyperphosphorylation, ROS, and neuroinflammation.	96.23 mg (1.375 mg/kg)	186.0 mg (2.66 mg/kg)	408.98 mg (5.84 mg/kg)
40 ppm in food pellets, healthy, normal B6C3F1 mice/7.2 mg/kg/11 weeks different age groups/[364]	Significant reduction in A β peptides in brain cortex tissues: 57% in A β 40 and 73% in A β 42; increased melatonin levels in cerebral cortex in all 3 treated age groups (12 > 6 > 27 mos) compared to untreated.	69.29 mg (0.99 mg/kg)	133.94 mg (1.91 mg/kg)	Not applicable
10 mg/kg IP injection, C57BL/6J mice treated with A β 1-42 peptide/daily IP injections for 3 wks/[365]	Reversed A β 1-42-induced synaptic disorder, memory deficit; prevented A β 1-42-induced apoptosis, neurodegeneration, and tau phosphorylation.	98.55 mg (1.41 mg/kg)	486.15 mg (6.95 mg/kg)	Not applicable

The selection of a “perfect” HED dose for melatonin under different contexts is ultimately at the sole discretion of the investigator(s) who will determine the “parameters to

be scaled, independent variables, and the mathematical relationship used in the scaling process" [438,439]. Therefore, the values presented in Table 3 are intended purely as an informative guide to various potentially effective HEDs for melatonin that can be applied in the regulation of phase separation in dementia under distinct conditions.

5. Conclusions

Modernization of infrastructure leads to inevitable environmental changes that restrict easy access to the ancient, dynamic synergy between light, water, and melatonin. Individuals who live in densely populated urban areas are affected by the lack of adequate greenness that limits exposure to red and infrared frequencies from sunlight, generously reflected by plants [205]. Furthermore, continuous exposure to low-level microwaves and varying levels of EMF can restructure hydrogen bonding to either decrease or increase intracellular viscosity [195–199]. Even exposure to magnetic fields at 0.5 T causes water molecules to form new hydrogen bonds resulting in larger-sized water clusters that increase viscosity but reduce the proportion of free water molecules [485]. At the same time, the endogenous production of melatonin may be impacted under some circumstances by constant exposure to 60 Hz magnetic field [424] and ambient light at night [425,426]. In older adults with varying risks for dementia, increased light exposure in the evening results in earlier dim light melatonin onset (DLMO) time. This shift in the circadian phase may disturb rhythmicity that is often associated with dementia [486–488].

Our brave, new world offers unlimited potential in technological advances in every frontier imaginable but exacts an exorbitant premium on our health by creating intracellular conditions that favor aberrant phase separation resulting in pathological protein aggregations that are associated with a wide range of health challenges, including dementia. The reinstatement of this powerful but lost synergy is a provocative proposal that entails the conditional rescaling of an ancient theme to harmonize with the cacophony of modern influences, restoring, once again, balance in optimum health.

Author Contributions: D.L.: Conceptualization and manuscript preparation. R.J.R.: Critical review and editing. All authors have read and agreed to the published version of the manuscript.

Funding: This research received no external funding.

Institutional Review Board Statement: Not applicable.

Informed Consent Statement: Not applicable.

Data Availability Statement: Not applicable.

Acknowledgments: Special thanks to Daniel Matrone for technical assistance. Figure 1 was created with [BioRender.com](https://www.biorender.com).

Conflicts of Interest: The authors declare no conflict of interest.

Abbreviations

6-OHMS	6-sulfatoxymelatonin
A β	amyloid- β
AD	Alzheimer's disease
AMP	adenosine monophosphate
α -syn	alpha-synuclein
ATP	adenosine triphosphate
CP	centipoise
COX	cytochrome C oxidase
EMF	electromagnetic fields
FTD	frontotemporal dementia
FUS	fused in sarcoma
H ₂ O ₂	hydrogen peroxide
IDP	intrinsically disordered protein

IP	intraperitoneal
IV	intravenous
LCD	low-complexity domain
MD	molecular dynamics
MLO	membraneless organelle
•OH	hydroxyl radical
PD	Parkinson's disease
pI	isoelectric point
ROS	reactive oxygen species
SD	Sprague Dawley
SG	stress granule
VaD	Vascular dementia

References

1. Qiu, S.; Miller, M.I.; Joshi, P.S.; Lee, J.C.; Xue, C.; Ni, Y.; Wang, Y.; De Anda-Duran, I.; Hwang, P.H.; Cramer, J.A.; et al. Multimodal Deep Learning for Alzheimer's Disease Dementia Assessment. *Nat. Commun.* **2022**, *13*, 3404. [[CrossRef](#)]
2. Anstey, K.J.; Peters, R.; Clare, L.; Lautenschlager, N.T.; Dodge, H.H.; Barnes, D.E.; Shahr, S.; Brodaty, H.; Rees, G. Joining Forces to Prevent Dementia: The International Research Network on Dementia Prevention (IRNDP). *Int. Psychogeriatr.* **2017**, *29*, 1757–1760. [[CrossRef](#)]
3. Qiu, C.; Kivipelto, M.; von Strauss, E. Epidemiology of Alzheimer's Disease: Occurrence, Determinants, and Strategies toward Intervention. *Dialogues Clin. Neurosci.* **2009**, *11*, 111–128. [[CrossRef](#)]
4. Piscopo, P.; Crestini, A.; Carbone, E.; Rivabene, R.; Ancidoni, A.; Lo Giudice, M.; Corbo, M.; Vanacore, N.; Lacorte, E. A Systematic Review on Drugs for Synaptic Plasticity in the Treatment of Dementia. *Ageing Res. Rev.* **2022**, *81*, 101726. [[CrossRef](#)] [[PubMed](#)]
5. Velandia, P.P.; Miller-Petrie, M.K.; Chen, C.; Chakrabarti, S.; Chapin, A.; Hay, S.; Tsakalos, G.; Wimo, A.; Dieleman, J.L. Global and Regional Spending on Dementia Care from 2000–2019 and Expected Future Health Spending Scenarios from 2020–2050: An Economic Modelling Exercise. *EClinicalMedicine* **2022**, *45*, 101337. [[CrossRef](#)] [[PubMed](#)]
6. McKhann, G.M.; Knopman, D.S.; Chertkow, H.; Hyman, B.T.; Jack, C.R.; Kawas, C.H.; Klunk, W.E.; Koroshetz, W.J.; Manly, J.J.; Mayeux, R.; et al. The Diagnosis of Dementia due to Alzheimer's Disease: Recommendations from the National Institute on Aging-Alzheimer's Association Workgroups on Diagnostic Guidelines for Alzheimer's Disease. *Alzheimer's Dement.* **2011**, *7*, 263–269. [[CrossRef](#)] [[PubMed](#)]
7. Hendrie, H.C. Epidemiology of Dementia and Alzheimer's Disease. *Am. J. Geriatr. Psychiatry* **1998**, *6* (Suppl. 1), S3–S18. [[CrossRef](#)]
8. O'Brien, J.T.; Thomas, A. Vascular Dementia. *Lancet* **2015**, *386*, 1698–1706. [[CrossRef](#)]
9. Iadecola, C. The Pathobiology of Vascular Dementia. *Neuron* **2013**, *80*, 844–866. [[CrossRef](#)]
10. Walker, Z.; Possin, K.L.; Boeve, B.F.; Aarsland, D. Lewy Body Dementias. *Lancet* **2015**, *386*, 1683–1697. [[CrossRef](#)]
11. Bang, J.; Spina, S.; Miller, B.L. Frontotemporal Dementia. *Lancet* **2015**, *386*, 1672–1682. [[CrossRef](#)]
12. Bolla, L.R.; Filley, C.M.; Palmer, R.M. Dementia DDX. Office Diagnosis of the Four Major Types of Dementia. *Geriatrics* **2000**, *55*, 34–37, 41, 42, 45, 46.
13. Li, M.; Fan, Y.; Li, Q.; Wang, X.; Zhao, L.; Zhu, M. Liquid-Liquid Phase Separation Promotes Protein Aggregation and Its Implications in Ferroptosis in Parkinson's Disease Dementia. *Oxidative Med. Cell. Longev.* **2022**, *2022*, 7165387. [[CrossRef](#)]
14. Alberti, S.; Hyman, A.A. Biomolecular Condensates at the Nexus of Cellular Stress, Protein Aggregation Disease and Ageing. *Nat. Rev. Mol. Cell Biol.* **2021**, *22*, 196–213. [[CrossRef](#)]
15. Mackenzie, I.R.; Nicholson, A.M.; Sarkar, M.; Messing, J.; Purice, M.D.; Pottier, C.; Annu, K.; Baker, M.; Perkerson, R.B.; Kurti, A.; et al. TIA1 Mutations in Amyotrophic Lateral Sclerosis and Frontotemporal Dementia Promote Phase Separation and Alter Stress Granule Dynamics. *Neuron* **2017**, *95*, 808–816.e9. [[CrossRef](#)]
16. Jack, C.R., Jr.; Therneau, T.M.; Lundt, E.S.; Wiste, H.J.; Mielke, M.M.; Knopman, D.S.; Graff-Radford, J.; Lowe, V.J.; Vemuri, P.; Schwarz, C.G.; et al. Long-Term Associations between Amyloid Positron Emission Tomography, Sex, Apolipoprotein E and Incident Dementia and Mortality among Individuals without Dementia: Hazard Ratios and Absolute Risk. *Brain Commun.* **2022**, *4*, fca017. [[CrossRef](#)]
17. Gottesman, R.F.; Wu, A.; Coresh, J.; Knopman, D.S.; Jack, C.R., Jr.; Rahmim, A.; Sharrett, A.R.; Spira, A.P.; Wong, D.F.; Wagenknecht, L.E.; et al. Associations of Vascular Risk and Amyloid Burden with Subsequent Dementia. *Ann. Neurol.* **2022**, *92*, 607–619. [[CrossRef](#)]
18. Banani, S.F.; Lee, H.O.; Hyman, A.A.; Rosen, M.K. Biomolecular Condensates: Organizers of Cellular Biochemistry. *Nat. Rev. Mol. Cell Biol.* **2017**, *18*, 285–298. [[CrossRef](#)] [[PubMed](#)]
19. Yoo, H.; Bard, J.A.M.; Pilipenko, E.; Drummond, D.A. Chaperones Directly and Efficiently Disperse Stress-Triggered Biomolecular Condensates. *bioRxiv* **2021**. [[CrossRef](#)]
20. Wen, Y.; Ma, J. Phase Separation Drives the Formation of Biomolecular Condensates in the Immune System. *Front. Immunol.* **2022**, *13*, 986589. [[CrossRef](#)]
21. Ditlev, J.A.; Case, L.B.; Rosen, M.K. Who's In and Who's Out-Compositional Control of Biomolecular Condensates. *J. Mol. Biol.* **2018**, *430*, 4666–4684. [[CrossRef](#)] [[PubMed](#)]

22. Yeong, V.; Werth, E.G.; Brown, L.M.; Obermeyer, A.C. Formation of Biomolecular Condensates in Bacteria by Tuning Protein Electrostatics. *ACS Cent. Sci.* **2020**, *6*, 2301–2310. [[CrossRef](#)]
23. Sagan, S.M.; Weber, S.C. Let's Phase It: Viruses Are Master Architects of Biomolecular Condensates. *Trends Biochem. Sci.* **2022**, *48*, 229–243. [[CrossRef](#)]
24. Geiger, F.; Acker, J.; Papa, G.; Wang, X.; Arter, W.E.; Saar, K.L.; Erkamp, N.A.; Qi, R.; Bravo, J.P.; Strauss, S.; et al. Liquid-Liquid Phase Separation Underpins the Formation of Replication Factories in Rotaviruses. *EMBO J.* **2021**, *40*, e107711. [[CrossRef](#)] [[PubMed](#)]
25. Ahn, J.H.; Davis, E.S.; Daugird, T.A.; Zhao, S.; Quiroga, I.Y.; Uryu, H.; Li, J.; Storey, A.J.; Tsai, Y.-H.; Keeley, D.P.; et al. Phase Separation Drives Aberrant Chromatin Looping and Cancer Development. *Nature* **2021**, *595*, 591–595. [[CrossRef](#)] [[PubMed](#)]
26. Zbinden, A.; Pérez-Berlanga, M.; De Rossi, P.; Polymenidou, M. Phase Separation and Neurodegenerative Diseases: A Disturbance in the Force. *Dev. Cell* **2020**, *55*, 45–68. [[CrossRef](#)]
27. Elbaum-Garfinkle, S. Matter over Mind: Liquid Phase Separation and Neurodegeneration. *J. Biol. Chem.* **2019**, *294*, 7160–7168. [[CrossRef](#)] [[PubMed](#)]
28. Boeynaems, S.; Alberti, S.; Fawzi, N.L.; Mittag, T.; Polymenidou, M.; Rousseau, F.; Schymkowitz, J.; Shorter, J.; Wolozin, B.; Van Den Bosch, L.; et al. Protein Phase Separation: A New Phase in Cell Biology. *Trends Cell Biol.* **2018**, *28*, 420–435. [[CrossRef](#)]
29. Aguzzi, A.; Altmeyer, M. Phase Separation: Linking Cellular Compartmentalization to Disease. *Trends Cell Biol.* **2016**, *26*, 547–558. [[CrossRef](#)] [[PubMed](#)]
30. Rowlinson, J.S. Translation of JD van der Waals' "The Thermodynamik Theory of Capillarity under the Hypothesis of a Continuous Variation of Density". *J. Stat. Phys.* **1979**, *20*, 197–200. [[CrossRef](#)]
31. Ginzburg, V.V.; Peng, G.; Qiu, F.; Jasnow, D.; Balazs, A.C. Kinetic Model of Phase Separation in Binary Mixtures with Hard Mobile Impurities. *Phys. Rev. E* **1999**, *60 Pt B*, 4352–4359. [[CrossRef](#)]
32. Alberti, S.; Saha, S.; Woodruff, J.B.; Franzmann, T.M.; Wang, J.; Hyman, A.A. A User's Guide for Phase Separation Assays with Purified Proteins. *J. Mol. Biol.* **2018**, *430*, 4806–4820. [[CrossRef](#)] [[PubMed](#)]
33. Himeno, H.; Shimokawa, N.; Komura, S.; Andelman, D.; Hamada, T.; Takagi, M. Charge-Induced Phase Separation in Lipid Membranes. *Soft Matter* **2014**, *10*, 7959–7967. [[CrossRef](#)] [[PubMed](#)]
34. Laradji, M.; Guo, H.; Grant, M.; Zuckermann, M.J. The Effect of Surfactants on the Dynamics of Phase Separation. *J. Phys. Condens. Matter* **1992**, *4*, 6715. [[CrossRef](#)]
35. Choi, J.-M.; Holehouse, A.S.; Pappu, R.V. Physical Principles Underlying the Complex Biology of Intracellular Phase Transitions. *Annu. Rev. Biophys.* **2020**, *49*, 107–133. [[CrossRef](#)]
36. De Sancho, D. Phase Separation in Amino Acid Mixtures Is Governed by Composition. *Biophys. J.* **2022**, *121*, 4119–4127. [[CrossRef](#)]
37. Choi, J.-M.; Dar, F.; Pappu, R.V. LASSI: A Lattice Model for Simulating Phase Transitions of Multivalent Proteins. *PLoS Comput. Biol.* **2019**, *15*, e1007028. [[CrossRef](#)] [[PubMed](#)]
38. Gereben, O.; Pusztai, L. Cluster Formation and Percolation in Ethanol-Water Mixtures. *Chem. Phys.* **2017**, *496*, 1–8. [[CrossRef](#)]
39. Servis, M.J.; Wu, D.T.; Braley, J.C. Network Analysis and Percolation Transition in Hydrogen Bonded Clusters: Nitric Acid and Water Extracted by Tributyl Phosphate. *Phys. Chem. Chem. Phys.* **2017**, *19*, 11326–11339. [[CrossRef](#)]
40. Pothoczki, S.; Pethes, I.; Pusztai, L.; Temleitner, L.; Csókás, D.; Kohara, S.; Ohara, K.; Bakó, I. Hydrogen Bonding and Percolation in Propan-2-Ol—Water Liquid Mixtures: X-Ray Diffraction Experiments and Computer Simulations. *J. Mol. Liq.* **2021**, *329*, 115592. [[CrossRef](#)]
41. Alshareedah, I.; Moosa, M.M.; Banerjee, P.R. Programmable Viscoelasticity in Protein-RNA Condensates with Disordered Sticker-Spacer Polypeptides. *bioRxiv* **2021**. [[CrossRef](#)]
42. Joseph, J.A.; Reinhardt, A.; Aguirre, A.; Chew, P.Y.; Russell, K.O.; Espinosa, J.R.; Garaizar, A.; Collepardo-Guevara, R. Physics-Driven Coarse-Grained Model for Biomolecular Phase Separation with near-Quantitative Accuracy. *Nat. Comput. Sci.* **2021**, *1*, 732–743. [[CrossRef](#)] [[PubMed](#)]
43. Deniz, A.A. Percolation Physics and Density Transition Frameworks Converge in Biomolecular Condensation. *Proc. Natl. Acad. Sci. USA* **2022**, *119*, e2210177119. [[CrossRef](#)]
44. Choi, J.-M.; Hyman, A.A.; Pappu, R.V. Generalized Models for Bond Percolation Transitions of Associative Polymers. *Phys. Rev. E* **2020**, *102*, 042403. [[CrossRef](#)]
45. Jadrlich, R.; Schweizer, K.S. Percolation, Phase Separation, and Gelation in Fluids and Mixtures of Spheres and Rods. *J. Chem. Phys.* **2011**, *135*, 234902. [[CrossRef](#)] [[PubMed](#)]
46. Binder, K. Percolation Effects in the Kinetics of Phase Separation. *Solid State Commun.* **1980**, *34*, 191–194. [[CrossRef](#)]
47. Kar, M.; Dar, F.; Welsh, T.J.; Vogel, L.T.; Kühnemuth, R.; Majumdar, A.; Krainer, G.; Franzmann, T.M.; Alberti, S.; Seidel, C.A.M.; et al. Phase-Separating RNA-Binding Proteins Form Heterogeneous Distributions of Clusters in Subsaturated Solutions. *Proc. Natl. Acad. Sci. USA* **2022**, *119*, e2202222119. [[CrossRef](#)]
48. Thomsen, C.; Grundevik, P.; Elias, P.; Ståhlberg, A.; Aman, P. A Conserved N-Terminal Motif Is Required for Complex Formation between FUS, EWSR1, TAF15 and Their Oncogenic Fusion Proteins. *FASEB J.* **2013**, *27*, 4965–4974. [[CrossRef](#)]
49. Andersson, M.K.; Ståhlberg, A.; Arvidsson, Y.; Olofsson, A.; Semb, H.; Stenman, G.; Nilsson, O.; Aman, P. The Multifunctional FUS, EWS and TAF15 Proto-Oncoproteins Show Cell Type-Specific Expression Patterns and Involvement in Cell Spreading and Stress Response. *BMC Cell Biol.* **2008**, *9*, 37. [[CrossRef](#)]

50. McSwiggen, D.T.; Mir, M.; Darzacq, X.; Tjian, R. Evaluating Phase Separation in Live Cells: Diagnosis, Caveats, and Functional Consequences. *Genes Dev.* **2019**, *33*, 1619–1634. [[CrossRef](#)]
51. Takamuku, M.; Sugishita, T.; Tamaki, H.; Dong, L.; So, M.; Fujiwara, T.; Matsuki, Y. Evolution of α -Synuclein Conformation Ensemble toward Amyloid Fibril via Liquid-Liquid Phase Separation (LLPS) as Investigated by Dynamic Nuclear Polarization-Enhanced Solid-State MAS NMR. *Neurochem. Int.* **2022**, *157*, 105345. [[CrossRef](#)] [[PubMed](#)]
52. Murray, D.T.; Kato, M.; Lin, Y.; Thurber, K.R.; Hung, L.; McKnight, S.L.; Tycko, R. Structure of FUS Protein Fibrils and Its Relevance to Self-Assembly and Phase Separation of Low-Complexity Domains. *Cell* **2017**, *171*, 615–627.e16. [[CrossRef](#)]
53. Mittag, T.; Pappu, R.V. A Conceptual Framework for Understanding Phase Separation and Addressing Open Questions and Challenges. *Mol. Cell* **2022**, *82*, 2201–2214. [[CrossRef](#)] [[PubMed](#)]
54. Hardy, J.A.; Higgins, G.A. Alzheimer's Disease: The Amyloid Cascade Hypothesis. *Science* **1992**, *256*, 184–185. [[CrossRef](#)] [[PubMed](#)]
55. Selkoe, D.J.; Hardy, J. The Amyloid Hypothesis of Alzheimer's Disease at 25 Years. *EMBO Mol. Med.* **2016**, *8*, 595–608. [[CrossRef](#)]
56. Hardy, J.; Selkoe, D.J. The Amyloid Hypothesis of Alzheimer's Disease: Progress and Problems on the Road to Therapeutics. *Science* **2002**, *297*, 353–356. [[CrossRef](#)]
57. Miller, R.L.; Dhavale, D.D.; O'Shea, J.Y.; Andruska, K.M.; Liu, J.; Franklin, E.E.; Buddhala, C.; Loftin, S.K.; Cirrito, J.R.; Perrin, R.J.; et al. Quantifying Regional α -Synuclein, Amyloid β , and Tau Accumulation in Lewy Body Dementia. *Ann. Clin. Transl. Neurol.* **2022**, *9*, 106–121. [[CrossRef](#)]
58. Meade, R.M.; Fairlie, D.P.; Mason, J.M. Alpha-Synuclein Structure and Parkinson's Disease—Lessons and Emerging Principles. *Mol. Neurodegener.* **2019**, *14*, 29. [[CrossRef](#)] [[PubMed](#)]
59. Benson, M.D.; Buxbaum, J.N.; Eisenberg, D.S.; Merlini, G.; Saraiva, M.J.M.; Sekijima, Y.; Sipe, J.D.; Westermarck, P. Amyloid Nomenclature 2018: Recommendations by the International Society of Amyloidosis (ISA) Nomenclature Committee. *Amyloid* **2018**, *25*, 215–219. [[CrossRef](#)]
60. Benson, M.D.; Buxbaum, J.N.; Eisenberg, D.S.; Merlini, G.; Saraiva, M.J.M.; Sekijima, Y.; Sipe, J.D.; Westermarck, P. Amyloid Nomenclature 2020: Update and Recommendations by the International Society of Amyloidosis (ISA) Nomenclature Committee. *Amyloid* **2020**, *27*, 217–222. [[CrossRef](#)]
61. Maji, S.K.; Wang, L.; Greenwald, J.; Riek, R. Structure-Activity Relationship of Amyloid Fibrils. *FEBS Lett.* **2009**, *583*, 2610–2617. [[CrossRef](#)]
62. Nelson, R.; Eisenberg, D. Recent Atomic Models of Amyloid Fibril Structure. *Curr. Opin. Struct. Biol.* **2006**, *16*, 260–265. [[CrossRef](#)]
63. Glabe, C.C. Amyloid Accumulation and Pathogenesis of Alzheimer's Disease: Significance of Monomeric, Oligomeric and Fibrillar A β . In *Alzheimer's Disease: Cellular and Molecular Aspects of Amyloid β* ; Harris, J.R., Fahrenholz, F., Eds.; Springer: Boston, MA, USA, 2005; pp. 167–177. [[CrossRef](#)]
64. Roeters, S.J.; Iyer, A.; Pletikapić, G.; Kogan, V.; Subramaniam, V.; Woutersen, S. Evidence for Intramolecular Antiparallel Beta-Sheet Structure in Alpha-Synuclein Fibrils from a Combination of Two-Dimensional Infrared Spectroscopy and Atomic Force Microscopy. *Sci. Rep.* **2017**, *7*, 41051. [[CrossRef](#)] [[PubMed](#)]
65. Park, S.-B.; Yoon, J.-S.; Jang, S.-M.; Lee, K.-H.; Shin, S.-M. Computational Study on Oligomer Formation of Fibril-Forming Peptide of α -Synuclein. *Bull. Korean Chem. Soc.* **2012**, *33*, 848–854. [[CrossRef](#)]
66. Serpell, L.C.; Berriman, J.; Jakes, R.; Goedert, M.; Crowther, R.A. Fiber Diffraction of Synthetic α -Synuclein Filaments Shows Amyloid-like Cross- β Conformation. *Proc. Natl. Acad. Sci. USA* **2000**, *97*, 4897–4902. [[CrossRef](#)]
67. Passarella, D.; Goedert, M. Beta-Sheet Assembly of Tau and Neurodegeneration in *Drosophila Melanogaster*. *Neurobiol. Aging* **2018**, *72*, 98–105. [[CrossRef](#)] [[PubMed](#)]
68. Daebel, V.; Chinnathambi, S.; Biernat, J.; Schwalbe, M.; Habenstein, B.; Loquet, A.; Akoury, E.; Tepper, K.; Müller, H.; Baldus, M.; et al. β -Sheet Core of Tau Paired Helical Filaments Revealed by Solid-State NMR. *J. Am. Chem. Soc.* **2012**, *134*, 13982–13989. [[CrossRef](#)]
69. von Bergen, M.; Barghorn, S.; Biernat, J.; Mandelkow, E.-M.; Mandelkow, E. Tau Aggregation Is Driven by a Transition from Random Coil to Beta Sheet Structure. *Biochim. Biophys. Acta* **2005**, *1739*, 158–166. [[CrossRef](#)] [[PubMed](#)]
70. Spillantini, M.G.; Divane, A.; Goedert, M. Assignment of Human Alpha-Synuclein (SNCA) and Beta-Synuclein (SNCB) Genes to Chromosomes 4q21 and 5q35. *Genomics* **1995**, *27*, 379–381. [[CrossRef](#)] [[PubMed](#)]
71. Jakes, R.; Spillantini, M.G.; Goedert, M. Identification of Two Distinct Synucleins from Human Brain. *FEBS Lett.* **1994**, *345*, 27–32. [[CrossRef](#)]
72. Coelho-Cerqueira, E.; Carmo-Gonçalves, P.; Pinheiro, A.S.; Cortines, J.; Follmer, C. α -Synuclein as an Intrinsically Disordered Monomer—Fact or Artefact? *FEBS J.* **2013**, *280*, 4915–4927. [[CrossRef](#)]
73. Hoppe, S.O.; Uzunoğlu, G.; Nussbaum-Krammer, C. α -Synuclein Strains: Does Amyloid Conformation Explain the Heterogeneity of Synucleinopathies? *Biomolecules* **2021**, *11*, 931. [[CrossRef](#)]
74. Winner, B.; Jappelli, R.; Maji, S.K.; Desplats, P.A.; Boyer, L.; Aigner, S.; Hetzer, C.; Loher, T.; Vilar, M.; Campioni, S.; et al. In Vivo Demonstration That α -Synuclein Oligomers Are Toxic. *Proc. Natl. Acad. Sci. USA* **2011**, *108*, 4194–4199. [[CrossRef](#)]
75. Poudyal, M.; Sakunthala, A.; Mukherjee, S.; Gadhe, L.; Maji, S.K. Phase Separation and Other Forms of α -Synuclein Self-Assemblies. *Essays Biochem.* **2022**, *66*, 987–1000. [[CrossRef](#)] [[PubMed](#)]

76. Mukherjee, S.; Sakunthala, A.; Gadhe, L.; Poudyal, M.; Sawner, A.S.; Kadu, P.; Maji, S.K. Liquid-Liquid Phase Separation of α -Synuclein: A New Mechanistic Insight for α -Synuclein Aggregation Associated with Parkinson's Disease Pathogenesis. *J. Mol. Biol.* **2022**, *435*, 167713. [[CrossRef](#)] [[PubMed](#)]
77. Huang, S.; Mo, X.; Wang, J.; Ye, X.; Yu, H.; Liu, Y. α -Synuclein Phase Separation and Amyloid Aggregation Are Modulated by C-Terminal Truncations. *FEBS Lett.* **2022**, *596*, 1388–1400. [[CrossRef](#)]
78. Hardenberg, M.C.; Sinnige, T.; Casford, S.; Dada, S.T.; Poudel, C.; Robinson, E.A.; Fuxreiter, M.; Kaminski, C.F.; Kaminski Schierle, G.S.; Nollen, E.A.A.; et al. Observation of an α -Synuclein Liquid Droplet State and Its Maturation into Lewy Body-like Assemblies. *J. Mol. Cell Biol.* **2021**, *13*, 282–294. [[CrossRef](#)] [[PubMed](#)]
79. Ray, S.; Singh, N.; Kumar, R.; Patel, K.; Pandey, S.; Datta, D.; Mahato, J.; Panigrahi, R.; Navalkar, A.; Mehra, S.; et al. α -Synuclein Aggregation Nucleates through Liquid-Liquid Phase Separation. *Nat. Chem.* **2020**, *12*, 705–716. [[CrossRef](#)]
80. Ray, S.; Singh, N.; Patel, K.; Krishnamoorthy, G.; Maji, S.K. FRAP and FRET Investigation of α -Synuclein Fibrillization via Liquid-Liquid Phase Separation In Vitro and in HeLa Cells. In *Protein Aggregation: Methods and Protocols*; Cieplak, A.S., Ed.; Springer: New York, NY, USA, 2023; pp. 395–423. [[CrossRef](#)]
81. Xu, B.; Mo, X.; Chen, J.; Yu, H.; Liu, Y. Myricetin Inhibits α -Synuclein Amyloid Aggregation by Delaying the Liquid-to-Solid Phase Transition. *Chembiochem* **2022**, *23*, e202200216. [[CrossRef](#)]
82. Davies, H.A.; Rigden, D.J.; Phelan, M.M.; Madine, J. Probing Medin Monomer Structure and Its Amyloid Nucleation Using ^{13}C -Direct Detection NMR in Combination with Structural Bioinformatics. *Sci. Rep.* **2017**, *7*, 45224. [[CrossRef](#)]
83. Larsson, A.; Söderberg, L.; Westermark, G.T.; Sletten, K.; Engström, U.; Tjernberg, L.O.; Näslund, J.; Westermark, P. Unwinding Fibril Formation of Medin, the Peptide of the Most Common Form of Human Amyloid. *Biochem. Biophys. Res. Commun.* **2007**, *361*, 822–828. [[CrossRef](#)]
84. Peng, S.; Glennert, J.; Westermark, P. Medin-Amyloid: A Recently Characterized Age-Associated Arterial Amyloid Form Affects Mainly Arteries in the Upper Part of the Body. *Amyloid* **2005**, *12*, 96–102. [[CrossRef](#)]
85. Marazuela, P.; Solé, M.; Bonaterra-Pastra, A.; Pizarro, J.; Camacho, J.; Martínez-Sáez, E.; Kuiperij, H.B.; Verbeek, M.M.; de Kort, A.M.; Schreuder, F.H.B.M.; et al. MFG-E8 (LACTADHERIN): A Novel Marker Associated with Cerebral Amyloid Angiopathy. *Acta Neuropathol. Commun.* **2021**, *9*, 154. [[CrossRef](#)]
86. Larsson, A.; Malmström, S.; Westermark, P. Signs of Cross-Seeding: Aortic Medin Amyloid as a Trigger for Protein AA Deposition. *Amyloid* **2011**, *18*, 229–234. [[CrossRef](#)] [[PubMed](#)]
87. Larsson, A.; Peng, S.; Persson, H.; Rosenbloom, J.; Abrams, W.R.; Wassberg, E.; Thelin, S.; Sletten, K.; Gerwins, P.; Westermark, P. Lactadherin Binds to Elastin—A Starting Point for Medin Amyloid Formation? *Amyloid* **2006**, *13*, 78–85. [[CrossRef](#)] [[PubMed](#)]
88. Wagner, J.; Degenhardt, K.; Veit, M.; Louros, N.; Konstantoulea, K.; Skodras, A.; Wild, K.; Liu, P.; Obermüller, U.; Bansal, V.; et al. Medin Co-Aggregates with Vascular Amyloid- β in Alzheimer's Disease. *Nature* **2022**, *612*, 123–131. [[CrossRef](#)]
89. Degenhardt, K.; Wagner, J.; Skodras, A.; Candlish, M.; Koppelman, A.J.; Wild, K.; Maxwell, R.; Rotermund, C.; von Zweydford, F.; Gloeckner, C.J.; et al. Medin Aggregation Causes Cerebrovascular Dysfunction in Aging Wild-Type Mice. *Proc. Natl. Acad. Sci. USA* **2020**, *117*, 23925–23931. [[CrossRef](#)] [[PubMed](#)]
90. Karamanova, N.; Truran, S.; Serrano, G.E.; Beach, T.G.; Madine, J.; Weissig, V.; Davies, H.A.; Veldhuizen, J.; Nikkhah, M.; Hansen, M.; et al. Endothelial Immune Activation by Medin: Potential Role in Cerebrovascular Disease and Reversal by Monosialoganglioside-Containing Nanoliposomes. *J. Am. Heart Assoc.* **2020**, *9*, e014810. [[CrossRef](#)] [[PubMed](#)]
91. Migrino, R.Q.; Karamanova, N.; Truran, S.; Serrano, G.E.; Davies, H.A.; Madine, J.; Beach, T.G. Cerebrovascular Medin Is Associated with Alzheimer's Disease and Vascular Dementia. *Alzheimer's Dement.* **2020**, *12*, e12072. [[CrossRef](#)]
92. Sabha, B.H.; Alzahrani, F.; Almehdar, H.A.; Uversky, V.N.; Redwan, E.M. Disorder in Milk Proteins: Lactadherin Multifunctionality and Structure. *Curr. Protein Pept. Sci.* **2018**, *19*, 983–997. [[CrossRef](#)]
93. Fens, M.H.A.M.; Mastrobattista, E.; de Graaff, A.M.; Flesch, F.M.; Ultee, A.; Rasmussen, J.T.; Molema, G.; Storm, G.; Schiffelers, R.M. Angiogenic Endothelium Shows Lactadherin-Dependent Phagocytosis of Aged Erythrocytes and Apoptotic Cells. *Blood* **2008**, *111*, 4542–4550. [[CrossRef](#)]
94. Silvestre, J.-S.; Théry, C.; Hamard, G.; Boddaert, J.; Aguilar, B.; Delcayre, A.; Houbbron, C.; Tamarat, R.; Blanc-Brude, O.; Heeneman, S.; et al. Lactadherin Promotes VEGF-Dependent Neovascularization. *Nat. Med.* **2005**, *11*, 499–506. [[CrossRef](#)]
95. Bu, H.-F.; Zuo, X.-L.; Wang, X.; Ensslin, M.A.; Koti, V.; Hsueh, W.; Raymond, A.S.; Shur, B.D.; Tan, X.-D. Milk Fat Globule-EGF Factor 8/lactadherin Plays a Crucial Role in Maintenance and Repair of Murine Intestinal Epithelium. *J. Clin. Investig.* **2007**, *117*, 3673–3683. [[CrossRef](#)]
96. Younger, S.; Jang, H.; Davies, H.A.; Niemiec, M.J.; Garcia, J.G.N.; Nussinov, R.; Migrino, R.Q.; Madine, J.; Arce, F.T. Medin Oligomer Membrane Pore Formation: A Potential Mechanism of Vascular Dysfunction. *Biophys. J.* **2020**, *118*, 2769–2782. [[CrossRef](#)] [[PubMed](#)]
97. Migrino, R.Q.; Davies, H.A.; Truran, S.; Karamanova, N.; Franco, D.A.; Beach, T.G.; Serrano, G.E.; Truong, D.; Nikkhah, M.; Madine, J. Amyloidogenic Medin Induces Endothelial Dysfunction and Vascular Inflammation through the Receptor for Advanced Glycation Endproducts. *Cardiovasc. Res.* **2017**, *113*, 1389–1402. [[CrossRef](#)]
98. Arispe, N.; Rojas, E.; Pollard, H.B. Alzheimer Disease Amyloid Beta Protein Forms Calcium Channels in Bilayer Membranes: Blockade by Tromethamine and Aluminum. *Proc. Natl. Acad. Sci. USA* **1993**, *90*, 567–571. [[CrossRef](#)] [[PubMed](#)]
99. Arispe, N.; Pollard, H.B.; Rojas, E. Zn^{2+} Interaction with Alzheimer Amyloid Beta Protein Calcium Channels. *Proc. Natl. Acad. Sci. USA* **1996**, *93*, 1710–1715. [[CrossRef](#)] [[PubMed](#)]

100. Konstantoulea, K.; Louros, N.; Rousseau, F.; Schymkowitz, J. Heterotypic Interactions in Amyloid Function and Disease. *FEBS J.* **2022**, *289*, 2025–2046. [[CrossRef](#)]
101. Nag, N.; Tripathi, T. Cross-Seeding with Homologous Sequences Alters Amyloid Aggregation Kinetics and Fibril Structure. *ACS Chem. Neurosci.* **2022**, *13*, 537–539. [[CrossRef](#)]
102. Mathieu, C.; Pappu, R.V.; Taylor, J.P. Beyond Aggregation: Pathological Phase Transitions in Neurodegenerative Disease. *Science* **2020**, *370*, 56–60. [[CrossRef](#)]
103. St George-Hyslop, P.; Lin, J.Q.; Miyashita, A.; Phillips, E.C.; Qamar, S.; Randle, S.J.; Wang, G. The Physiological and Pathological Biophysics of Phase Separation and Gelation of RNA Binding Proteins in Amyotrophic Lateral Sclerosis and Fronto-Temporal Lobar Degeneration. *Brain Res.* **2018**, *1693 Pt A*, 11–23. [[CrossRef](#)]
104. Vanderweyde, T.; Apicco, D.J.; Youmans-Kidder, K.; Ash, P.E.A.; Cook, C.; da Rocha, E.L.; Jansen-West, K.; Frame, A.A.; Citro, A.; Leszyk, J.D.; et al. Interaction of Tau with the RNA-Binding Protein TIA1 Regulates Tau Pathophysiology and Toxicity. *Cell Rep.* **2016**, *15*, 1455–1466. [[CrossRef](#)]
105. Gui, X.; Luo, F.; Li, Y.; Zhou, H.; Qin, Z.; Liu, Z.; Gu, J.; Xie, M.; Zhao, K.; Dai, B.; et al. Structural Basis for Reversible Amyloids of hnRNPA1 Elucidates Their Role in Stress Granule Assembly. *Nat. Commun.* **2019**, *10*, 2006. [[CrossRef](#)]
106. Ayyadevara, S.; Balasubramaniam, M.; Parcon, P.A.; Barger, S.W.; Griffin, W.S.T.; Alla, R.; Tackett, A.J.; Mackintosh, S.G.; Petricoin, E.; Zhou, W.; et al. Proteins That Mediate Protein Aggregation and Cytotoxicity Distinguish Alzheimer’s Hippocampus from Normal Controls. *Aging Cell* **2016**, *15*, 924–939. [[CrossRef](#)] [[PubMed](#)]
107. Brunello, C.A.; Yan, X.; Huttunen, H.J. Internalized Tau Sensitizes Cells to Stress by Promoting Formation and Stability of Stress Granules. *Sci. Rep.* **2016**, *6*, 30498. [[CrossRef](#)] [[PubMed](#)]
108. Maziuk, B.; Ballance, H.I.; Wolozin, B. Dysregulation of RNA Binding Protein Aggregation in Neurodegenerative Disorders. *Front. Mol. Neurosci.* **2017**, *10*, 89. [[CrossRef](#)]
109. Bishof, I.; Dammer, E.B.; Duong, D.M.; Kunding, S.R.; Gearing, M.; Lah, J.J.; Levey, A.I.; Seyfried, N.T. RNA-Binding Proteins with Basic-Acidic Dipeptide (BAD) Domains Self-Assemble and Aggregate in Alzheimer’s Disease. *J. Biol. Chem.* **2018**, *293*, 11047–11066. [[CrossRef](#)]
110. Kapeli, K.; Martinez, F.J.; Yeo, G.W. Genetic Mutations in RNA-Binding Proteins and Their Roles in ALS. *Hum. Genet.* **2017**, *136*, 1193–1214. [[CrossRef](#)]
111. Cookson, M.R. RNA-Binding Proteins Implicated in Neurodegenerative Diseases. *Wiley Interdiscip. Rev. RNA* **2017**, *8*, e1397. [[CrossRef](#)] [[PubMed](#)]
112. Cascarina, S.M.; Elder, M.R.; Ross, E.D. Atypical Structural Tendencies among Low-Complexity Domains in the Protein Data Bank Proteome. *PLoS Comput. Biol.* **2020**, *16*, e1007487. [[CrossRef](#)]
113. Posey, A.E.; Holehouse, A.S.; Pappu, R.V. Phase Separation of Intrinsically Disordered Proteins. *Methods Enzymol.* **2018**, *611*, 1–30. [[CrossRef](#)] [[PubMed](#)]
114. Uversky, V.N. Intrinsically Disordered Proteins in Overcrowded Milieu: Membrane-Less Organelles, Phase Separation, and Intrinsic Disorder. *Curr. Opin. Struct. Biol.* **2017**, *44*, 18–30. [[CrossRef](#)] [[PubMed](#)]
115. Hyman, A.A.; Weber, C.A.; Jülicher, F. Liquid-Liquid Phase Separation in Biology. *Annu. Rev. Cell Dev. Biol.* **2014**, *30*, 39–58. [[CrossRef](#)]
116. Kragelj, J.; Orand, T.; Delaforge, E.; Tengo, L.; Blackledge, M.; Palencia, A.; Jensen, M.R. Enthalpy-Entropy Compensation in the Promiscuous Interaction of an Intrinsically Disordered Protein with Homologous Protein Partners. *Biomolecules* **2021**, *11*, 1204. [[CrossRef](#)] [[PubMed](#)]
117. Arbesú, M.; Iruela, G.; Fuentes, H.; Teixeira, J.M.C.; Pons, M. Intramolecular Fuzzy Interactions Involving Intrinsically Disordered Domains. *Front. Mol. Biosci.* **2018**, *5*, 39. [[CrossRef](#)] [[PubMed](#)]
118. Flock, T.; Weatheritt, R.J.; Latysheva, N.S.; Babu, M.M. Controlling Entropy to Tune the Functions of Intrinsically Disordered Regions. *Curr. Opin. Struct. Biol.* **2014**, *26*, 62–72. [[CrossRef](#)]
119. Workman, R.J.; Drake, J.A.; Pettitt, B.M. Chapter 4—Thermodynamic Perspective of Protein Disorder and Phase Separation: Model Systems. In *Structure and Intrinsic Disorder in Enzymology*; Gupta, M.N., Uversky, V.N., Eds.; Academic Press: Cambridge, MA, USA, 2023; pp. 97–126. [[CrossRef](#)]
120. Flory, P.J. Thermodynamics of High Polymer Solutions. *J. Chem. Phys.* **1942**, *10*, 51–61. [[CrossRef](#)]
121. Huggins, M.L. Some Properties of Solutions of Long-Chain Compounds. *J. Phys. Chem.* **1942**, *46*, 151–158. [[CrossRef](#)]
122. Dignon, G.L.; Best, R.B.; Mittal, J. Biomolecular Phase Separation: From Molecular Driving Forces to Macroscopic Properties. *Annu. Rev. Phys. Chem.* **2020**, *71*, 53–75. [[CrossRef](#)]
123. Qian, H.; Hopfield, J.J. Entropy-enthalpy Compensation: Perturbation and Relaxation in Thermodynamic Systems. *J. Chem. Phys.* **1996**, *105*, 9292–9298. [[CrossRef](#)]
124. Jacobson, K.; Papahadjopoulos, D. Phase Transitions and Phase Separations in Phospholipid Membranes Induced by Changes in Temperature, pH, and Concentration of Bivalent Cations. *Biochemistry* **1975**, *14*, 152–161. [[CrossRef](#)] [[PubMed](#)]
125. Nott, T.J.; Petsalaki, E.; Farber, P.; Jervis, D.; Fussner, E.; Plochowitz, A.; Craggs, T.D.; Bazett-Jones, D.P.; Pawson, T.; Forman-Kay, J.D.; et al. Phase Transition of a Disordered Nuage Protein Generates Environmentally Responsive Membraneless Organelles. *Mol. Cell* **2015**, *57*, 936–947. [[CrossRef](#)]
126. Molliex, A.; Temirov, J.; Lee, J.; Coughlin, M.; Kanagaraj, A.P.; Kim, H.J.; Mittag, T.; Taylor, J.P. Phase Separation by Low Complexity Domains Promotes Stress Granule Assembly and Drives Pathological Fibrillization. *Cell* **2015**, *163*, 123–133. [[CrossRef](#)] [[PubMed](#)]

127. Riback, J.A.; Katanski, C.D.; Kear-Scott, J.L.; Pilipenko, E.V.; Rojek, A.E.; Sosnick, T.R.; Drummond, D.A. Stress-Triggered Phase Separation Is an Adaptive, Evolutionarily Tuned Response. *Cell* **2017**, *168*, 1028–1040.e19. [[CrossRef](#)] [[PubMed](#)]
128. Cinar, H.; Fetahaj, Z.; Cinar, S.; Vernon, R.M.; Chan, H.S.; Winter, R.H.A. Temperature, Hydrostatic Pressure, and Osmolyte Effects on Liquid-Liquid Phase Separation in Protein Condensates: Physical Chemistry and Biological Implications. *Chemistry* **2019**, *25*, 13049–13069. [[CrossRef](#)]
129. Protter, D.S.W.; Parker, R. Principles and Properties of Stress Granules. *Trends Cell Biol.* **2016**, *26*, 668–679. [[CrossRef](#)] [[PubMed](#)]
130. Tamaki, M.; Kojima, C. pH-Switchable LCST/UCST-Type Thermosensitive Behaviors of Phenylalanine-Modified Zwitterionic Dendrimers. *RSC Adv.* **2020**, *10*, 10452–10460. [[CrossRef](#)]
131. Zhang, H.; Zhang, J.; Dai, W.; Zhao, Y. Facile Synthesis of Thermo-, pH-, CO₂- and Oxidation-Responsive Poly(amido Thioether)s with Tunable LCST and UCST Behaviors. *Polym. Chem.* **2017**, *8*, 5749–5760. [[CrossRef](#)]
132. Jin, X.; Zhou, M.; Chen, S.; Li, D.; Cao, X.; Liu, B. Effects of pH Alterations on Stress- and Aging-Induced Protein Phase Separation. *Cell. Mol. Life Sci.* **2022**, *79*, 380. [[CrossRef](#)]
133. Orij, R.; Brul, S.; Smits, G.J. Intracellular pH Is a Tightly Controlled Signal in Yeast. *Biochim. Biophys. Acta* **2011**, *1810*, 933–944. [[CrossRef](#)]
134. Kroschwald, S.; Munder, M.C.; Maharana, S.; Franzmann, T.M.; Richter, D.; Ruer, M.; Hyman, A.A.; Alberti, S. Different Material States of Pub1 Condensates Define Distinct Modes of Stress Adaptation and Recovery. *Cell Rep.* **2018**, *23*, 3327–3339. [[CrossRef](#)] [[PubMed](#)]
135. Lin, Y.; Fichou, Y.; Longhini, A.P.; Llanes, L.C.; Yin, P.; Bazan, G.C.; Kosik, K.S.; Han, S. Liquid-Liquid Phase Separation of Tau Driven by Hydrophobic Interaction Facilitates Fibrillization of Tau. *J. Mol. Biol.* **2021**, *433*, 166731. [[CrossRef](#)] [[PubMed](#)]
136. Park, S.; Barnes, R.; Lin, Y.; Jeon, B.-J.; Najafi, S.; Delaney, K.T.; Fredrickson, G.H.; Shea, J.-E.; Hwang, D.S.; Han, S. Dehydration Entropy Drives Liquid-Liquid Phase Separation by Molecular Crowding. *Commun. Chem.* **2020**, *3*, 83. [[CrossRef](#)]
137. Elbaum-Garfinkle, S.; Kim, Y.; Szczepaniak, K.; Chen, C.C.-H.; Eckmann, C.R.; Myong, S.; Brangwynne, C.P. The Disordered P Granule Protein LAF-1 Drives Phase Separation into Droplets with Tunable Viscosity and Dynamics. *Proc. Natl. Acad. Sci. USA* **2015**, *112*, 7189–7194. [[CrossRef](#)] [[PubMed](#)]
138. Salis, A.; Ninham, B.W. Models and Mechanisms of Hofmeister Effects in Electrolyte Solutions, and Colloid and Protein Systems Revisited. *Chem. Soc. Rev.* **2014**, *43*, 7358–7377. [[CrossRef](#)]
139. Kalra, A.; Tugcu, N.; Cramer, S.M.; Garde, S. Salting-in and Salting-out of Hydrophobic Solutes in Aqueous Salt Solutions. *J. Phys. Chem. B* **2001**, *105*, 6380–6386. [[CrossRef](#)]
140. Melander, W.; Horváth, C. Salt Effect on Hydrophobic Interactions in Precipitation and Chromatography of Proteins: An Interpretation of the Lyotropic Series. *Arch. Biochem. Biophys.* **1977**, *183*, 200–215. [[CrossRef](#)]
141. Collins, K.D.; Washabaugh, M.W. The Hofmeister Effect and the Behaviour of Water at Interfaces. *Q. Rev. Biophys.* **1985**, *18*, 323–422. [[CrossRef](#)]
142. Friberg, S.E.; Chiu, M. Hydrotropes. *J. Dispers. Sci. Technol.* **1988**, *9*, 443–457. [[CrossRef](#)]
143. Schwierz, N.; Horinek, D.; Netz, R.R. Anionic and Cationic Hofmeister Effects on Hydrophobic and Hydrophilic Surfaces. *Langmuir* **2013**, *29*, 2602–2614. [[CrossRef](#)]
144. Furukawa, K.; Aguirre, C.; So, M.; Sasahara, K.; Miyanoiri, Y.; Sakurai, K.; Yamaguchi, K.; Ikenaka, K.; Mochizuki, H.; Kardos, J.; et al. Isoelectric Point-Amyloid Formation of α -Synuclein Extends the Generality of the Solubility and Supersaturation-Limited Mechanism. *Curr. Res. Struct. Biol.* **2020**, *2*, 35–44. [[CrossRef](#)]
145. Vugmeyster, L.; Clark, M.A.; Falconer, I.B.; Ostrovsky, D.; Gantz, D.; Qiang, W.; Hoatson, G.L. Flexibility and Solvation of Amyloid- β Hydrophobic Core. *J. Biol. Chem.* **2016**, *291*, 18484–18495. [[CrossRef](#)] [[PubMed](#)]
146. Kawai, R.; Chiba, S.; Okuwaki, K.; Kanada, R.; Doi, H.; Ono, M.; Mochizuki, Y.; Okuno, Y. Stabilization Mechanism for a Nonfibrillar Amyloid β Oligomer Based on Formation of a Hydrophobic Core Determined by Dissipative Particle Dynamics. *ACS Chem. Neurosci.* **2020**, *11*, 385–394. [[CrossRef](#)] [[PubMed](#)]
147. Majumdar, A.; Das, D.; Madhu, P.; Avni, A.; Mukhopadhyay, S. Excitation Energy Migration Unveils Fuzzy Interfaces within the Amyloid Architecture. *Biophys. J.* **2020**, *118*, 2621–2626. [[CrossRef](#)]
148. Fernández, A. Time-Resolved Backbone Desolvation and Mutational Hot Spots in Folding Proteins. *Proteins* **2002**, *47*, 447–457. [[CrossRef](#)]
149. Nakagawa, H.; Tamada, T. Hydration and Its Hydrogen Bonding State on a Protein Surface in the Crystalline State as Revealed by Molecular Dynamics Simulation. *Front. Chem.* **2021**, *9*, 738077. [[CrossRef](#)]
150. Bellissent-Funel, M.-C.; Hassanali, A.; Havenith, M.; Henchman, R.; Pohl, P.; Sterpone, F.; van der Spoel, D.; Xu, Y.; Garcia, A.E. Water Determines the Structure and Dynamics of Proteins. *Chem. Rev.* **2016**, *116*, 7673–7697. [[CrossRef](#)] [[PubMed](#)]
151. Levy, Y.; Onuchic, J.N. Water Mediation in Protein Folding and Molecular Recognition. *Annu. Rev. Biophys. Biomol. Struct.* **2006**, *35*, 389–415. [[CrossRef](#)]
152. Chaplin, M. Do We Underestimate the Importance of Water in Cell Biology? *Nat. Rev. Mol. Cell Biol.* **2006**, *7*, 861–866. [[CrossRef](#)]
153. Lum, K.; Chandler, D.; Weeks, J.D. Hydrophobicity at Small and Large Length Scales. *J. Phys. Chem. B* **1999**, *103*, 4570–4577. [[CrossRef](#)]
154. Ahlers, J.; Adams, E.M.; Bader, V.; Pezzotti, S.; Winklhofer, K.F.; Tatzelt, J.; Havenith, M. The Key Role of Solvent in Condensation: Mapping Water in Liquid-Liquid Phase-Separated FUS. *Biophys. J.* **2021**, *120*, 1266–1275. [[CrossRef](#)]

155. Conti Nibali, V.; Pezzotti, S.; Sebastiani, F.; Galimberti, D.R.; Schwaab, G.; Heyden, M.; Gaigeot, M.-P.; Havenith, M. Wrapping Up Hydrophobic Hydration: Locality Matters. *J. Phys. Chem. Lett.* **2020**, *11*, 4809–4816. [[CrossRef](#)]
156. Laage, D.; Elsaesser, T.; Hynes, J.T. Water Dynamics in the Hydration Shells of Biomolecules. *Chem. Rev.* **2017**, *117*, 10694–10725. [[CrossRef](#)] [[PubMed](#)]
157. Fogarty, A.C.; Laage, D. Water Dynamics in Protein Hydration Shells: The Molecular Origins of the Dynamical Perturbation. *J. Phys. Chem. B* **2014**, *118*, 7715–7729. [[CrossRef](#)] [[PubMed](#)]
158. Liu, Z.; Chan, H.S. Desolvation Is a Likely Origin of Robust Enthalpic Barriers to Protein Folding. *J. Mol. Biol.* **2005**, *349*, 872–889. [[CrossRef](#)]
159. Camino, J.D.; Gracia, P.; Cremades, N. The Role of Water in the Primary Nucleation of Protein Amyloid Aggregation. *Biophys. Chem.* **2021**, *269*, 106520. [[CrossRef](#)] [[PubMed](#)]
160. Castellano, B.M.; Eggers, D.K. Experimental Support for a Desolvation Energy Term in Governing Equations for Binding Equilibria. *J. Phys. Chem. B* **2013**, *117*, 8180–8188. [[CrossRef](#)]
161. Kauzmann, W. Some Factors in the Interpretation of Protein Denaturation. *Adv. Protein Chem.* **1959**, *14*, 1–63. [[CrossRef](#)]
162. Blokzijl, W.; Engberts, J.B.F.N. Hydrophobic Effects. Opinions and Facts. *Angew. Chem. Int. Ed. Engl.* **1993**, *32*, 1545–1579. [[CrossRef](#)]
163. Muller, N. Search for a Realistic View of Hydrophobic Effects. *Acc. Chem. Res.* **1990**, *23*, 23–28. [[CrossRef](#)]
164. Hamaker, H.C. The London—Van Der Waals Attraction between Spherical Particles. *Physica* **1937**, *4*, 1058–1072. [[CrossRef](#)]
165. Davis, J.G.; Gierszal, K.P.; Wang, P.; Ben-Amotz, D. Water Structural Transformation at Molecular Hydrophobic Interfaces. *Nature* **2012**, *491*, 582–585. [[CrossRef](#)] [[PubMed](#)]
166. Baldwin, R.L. Dynamic Hydration Shell Restores Kauzmann’s 1959 Explanation of How the Hydrophobic Factor Drives Protein Folding. *Proc. Natl. Acad. Sci. USA* **2014**, *111*, 13052–13056. [[CrossRef](#)]
167. Li, J.; Hou, C.; Ma, X.; Guo, S.; Zhang, H.; Shi, L.; Liao, C.; Zheng, B.; Ye, L.; Yang, L.; et al. Entropy-Enthalpy Compensations Fold Proteins in Precise Ways. *Int. J. Mol. Sci.* **2021**, *22*, 9653. [[CrossRef](#)]
168. Mancera, R.L. Computer Simulation of the Effect of Salt on the Hydrophobic Effect. *J. Chem. Soc. Faraday Trans.* **1998**, *94*, 3549–3559. [[CrossRef](#)]
169. Tuladhar, A.; Dewan, S.; Pezzotti, S.; Brigiano, F.S.; Creazzo, F.; Gaigeot, M.-P.; Borguet, E. Ions Tune Interfacial Water Structure and Modulate Hydrophobic Interactions at Silica Surfaces. *J. Am. Chem. Soc.* **2020**, *142*, 6991–7000. [[CrossRef](#)] [[PubMed](#)]
170. Arya, S.; Singh, A.K.; Bhasne, K.; Dogra, P.; Datta, A.; Das, P.; Mukhopadhyay, S. Femtosecond Hydration Map of Intrinsically Disordered α -Synuclein. *Biophys. J.* **2018**, *114*, 2540–2551. [[CrossRef](#)] [[PubMed](#)]
171. Rodriguez, J.A.; Ivanova, M.I.; Sawaya, M.R.; Cascio, D.; Reyes, F.E.; Shi, D.; Sangwan, S.; Guenther, E.L.; Johnson, L.M.; Zhang, M.; et al. Structure of the Toxic Core of α -Synuclein from Invisible Crystals. *Nature* **2015**, *525*, 486–490. [[CrossRef](#)]
172. Thirumalai, D.; Reddy, G.; Straub, J.E. Role of Water in Protein Aggregation and Amyloid Polymorphism. *Acc. Chem. Res.* **2012**, *45*, 83–92. [[CrossRef](#)]
173. Krone, M.G.; Hua, L.; Soto, P.; Zhou, R.; Berne, B.J.; Shea, J.-E. Role of Water in Mediating the Assembly of Alzheimer Amyloid-Beta A β 16–22 Protofilaments. *J. Am. Chem. Soc.* **2008**, *130*, 11066–11072. [[CrossRef](#)]
174. Klement, K.; Wieligmann, K.; Meinhardt, J.; Hortschansky, P.; Richter, W.; Fändrich, M. Effect of Different Salt Ions on the Propensity of Aggregation and on the Structure of Alzheimer’s α 1–40 Amyloid Fibrils. *J. Mol. Biol.* **2007**, *373*, 1321–1333. [[CrossRef](#)] [[PubMed](#)]
175. van der Lubbe, S.C.C.; Fonseca Guerra, C. The Nature of Hydrogen Bonds: A Delineation of the Role of Different Energy Components on Hydrogen Bond Strengths and Lengths. *Chem. Asian J.* **2019**, *14*, 2760–2769. [[CrossRef](#)] [[PubMed](#)]
176. Muthachikavil, A.V.; Peng, B.; Kontogeorgis, G.M.; Liang, X. Distinguishing Weak and Strong Hydrogen Bonds in Liquid Water—A Potential of Mean Force-Based Approach. *J. Phys. Chem. B* **2021**, *125*, 7187–7198. [[CrossRef](#)] [[PubMed](#)]
177. Lin, Y.; Fichou, Y.; Zeng, Z.; Hu, N.Y.; Han, S. Electrostatically Driven Complex Coacervation and Amyloid Aggregation of Tau Are Independent Processes with Overlapping Conditions. *ACS Chem. Neurosci.* **2020**, *11*, 615–627. [[CrossRef](#)] [[PubMed](#)]
178. Camino, J.D.; Gracia, P.; Chen, S.W.; Sot, J.; de la Arada, I.; Sebastián, V.; Arrondo, J.L.R.; Goñi, F.M.; Dobson, C.M.; Cremades, N. The Extent of Protein Hydration Dictates the Preference for Heterogeneous or Homogeneous Nucleation Generating Either Parallel or Antiparallel β -Sheet α -Synuclein Aggregates. *Chem. Sci.* **2020**, *11*, 11902–11914. [[CrossRef](#)] [[PubMed](#)]
179. Tarus, B.; Straub, J.E.; Thirumalai, D. Probing the Initial Stage of Aggregation of the A β (10–35)-Protein: Assessing the Propensity for Peptide Dimerization. *J. Mol. Biol.* **2005**, *345*, 1141–1156. [[CrossRef](#)]
180. Esler, W.P.; Felix, A.M.; Stimson, E.R.; Lachenmann, M.J.; Ghilardi, J.R.; Lu, Y.A.; Vinters, H.V.; Mantyh, P.W.; Lee, J.P.; Maggio, J.E. Activation Barriers to Structural Transition Determine Deposition Rates of Alzheimer’s Disease a Beta Amyloid. *J. Struct. Biol.* **2000**, *130*, 174–183. [[CrossRef](#)]
181. Chang, L.; Ernst, T.; Poland, R.E.; Jenden, D.J. In Vivo Proton Magnetic Resonance Spectroscopy of the Normal Aging Human Brain. *Life Sci.* **1996**, *58*, 2049–2056. [[CrossRef](#)]
182. Naber, D.; Korte, U.; Krack, K. Content of Water-Soluble and Total Proteins in the Aging Human Brain. *Exp. Gerontol.* **1979**, *14*, 59–63. [[CrossRef](#)]
183. Chong, S.-H.; Ham, S. Dynamics of Hydration Water Plays a Key Role in Determining the Binding Thermodynamics of Protein Complexes. *Sci. Rep.* **2017**, *7*, 8744. [[CrossRef](#)]

184. Ribeiro, S.S.; Samanta, N.; Ebbinghaus, S.; Marcos, J.C. The Synergic Effect of Water and Biomolecules in Intracellular Phase Separation. *Nat. Rev. Chem.* **2019**, *3*, 552–561. [[CrossRef](#)]
185. Wang, T.; Jo, H.; DeGrado, W.F.; Hong, M. Water Distribution, Dynamics, and Interactions with Alzheimer's β -Amyloid Fibrils Investigated by Solid-State NMR. *J. Am. Chem. Soc.* **2017**, *139*, 6242–6252. [[CrossRef](#)] [[PubMed](#)]
186. Schwierz, N.; Frost, C.V.; Geissler, P.L.; Zacharias, M. Dynamics of Seeded A β 40-Fibril Growth from Atomistic Molecular Dynamics Simulations: Kinetic Trapping and Reduced Water Mobility in the Locking Step. *J. Am. Chem. Soc.* **2016**, *138*, 527–539. [[CrossRef](#)] [[PubMed](#)]
187. van der Spoel, D.; van Maaren, P.J.; Larsson, P.; Timneanu, N. Thermodynamics of Hydrogen Bonding in Hydrophilic and Hydrophobic Media. *J. Phys. Chem. B* **2006**, *110*, 4393–4398. [[CrossRef](#)] [[PubMed](#)]
188. Arunan, E.; Desiraju, G.R.; Klein, R.A.; Sadlej, J.; Scheiner, S.; Alkorta, I.; Clary, D.C.; Crabtree, R.H.; Dannenberg, J.J.; Hobza, P.; et al. Definition of the hydrogen bond (IUPAC Recommendations 2011). *J. Macromol. Sci. Part A Pure Appl. Chem.* **2011**, *83*, 1637–1641. [[CrossRef](#)]
189. Dong, K.; Zhang, S.; Wang, J. Understanding the Hydrogen Bonds in Ionic Liquids and Their Roles in Properties and Reactions. *Chem. Commun.* **2016**, *52*, 6744–6764. [[CrossRef](#)] [[PubMed](#)]
190. Jiang, K.; Liu, L.; Liu, X.; Zhang, X.; Zhang, S. Insight into the Relationship between Viscosity and Hydrogen Bond of a Series of Imidazolium Ionic Liquids: A Molecular Dynamics and Density Functional Theory Study. *Ind. Eng. Chem. Res.* **2019**, *58*, 18848–18854. [[CrossRef](#)]
191. Ma, Y.; Liu, Y.; Su, H.; Wang, L.; Zhang, J. Relationship between Hydrogen Bond and Viscosity for a Series of Pyridinium Ionic Liquids: Molecular Dynamics and Quantum Chemistry. *J. Mol. Liq.* **2018**, *255*, 176–184. [[CrossRef](#)]
192. Goertz, M.P.; Houston, J.E.; Zhu, X.-Y. Hydrophilicity and the Viscosity of Interfacial Water. *Langmuir* **2007**, *23*, 5491–5497. [[CrossRef](#)]
193. Luzar, A.; Chandler, D. Hydrogen-Bond Kinetics in Liquid Water. *Nature* **1996**, *379*, 55–57. [[CrossRef](#)]
194. Beal, C. The Viscosity of Air, Water, Natural Gas, Crude Oil and Its Associated Gases at Oil Field Temperatures and Pressures. *Trans. AIME* **1946**, *165*, 94–115. [[CrossRef](#)]
195. Hinrikus, H.; Bachmann, M.; Lass, J. Understanding Physical Mechanism of Low-Level Microwave Radiation Effect. *Int. J. Radiat. Biol.* **2018**, *94*, 877–882. [[CrossRef](#)]
196. Zong, D.; Hu, H.; Duan, Y.; Sun, Y. Viscosity of Water under Electric Field: Anisotropy Induced by Redistribution of Hydrogen Bonds. *J. Phys. Chem. B* **2016**, *120*, 4818–4827. [[CrossRef](#)] [[PubMed](#)]
197. Tatoń, G. The Influence of Electromagnetic Wave Originating from WiFi Router on Water Viscosity. *Prz. Elektrotech.* **2018**, *1*, 280–282. [[CrossRef](#)]
198. Hinrikus, H.; Lass, J.; Karai, D.; Pilt, K.; Bachmann, M. Microwave Effect on Diffusion: A Possible Mechanism for Non-Thermal Effect. *Electromagn. Biol. Med.* **2015**, *34*, 327–333. [[CrossRef](#)]
199. Ghauri, S.A.; Ansari, M.S. Increase of Water Viscosity under the Influence of Magnetic Field. *J. Appl. Phys.* **2006**, *100*, 066101. [[CrossRef](#)]
200. Read, F.H. *Electromagnetic Radiation*; John Wiley and Sons: Chichester, UK; New York, NY, USA, 1980.
201. Sellers, P.J.; Berry, J.A.; Collatz, G.J.; Field, C.B.; Hall, F.G. Canopy Reflectance, Photosynthesis, and Transpiration. III. A Reanalysis Using Improved Leaf Models and a New Canopy Integration Scheme. *Remote Sens. Environ.* **1992**, *42*, 187–216. [[CrossRef](#)]
202. Sellers, P.J. Canopy Reflectance, Photosynthesis, and Transpiration, II. The Role of Biophysics in the Linearity of Their Interdependence. *Remote Sens. Environ.* **1987**, *21*, 143–183. [[CrossRef](#)]
203. Gates, D.M.; Tantraporn, W. The Reflectivity of Deciduous Trees and Herbaceous Plants in the Infrared to 25 Microns. *Science* **1952**, *115*, 613–616. [[CrossRef](#)] [[PubMed](#)]
204. Baldocchi, D.D.; Ryu, Y.; Dechant, B.; Eichelmann, E.; Hemes, K.; Ma, S.; Sanchez, C.R.; Shortt, R.; Szutu, D.; Valach, A.; et al. Outgoing Near-infrared Radiation from Vegetation Scales with Canopy Photosynthesis across a Spectrum of Function, Structure, Physiological Capacity, and Weather. *J. Geophys. Res. Biogeosci.* **2020**, *125*, e2019JG005534. [[CrossRef](#)]
205. Aitken, W.W.; Lombard, J.; Wang, K.; Toro, M.; Byrne, M.; Nardi, M.I.; Kardys, J.; Parrish, A.; Dong, C.; Szapocznik, J.; et al. Relationship of Neighborhood Greenness to Alzheimer's Disease and Non-Alzheimer's Dementia among 249,405 U.S. Medicare Beneficiaries. *J. Alzheimer's Dis.* **2021**, *81*, 597–606. [[CrossRef](#)] [[PubMed](#)]
206. Veleva, B.I.; Caljouw, M.A.A.; van der Steen, J.T.; Mertens, B.J.A.; Chel, V.G.M.; Numans, M.E. The Effect of Ultraviolet B Irradiation Compared with Oral Vitamin D Supplementation on the Well-Being of Nursing Home Residents with Dementia: A Randomized Controlled Trial. *Int. J. Environ. Res. Public Health* **2020**, *17*, 1684. [[CrossRef](#)] [[PubMed](#)]
207. Purushothuman, S.; Johnstone, D.M.; Nandasena, C.; van Eersel, J.; Ittner, L.M.; Mitrofanis, J.; Stone, J. Near Infrared Light Mitigates Cerebellar Pathology in Transgenic Mouse Models of Dementia. *Neurosci. Lett.* **2015**, *591*, 155–159. [[CrossRef](#)]
208. Purushothuman, S.; Johnstone, D.M.; Nandasena, C.; Mitrofanis, J.; Stone, J. Photobiomodulation with near Infrared Light Mitigates Alzheimer's Disease-Related Pathology in Cerebral Cortex—Evidence from Two Transgenic Mouse Models. *Alzheimer's Res. Ther.* **2014**, *6*, 2. [[CrossRef](#)]
209. Comerota, M.M.; Krishnan, B.; Taglialatela, G. Near Infrared Light Decreases Synaptic Vulnerability to Amyloid Beta Oligomers. *Sci. Rep.* **2017**, *7*, 15012. [[CrossRef](#)]

210. Comerota, M.M.; Tumurbaatar, B.; Krishnan, B.; Kayed, R.; Taglialatela, G. Near Infrared Light Treatment Reduces Synaptic Levels of Toxic Tau Oligomers in Two Transgenic Mouse Models of Human Tauopathies. *Mol. Neurobiol.* **2019**, *56*, 3341–3355. [[CrossRef](#)] [[PubMed](#)]
211. Stepanov, Y.V.; Golovynska, I.; Zhang, R.; Golovynskyi, S.; Stepanova, L.I.; Gorbach, O.; Dovbynychuk, T.; Garmanchuk, L.V.; Ohulchanskyi, T.Y.; Qu, J. Near-Infrared Light Reduces β -Amyloid-Stimulated Microglial Toxicity and Enhances Survival of Neurons: Mechanisms of Light Therapy for Alzheimer's Disease. *Alzheimer's Res. Ther.* **2022**, *14*, 84. [[CrossRef](#)] [[PubMed](#)]
212. Chao, L.L. Effects of Home Photobiomodulation Treatments on Cognitive and Behavioral Function, Cerebral Perfusion, and Resting-State Functional Connectivity in Patients with Dementia: A Pilot Trial. *Photobiomodulation Photomed. Laser Surg.* **2019**, *37*, 133–141. [[CrossRef](#)]
213. Berman, M.H.; Halper, J.P.; Nichols, T.W.; Jarrett, H.; Lundy, A.; Huang, J.H. Photobiomodulation with Near Infrared Light Helmet in a Pilot, Placebo Controlled Clinical Trial in Dementia Patients Testing Memory and Cognition. *J. Neurol. Neurosci.* **2017**, *8*, 176. [[CrossRef](#)]
214. Nizamutdinov, D.; Qi, X.; Berman, M.H.; Dougal, G.; Dayawansa, S.; Wu, E.; Yi, S.S.; Stevens, A.B.; Huang, J.H. Transcranial Near Infrared Light Stimulations Improve Cognition in Patients with Dementia. *Aging Dis.* **2021**, *12*, 954–963. [[CrossRef](#)]
215. Dougal, G.; Ennaceur, A.; Chazot, P.L. Effect of Transcranial Near-Infrared Light 1068 Nm Upon Memory Performance in Aging Healthy Individuals: A Pilot Study. *Photobiomodulation Photomed. Laser Surg.* **2021**, *39*, 654–660. [[CrossRef](#)]
216. Han, M.; Wang, Q.; Wang, X.; Zeng, Y.; Huang, Y.; Meng, Q.; Zhang, J.; Wei, X. Near Infra-Red Light Treatment of Alzheimer's Disease. *J. Innov. Opt. Health Sci.* **2018**, *11*, 1750012. [[CrossRef](#)]
217. Li, Q.; Peng, J.; Luo, Y.; Zhou, J.; Li, T.; Cao, L.; Peng, S.; Zuo, Z.; Wang, Z. Far Infrared Light Irradiation Enhances A β Clearance via Increased Exocytotic Microglial ATP and Ameliorates Cognitive Deficit in Alzheimer's Disease-like Mice. *J. Neuroinflamm.* **2022**, *19*, 145. [[CrossRef](#)] [[PubMed](#)]
218. Tan, D.-X.; Reiter, R.J.; Zimmerman, S.; Hardeland, R. Melatonin: Both a Messenger of Darkness and a Participant in the Cellular Actions of Non-Visible Solar Radiation of Near Infrared Light. *Biology* **2023**, *12*, 89. [[CrossRef](#)]
219. Zimmerman, S.; Reiter, R.J. Melatonin and the Optics of the Human Body. *Melatonin Res.* **2019**, *2*, 138–160. [[CrossRef](#)]
220. Chang, S.-Y.; Lee, M.Y.; Chung, P.-S.; Kim, S.; Choi, B.; Suh, M.-W.; Rhee, C.-K.; Jung, J.Y. Enhanced Mitochondrial Membrane Potential and ATP Synthesis by Photobiomodulation Increases Viability of the Auditory Cell Line after Gentamicin-Induced Intrinsic Apoptosis. *Sci. Rep.* **2019**, *9*, 19248. [[CrossRef](#)]
221. Hamblin, M.R. Mechanisms and Applications of the Anti-Inflammatory Effects of Photobiomodulation. *AIMS Biophys.* **2017**, *4*, 337–361. [[CrossRef](#)]
222. Karu, T. Mitochondrial Mechanisms of Photobiomodulation in Context of New Data about Multiple Roles of ATP. *Photomed. Laser Surg.* **2010**, *28*, 159–160. [[CrossRef](#)] [[PubMed](#)]
223. Coon, S.L.; Klein, D.C. Evolution of Arylalkylamine N-Acetyltransferase: Emergence and Divergence. *Mol. Cell. Endocrinol.* **2006**, *252*, 2–10. [[CrossRef](#)]
224. Lee, K.; Choi, G.-H.; Back, K. Functional Characterization of Serotonin N-Acetyltransferase in Archaeon *Thermoplasma Volcanium*. *Antioxidants* **2022**, *11*, 596. [[CrossRef](#)]
225. Kang, K.; Lee, K.; Park, S.; Byeon, Y.; Back, K. Molecular Cloning of Rice Serotonin N-Acetyltransferase, the Penultimate Gene in Plant Melatonin Biosynthesis. *J. Pineal Res.* **2013**, *55*, 7–13. [[CrossRef](#)]
226. Yoshizawa, T.; Nozawa, R.-S.; Jia, T.Z.; Saio, T.; Mori, E. Biological Phase Separation: Cell Biology Meets Biophysics. *Biophys. Rev.* **2020**, *12*, 519–539. [[CrossRef](#)] [[PubMed](#)]
227. King, J.T.; Shakya, A. Phase Separation of DNA: From Past to Present. *Biophys. J.* **2021**, *120*, 1139–1149. [[CrossRef](#)]
228. Dion, W.; Ballance, H.; Lee, J.; Pan, Y.; Irfan, S.; Edwards, C.; Sun, M.; Zhang, J.; Zhang, X.; Liu, S.; et al. Four-Dimensional Nuclear Speckle Phase Separation Dynamics Regulate Proteostasis. *Sci. Adv.* **2022**, *8*, eabl4150. [[CrossRef](#)]
229. Poudyal, R.R.; Pir Cakmak, F.; Keating, C.D.; Bevilacqua, P.C. Physical Principles and Extant Biology Reveal Roles for RNA-Containing Membraneless Compartments in Origins of Life Chemistry. *Biochemistry* **2018**, *57*, 2509–2519. [[CrossRef](#)]
230. Loh, D.; Reiter, R.J. Melatonin: Regulation of Biomolecular Condensates in Neurodegenerative Disorders. *Antioxidants* **2021**, *10*, 1483. [[CrossRef](#)] [[PubMed](#)]
231. Chu, X.-Y.; Xu, Y.-Y.; Tong, X.-Y.; Wang, G.; Zhang, H.-Y. The Legend of ATP: From Origin of Life to Precision Medicine. *Metabolites* **2022**, *12*, 461. [[CrossRef](#)]
232. Franzmann, T.M.; Alberti, S. Protein Phase Separation as a Stress Survival Strategy. *Cold Spring Harb. Perspect. Biol.* **2019**, *11*, a034058. [[CrossRef](#)]
233. Lerner, A.B.; Case, J.D.; Takahashi, Y.; Lee, T.H.; Mori, W. Isolation of melatonin, the pineal gland factor that lightens melanocytes. *J. Am. Chem. Soc.* **1958**, *80*, 2587. [[CrossRef](#)]
234. Loh, D.; Reiter, R.J. Melatonin and Phase Separation: Potential Interactions and Significance. *Melatonin Res.* **2022**, *5*, 186–191. [[CrossRef](#)]
235. Loh, D.; Reiter, R.J. Melatonin: Regulation of Prion Protein Phase Separation in Cancer Multidrug Resistance. *Molecules* **2022**, *27*, 705. [[CrossRef](#)]
236. Loh, D.; Reiter, R.J. Melatonin: Regulation of Viral Phase Separation and Epitranscriptomics in Post-Acute Sequelae of COVID-19. *Int. J. Mol. Sci.* **2022**, *23*, 8122. [[CrossRef](#)] [[PubMed](#)]

237. Li, C.; Akinc, M.; Wiench, J.; Pruski, M.; Schilling, C.H. Relationship between Water Mobility and Viscosity of Nanometric Alumina Suspensions. *J. Am. Ceram. Soc.* **2005**, *88*, 2762–2768. [[CrossRef](#)]
238. Ye, H.; Zhang, H.; Zhang, Z.; Zheng, Y. Size and Temperature Effects on the Viscosity of Water inside Carbon Nanotubes. *Nanoscale Res. Lett.* **2011**, *6*, 87. [[CrossRef](#)] [[PubMed](#)]
239. Shaat, M.; Zheng, Y. Fluidity and Phase Transitions of Water in Hydrophobic and Hydrophilic Nanotubes. *Sci. Rep.* **2019**, *9*, 5689. [[CrossRef](#)] [[PubMed](#)]
240. Chaban, V.V.; Prezhdo, V.V.; Prezhdo, O.V. Confinement by Carbon Nanotubes Drastically Alters the Boiling and Critical Behavior of Water Droplets. *ACS Nano* **2012**, *6*, 2766–2773. [[CrossRef](#)]
241. Striolo, A. Water Self-Diffusion through Narrow Oxygenated Carbon Nanotubes. *Nanotechnology* **2007**, *18*, 475704. [[CrossRef](#)]
242. Babu, J.S.; Sathian, S.P. The Role of Activation Energy and Reduced Viscosity on the Enhancement of Water Flow through Carbon Nanotubes. *J. Chem. Phys.* **2011**, *134*, 194509. [[CrossRef](#)]
243. Zhang, D.; Yang, X.; Jiang, W.; Jin, L.; Gao, Y.; Wang, Z. Pauli Repulsion Enhances Mobility of Ultraconfined Water. *ACS Nano* **2021**, *15*, 2490–2496. [[CrossRef](#)]
244. Najafi, S.; Lin, Y.; Longhini, A.P.; Zhang, X.; Delaney, K.T.; Kosik, K.S.; Fredrickson, G.H.; Shea, J.-E.; Han, S. Liquid-Liquid Phase Separation of Tau by Self and Complex Coacervation. *Protein Sci.* **2021**, *30*, 1393–1407. [[CrossRef](#)]
245. Jawerth, L.; Fischer-Friedrich, E.; Saha, S.; Wang, J.; Franzmann, T.; Zhang, X.; Sachweh, J.; Ruer, M.; Ijavi, M.; Saha, S.; et al. Protein Condensates as Aging Maxwell Fluids. *Science* **2020**, *370*, 1317–1323. [[CrossRef](#)] [[PubMed](#)]
246. Tejedor, A.R.; Sanchez-Burgos, I.; Estevez-Espinosa, M.; Garaizar, A.; Collepardo-Guevara, R.; Ramirez, J.; Espinosa, J.R. Protein Structural Transitions Critically Transform the Network Connectivity and Viscoelasticity of RNA-Binding Protein Condensates but RNA Can Prevent It. *Nat. Commun.* **2022**, *13*, 5717. [[CrossRef](#)] [[PubMed](#)]
247. Chen, H.-C.; Mai, F.-D.; Yang, K.-H.; Chen, L.-Y.; Yang, C.-P.; Liu, Y.-C. Quantitative Evaluation on Activated Property-Tunable Bulk Liquid Water with Reduced Hydrogen Bonds Using Deconvoluted Raman Spectroscopy. *Anal. Chem.* **2015**, *87*, 808–815. [[CrossRef](#)] [[PubMed](#)]
248. Yu, S.-H.; Chang, C.-C.; Mai, F.-D.; Yang, C.-P.; Liu, Y.-C. Plasmon-Activated Water Can Form Stronger Intermolecular Hydrogen Bonding with Water-Soluble Alcohols and Dissolve More Hydrophobic Solutes. *Chem. Eng. J.* **2022**, *427*, 131949. [[CrossRef](#)]
249. Zhang, J.; Yan, X.; Tian, Y.; Li, W.; Wang, H.; Li, Q.; Li, Y.; Li, Z.; Wu, T. Synthesis of a New Water-Soluble Melatonin Derivative with Low Toxicity and a Strong Effect on Sleep Aid. *ACS Omega* **2020**, *5*, 6494–6499. [[CrossRef](#)]
250. Renn, T.-Y.; Yang, C.-P.; Wu, U.-I.; Chen, L.-Y.; Mai, F.-D.; Tikhonova, M.A.; Amstislavskaya, T.G.; Liao, W.-C.; Lin, C.-T.; Liu, Y.-C.; et al. Water Composed of Reduced Hydrogen Bonds Activated by Localized Surface Plasmon Resonance Effectively Enhances Anti-Viral and Anti-Oxidative Activities of Melatonin. *Chem. Eng. J.* **2022**, *427*, 131626. [[CrossRef](#)]
251. Rodrigues, A.C.C.; de M. Camargo, L.T.F.; Lopes, Y.F.; Sallum, L.O.; Napolitano, H.B.; Camargo, A.J. Aqueous Solvation Study of Melatonin Using Ab Initio Molecular Dynamics. *J. Mol. Liq.* **2021**, *343*, 117451. [[CrossRef](#)]
252. Florio, G.M.; Zwier, T.S. Solvation of a Flexible Biomolecule in the Gas Phase: The Ultraviolet and Infrared Spectroscopy of Melatonin–Water Clusters. *J. Phys. Chem. A* **2003**, *107*, 974–983. [[CrossRef](#)]
253. Ritwiset, A.; Khajonrit, J.; Kongsuk, S.; Maensiri, S. Molecular Insight on the Formation Structure and Dynamics of Melatonin in an Aqueous Solution and at the Water-Air Interface: A Molecular Dynamics Study. *J. Mol. Graph. Model.* **2021**, *108*, 107983. [[CrossRef](#)] [[PubMed](#)]
254. Chang, H.-M.; Wu, U.-I.; Lin, T.-B.; Lan, C.-T.; Chien, W.-C.; Huang, W.-L.; Shieh, J.-Y. Total Sleep Deprivation Inhibits the Neuronal Nitric Oxide Synthase and Cytochrome Oxidase Reactivities in the Nodose Ganglion of Adult Rats. *J. Anat.* **2006**, *209*, 239–250. [[CrossRef](#)]
255. Cheng, C.-H.; Lin, K.-J.; Hong, C.-T.; Wu, D.; Chang, H.-M.; Liu, C.-H.; Hsiao, I.-T.; Yang, C.-P.; Liu, Y.-C.; Hu, C.-J. Plasmon-Activated Water Reduces Amyloid Burden and Improves Memory in Animals with Alzheimer’s Disease. *Sci. Rep.* **2019**, *9*, 13252. [[CrossRef](#)]
256. Chen, H.-C.; Cheng, C.-Y.; Chen, L.-Y.; Chang, C.-C.; Yang, C.-P.; Mai, F.-D.; Liao, W.-C.; Chang, H.-M.; Liu, Y.-C. Plasmon-Activated Water Effectively Relieves Hepatic Oxidative Damage Resulting from Chronic Sleep Deprivation. *RSC Adv.* **2018**, *8*, 9618–9626. [[CrossRef](#)]
257. Mitroka, S.; Zimmeck, S.; Troya, D.; Tanko, J.M. How Solvent Modulates Hydroxyl Radical Reactivity in Hydrogen Atom Abstractions. *J. Am. Chem. Soc.* **2010**, *132*, 2907–2913. [[CrossRef](#)]
258. Vassilev, P.; Louwse, M.J.; Baerends, E.J. Hydroxyl Radical and Hydroxide Ion in Liquid Water: A Comparative Electron Density Functional Theory Study. *J. Phys. Chem. B* **2005**, *109*, 23605–23610. [[CrossRef](#)]
259. Wong, H.-S.; Dighe, P.A.; Mezera, V.; Monternier, P.-A.; Brand, M.D. Production of Superoxide and Hydrogen Peroxide from Specific Mitochondrial Sites under Different Bioenergetic Conditions. *J. Biol. Chem.* **2017**, *292*, 16804–16809. [[CrossRef](#)] [[PubMed](#)]
260. Giulivi, C.; Boveris, A.; Cadenas, E. Hydroxyl Radical Generation during Mitochondrial Electron Transfer and the Formation of 8-Hydroxydesoxyguanosine in Mitochondrial DNA. *Arch. Biochem. Biophys.* **1995**, *316*, 909–916. [[CrossRef](#)] [[PubMed](#)]
261. Aleardi, A.M.; Benard, G.; Augereau, O.; Malgat, M.; Talbot, J.C.; Mazat, J.P.; Letellier, T.; Dachary-Prigent, J.; Solaini, G.C.; Rossignol, R. Gradual Alteration of Mitochondrial Structure and Function by Beta-Amyloids: Importance of Membrane Viscosity Changes, Energy Deprivation, Reactive Oxygen Species Production, and Cytochrome c Release. *J. Bioenerg. Biomembr.* **2005**, *37*, 207–225. [[CrossRef](#)] [[PubMed](#)]
262. Gough, D.R.; Cotter, T.G. Hydrogen Peroxide: A Jekyll and Hyde Signalling Molecule. *Cell Death Dis.* **2011**, *2*, e213. [[CrossRef](#)]

263. Ren, M.; Deng, B.; Zhou, K.; Kong, X.; Wang, J.-Y.; Lin, W. Single Fluorescent Probe for Dual-Imaging Viscosity and H₂O₂ in Mitochondria with Different Fluorescence Signals in Living Cells. *Anal. Chem.* **2017**, *89*, 552–555. [[CrossRef](#)]
264. Zheng, A.; Liu, H.; Gao, X.; Xu, K.; Tang, B. A Mitochondrial-Targeting Near-Infrared Fluorescent Probe for Revealing the Effects of Hydrogen Peroxide And Heavy Metal Ions on Viscosity. *Anal. Chem.* **2021**, *93*, 9244–9249. [[CrossRef](#)]
265. Li, S.; Wang, P.; Feng, W.; Xiang, Y.; Dou, K.; Liu, Z. Simultaneous Imaging of Mitochondrial Viscosity and Hydrogen Peroxide in Alzheimer's Disease by a Single near-Infrared Fluorescent Probe with a Large Stokes Shift. *Chem. Commun.* **2020**, *56*, 1050–1053. [[CrossRef](#)] [[PubMed](#)]
266. Tan, D.X.; Manchester, L.C.; Reiter, R.J.; Plummer, B.F. Cyclic 3-Hydroxymelatonin: A Melatonin Metabolite Generated as a Result of Hydroxyl Radical Scavenging. *Biol. Signals Recept.* **1999**, *8*, 70–74. [[CrossRef](#)]
267. Galano, A. On the Direct Scavenging Activity of Melatonin towards Hydroxyl and a Series of Peroxyl Radicals. *Phys. Chem. Chem. Phys.* **2011**, *13*, 7178–7188. [[CrossRef](#)] [[PubMed](#)]
268. Bandyopadhyay, D.; Biswas, K.; Bandyopadhyay, U.; Reiter, R.J.; Banerjee, R.K. Melatonin Protects against Stress-Induced Gastric Lesions by Scavenging the Hydroxyl Radical. *J. Pineal Res.* **2000**, *29*, 143–151. [[CrossRef](#)]
269. Reiter, R.J.; Tan, D.X.; Osuna, C.; Gitto, E. Actions of Melatonin in the Reduction of Oxidative Stress. A Review. *J. Biomed. Sci.* **2000**, *7*, 444–458. [[CrossRef](#)] [[PubMed](#)]
270. Galano, A.; Reiter, R.J. Melatonin and Its Metabolites vs Oxidative Stress: From Individual Actions to Collective Protection. *J. Pineal Res.* **2018**, *65*, e12514. [[CrossRef](#)]
271. Purushothaman, A.; Sheeja, A.A.; Janardanan, D. Hydroxyl Radical Scavenging Activity of Melatonin and Its Related Indolamines. *Free Radic. Res.* **2020**, *54*, 373–383. [[CrossRef](#)] [[PubMed](#)]
272. Persson, L.B.; Ambati, V.S.; Brandman, O. Cellular Control of Viscosity Counters Changes in Temperature and Energy Availability. *Cell* **2020**, *183*, 1572–1585.e16. [[CrossRef](#)]
273. Scalettar, B.A.; Abney, J.R.; Hackenbrock, C.R. Dynamics, Structure, and Function Are Coupled in the Mitochondrial Matrix. *Proc. Natl. Acad. Sci. USA* **1991**, *88*, 8057–8061. [[CrossRef](#)]
274. Hao, X.; Zhan, J.; Geng, C.; Lin, W. Discriminating Normal and Inflammatory Mice Models by Viscosity Changes with a Two-Photon Fluorescent Probe. *Spectrochim. Acta Part A Mol. Biomol. Spectrosc.* **2023**, *284*, 121807. [[CrossRef](#)]
275. Guan, X.; Hong, J.; Li, Q.; Feng, G. High-Fidelity Imaging Probe for Lysosomes and Selective Visualization of Cancer Cells and Tissues. *Sens. Actuators B Chem.* **2022**, *369*, 132325. [[CrossRef](#)]
276. Song, H.; Zhang, W.; Zhang, Y.; Yin, C.; Huo, F. Viscosity Activated NIR Fluorescent Probe for Visualizing Mitochondrial Viscosity Dynamic and Fatty Liver Mice. *Chem. Eng. J.* **2022**, *445*, 136448. [[CrossRef](#)]
277. Li, S.; Huo, F.; Yin, C. NIR Fluorescent Probe for Dual-Response Viscosity and Hydrogen Sulfide and Its Application in Parkinson's Disease Model. *Dyes Pigments* **2022**, *197*, 109825. [[CrossRef](#)]
278. Pan, W.; Han, L.; Cao, X.; Shen, S.; Pang, X.; Zhu, Y. Dual-Response near-Infrared Fluorescent Probe for Detecting Cyanide and Mitochondrial Viscosity and Its Application in Bioimaging. *Food Chem.* **2022**, *407*, 135163. [[CrossRef](#)] [[PubMed](#)]
279. Li, S.; Huo, F.; Wen, Y.; Yin, C. A Dual-Response NIR Probe Reveals Positive Correlation between Biothiols and Viscosity under Cellular Stress Change. *Chem. Commun.* **2022**, *58*, 4881–4884. [[CrossRef](#)] [[PubMed](#)]
280. Zhang, Y.; Zhou, Q.; Bu, Y.; Xu, T.; Zhu, X.; Zhang, J.; Yu, Z.; Wang, L.; Zhong, F.; Zhou, H. Real-Time Imaging Mitochondrial Viscosity Dynamic during Mitophagy Mediated by Photodynamic Therapy. *Anal. Chim. Acta* **2021**, *1178*, 338847. [[CrossRef](#)]
281. Zhou, Y.; Liu, Z.; Qiao, G.; Tang, B.; Li, P. Visualization of Endoplasmic Reticulum Viscosity in the Liver of Mice with Nonalcoholic Fatty Liver Disease by a near-Infrared Fluorescence Probe. *Chin. Chem. Lett.* **2021**, *32*, 3641–3645. [[CrossRef](#)]
282. Liu, Y.; Ma, Y.; Gao, W.; Ma, S.; Lin, W. Construction of a Fluorescent Probe with Large Stokes Shift and Deep Red Emission for Sensing of the Viscosity in Hyperglycemic Mice. *Dyes Pigments* **2021**, *195*, 109674. [[CrossRef](#)]
283. Xiao, H.; Li, P.; Tang, B. Small Molecular Fluorescent Probes for Imaging of Viscosity in Living Biosystems. *Chemistry* **2021**, *27*, 6880–6898. [[CrossRef](#)]
284. Shen, W.; Wang, P.; Xie, Z.; Zhou, H.; Hu, Y.; Fu, M.; Zhu, Q. A Bifunctional Probe Reveals Increased Viscosity and Hydrogen Sulfide in Zebra Fish Model of Parkinson's Disease. *Talanta* **2021**, *234*, 122621. [[CrossRef](#)]
285. Fang, Z.; Su, Z.; Qin, W.; Li, H.; Fang, B.; Du, W.; Wu, Q.; Peng, B.; Li, P.; Yu, H.; et al. Two-Photon Dual-Channel Fluorogenic Probe for in Situ Imaging the Mitochondrial H₂S/viscosity in the Brain of Drosophila Parkinson's Disease Model. *Chin. Chem. Lett.* **2020**, *31*, 2903–2908. [[CrossRef](#)]
286. Park, S.J.; Shin, B.K.; Lee, H.W.; Song, J.M.; Je, J.T.; Kim, H.M. Asymmetric Cyanine as a Far-Red Fluorescence Probe for Mitochondrial Viscosity. *Dyes Pigments* **2020**, *174*, 108080. [[CrossRef](#)]
287. Yang, J.; Guo, Y.; Pistolozzi, M.; Yan, J. Research Progress of Multi-Functional Fluorescent Probes for Alzheimer's Disease Monitoring. *Dyes Pigments* **2021**, *193*, 109466. [[CrossRef](#)]
288. Zhu, L.; Fu, M.; Yin, B.; Wang, L.; Chen, Y.; Zhu, Q. A Red-Emitting Fluorescent Probe for Mitochondria-Target Microviscosity in Living Cells and Blood Viscosity Detection in Hyperglycemia Mice. *Dyes Pigments* **2020**, *172*, 107859. [[CrossRef](#)]
289. Tan, H.-Y.; Qiu, Y.-T.; Sun, H.; Yan, J.-W.; Zhang, L. A Lysosome-Targeting Dual-Functional Fluorescent Probe for Imaging Intracellular Viscosity and Beta-Amyloid. *Chem. Commun.* **2019**, *55*, 2688–2691. [[CrossRef](#)]
290. Li, H.; Xin, C.; Zhang, G.; Han, X.; Qin, W.; Zhang, C.-W.; Yu, C.; Jing, S.; Li, L.; Huang, W. A Mitochondria-Targeted Two-Photon Fluorogenic Probe for the Dual-Imaging of Viscosity and H₂O₂ Levels in Parkinson's Disease Models. *J. Mater. Chem. B Mater. Biol. Med.* **2019**, *7*, 4243–4251. [[CrossRef](#)]

291. Yin, J.; Peng, M.; Lin, W. Visualization of Mitochondrial Viscosity in Inflammation, Fatty Liver, and Cancer Living Mice by a Robust Fluorescent Probe. *Anal. Chem.* **2019**, *91*, 8415–8421. [[CrossRef](#)] [[PubMed](#)]
292. Ren, M.; Zhou, K.; Wang, L.; Liu, K.; Lin, W. Construction of a Ratiometric Two-Photon Fluorescent Probe to Monitor the Changes of Mitochondrial Viscosity. *Sens. Actuators B Chem.* **2018**, *262*, 452–459. [[CrossRef](#)]
293. Jiang, N.; Fan, J.; Zhang, S.; Wu, T.; Wang, J.; Gao, P.; Qu, J.; Zhou, F.; Peng, X. Dual Mode Monitoring Probe for Mitochondrial Viscosity in Single Cell. *Sens. Actuators B Chem.* **2014**, *190*, 685–693. [[CrossRef](#)]
294. Aras, S.; Tek, I.; Varli, M.; Yalcin, A.; Cengiz, O.K.; Atmis, V.; Atli, T. Plasma Viscosity: Is a Biomarker for the Differential Diagnosis of Alzheimer's Disease and Vascular Dementia? *Am. J. Alzheimer's Dis. Other Dement.* **2013**, *28*, 62–68. [[CrossRef](#)] [[PubMed](#)]
295. Tang, Y.; Peng, J.; Zhang, Q.; Song, S.; Lin, W. A New NIR Emission Mitochondrial Targetable Fluorescent Probe and Its Application in Detecting Viscosity Changes in Mouse Liver and Kidney Injury. *Talanta* **2022**, *249*, 123647. [[CrossRef](#)]
296. Yu, F.-T.; Huang, Z.; Yang, J.-X.; Yang, L.-M.; Xu, X.-Y.; Huang, J.-Y.; Kong, L. Two Quinoline-Based Two-Photon Fluorescent Probes for Imaging of Viscosity in Subcellular Organelles of Living HeLa Cells. *Spectrochim. Acta Part A Mol. Biomol. Spectrosc.* **2022**, *283*, 121769. [[CrossRef](#)]
297. Wei, Y.-F.; Weng, X.-F.; Sha, X.-L.; Sun, R.; Xu, Y.-J.; Ge, J.-F. Simultaneous Imaging of Lysosomal and Mitochondrial Viscosity under Different Conditions Using a NIR Probe. *Sens. Actuators B Chem.* **2021**, *326*, 128954. [[CrossRef](#)]
298. Yan, F.; Sun, X.; Ma, T.; Zhang, Y.; Jiang, Y.; Wang, R.; Ma, C.; Wei, J.; Chen, L.; Cui, Y. A Viscosity-Dependent Carbon Dots with Anti-VEGF Properties for Monitoring and Promoting Apoptosis in Cancerous Cell. *Chem. Eng. J.* **2021**, *407*, 127801. [[CrossRef](#)]
299. Wu, Y.; Shu, W.; Zeng, C.; Guo, B.; Shi, J.; Jing, J.; Zhang, X. A Mitochondria Targetable and Viscosity Sensitive Fluorescent Probe and Its Applications for Distinguishing Cancerous Cells. *Dyes Pigments* **2019**, *168*, 134–139. [[CrossRef](#)]
300. Yang, Z.; He, Y.; Lee, J.-H.; Park, N.; Suh, M.; Chae, W.-S.; Cao, J.; Peng, X.; Jung, H.; Kang, C.; et al. A Self-Calibrating Bipartite Viscosity Sensor for Mitochondria. *J. Am. Chem. Soc.* **2013**, *135*, 9181–9185. [[CrossRef](#)]
301. Liang, L.-F.; Da, X.; Chen, T.-S.; Pei, Y.-H. Nucleoplasmic viscosity of living cells investigated by fluorescence correlation spectroscopy. *Guang Pu Xue Yu Guang Pu Fen Xi* **2009**, *29*, 459–462. [[PubMed](#)]
302. Zhang, S.; Zhang, Y.; Zhao, L.; Xu, L.; Han, H.; Huang, Y.; Fei, Q.; Sun, Y.; Ma, P.; Song, D. A Novel Water-Soluble near-Infrared Fluorescent Probe for Monitoring Mitochondrial Viscosity. *Talanta* **2021**, *233*, 122592. [[CrossRef](#)]
303. Chernyak, B.V.; Izyumov, D.S.; Lyamzaev, K.G.; Pashkovskaya, A.A.; Pletjushkina, O.Y.; Antonenko, Y.N.; Sakharov, D.V.; Wirtz, K.W.A.; Skulachev, V.P. Production of Reactive Oxygen Species in Mitochondria of HeLa Cells under Oxidative Stress. *Biochim. Biophys. Acta* **2006**, *1757*, 525–534. [[CrossRef](#)]
304. Sun, W.; Shi, Y.-D.; Ding, A.-X.; Tan, Z.-L.; Chen, H.; Liu, R.; Wang, R.; Lu, Z.-L. Imaging Viscosity and Peroxynitrite by a Mitochondria-Targeting Two-Photon Ratiometric Fluorescent Probe. *Sens. Actuators B Chem.* **2018**, *276*, 238–246. [[CrossRef](#)]
305. Xu, T.; Pagadala, V.; Mueller, D.M. Understanding Structure, Function, and Mutations in the Mitochondrial ATP Synthase. *Microb. Cell Factories* **2015**, *2*, 105–125. [[CrossRef](#)] [[PubMed](#)]
306. Nakamoto, R.K.; Scanlon, J.A.B.; Al-Shawi, M.K. The Rotary Mechanism of the ATP Synthase. *Arch. Biochem. Biophys.* **2008**, *476*, 43–50. [[CrossRef](#)]
307. Stock, D.; Gibbons, C.; Arechaga, I.; Leslie, A.G.; Walker, J.E. The Rotary Mechanism of ATP Synthase. *Curr. Opin. Struct. Biol.* **2000**, *10*, 672–679. [[CrossRef](#)]
308. Usukura, E.; Suzuki, T.; Furuike, S.; Soga, N.; Saita, E.-I.; Hisabori, T.; Kinoshita, K., Jr.; Yoshida, M. Torque Generation and Utilization in Motor Enzyme F₀F₁-ATP Synthase: Half-Torque F₁ with Short-Sized Pushrod Helix and Reduced ATP Synthesis by Half-Torque F₀F₁. *J. Biol. Chem.* **2012**, *287*, 1884–1891. [[CrossRef](#)]
309. Novichkova, N.S.; Malyan, A.N. The Effect of the Viscosity of a Trehalose Solution on ATP Hydrolysis by Chloroplast F₁-ATPase. *Biophysics* **2019**, *64*, 853–857. [[CrossRef](#)]
310. Nakanishi-Matsui, M.; Kashiwagi, S.; Hosokawa, H.; Cipriano, D.J.; Dunn, S.D.; Wada, Y.; Futai, M. Stochastic High-Speed Rotation of Escherichia Coli ATP Synthase F₁ Sector: The Epsilon Subunit-Sensitive Rotation. *J. Biol. Chem.* **2006**, *281*, 4126–4131. [[CrossRef](#)]
311. Capaldi, R.A.; Aggeler, R. Mechanism of the F₁(F₀)-Type ATP Synthase, a Biological Rotary Motor. *Trends Biochem. Sci.* **2002**, *27*, 154–160. [[CrossRef](#)]
312. Martin, J.L.; Ishmukhametov, R.; Hornung, T.; Ahmad, Z.; Frasch, W.D. Anatomy of F₁-ATPase Powered Rotation. *Proc. Natl. Acad. Sci. USA* **2014**, *111*, 3715–3720. [[CrossRef](#)]
313. Spetzler, D.; Ishmukhametov, R.; Hornung, T.; Day, L.J.; Martin, J.; Frasch, W.D. Single Molecule Measurements of F₁-ATPase Reveal an Interdependence between the Power Stroke and the Dwell Duration. *Biochemistry* **2009**, *48*, 7979–7985. [[CrossRef](#)] [[PubMed](#)]
314. Omote, H.; Sambonmatsu, N.; Saito, K.; Sambongi, Y.; Iwamoto-Kihara, A.; Yanagida, T.; Wada, Y.; Futai, M. The γ -Subunit Rotation and Torque Generation in F₁-ATPase from Wild-Type or Uncoupled Mutant *Escherichia coli*. *Proc. Natl. Acad. Sci. USA* **1999**, *96*, 7780–7784. [[CrossRef](#)]
315. Watanabe, R.; Hayashi, K.; Ueno, H.; Noji, H. Catalysis-Enhancement via Rotary Fluctuation of F₁-ATPase. *Biophys. J.* **2013**, *105*, 2385–2391. [[CrossRef](#)] [[PubMed](#)]
316. Begum, R.; Powner, M.B.; Hudson, N.; Hogg, C.; Jeffery, G. Treatment with 670 Nm Light up Regulates Cytochrome C Oxidase Expression and Reduces Inflammation in an Age-Related Macular Degeneration Model. *PLoS ONE* **2013**, *8*, e57828. [[CrossRef](#)]

317. Ahamed Basha, A.; Mathangi, D.C.; Shyamala, R. Effect of LED Photobiomodulation on Fluorescent Light Induced Changes in Cellular ATPases and Cytochrome c Oxidase Activity in Wistar Rat. *Lasers Med. Sci.* **2016**, *31*, 1803–1809. [[CrossRef](#)]
318. Gkotsi, D.; Begum, R.; Salt, T.; Lascaratos, G.; Hogg, C.; Chau, K.-Y.; Schapira, A.H.V.; Jeffery, G. Recharging Mitochondrial Batteries in Old Eyes. Near Infra-Red Increases ATP. *Exp. Eye Res.* **2014**, *122*, 50–53. [[CrossRef](#)] [[PubMed](#)]
319. Wong-Riley, M.T.T.; Liang, H.L.; Eells, J.T.; Chance, B.; Henry, M.M.; Buchmann, E.; Kane, M.; Whelan, H.T. Photobiomodulation Directly Benefits Primary Neurons Functionally Inactivated by Toxins: Role of cytochrome c oxidase *. *J. Biol. Chem.* **2005**, *280*, 4761–4771. [[CrossRef](#)] [[PubMed](#)]
320. Li, Y.; Park, J.-S.; Deng, J.-H.; Bai, Y. Cytochrome c Oxidase Subunit IV Is Essential for Assembly and Respiratory Function of the Enzyme Complex. *J. Bioenerg. Biomembr.* **2006**, *38*, 283–291. [[CrossRef](#)] [[PubMed](#)]
321. Sedlák, E.; Fabian, M.; Robinson, N.C.; Musatov, A. Ferricytochrome c Protects Mitochondrial Cytochrome c Oxidase against Hydrogen Peroxide-Induced Oxidative Damage. *Free Radic. Biol. Med.* **2010**, *49*, 1574–1581. [[CrossRef](#)] [[PubMed](#)]
322. Musatov, A.; Robinson, N.C. Susceptibility of Mitochondrial Electron-Transport Complexes to Oxidative Damage. Focus on Cytochrome c Oxidase. *Free Radic. Res.* **2012**, *46*, 1313–1326. [[CrossRef](#)]
323. Choksi, K.B.; Nuss, J.E.; Boylston, W.H.; Rabek, J.P.; Papaconstantinou, J. Age-Related Increases in Oxidatively Damaged Proteins of Mouse Kidney Mitochondrial Electron Transport Chain Complexes. *Free Radic. Biol. Med.* **2007**, *43*, 1423–1438. [[CrossRef](#)] [[PubMed](#)]
324. Zhang, Y.; Marcillat, O.; Giulivi, C.; Ernster, L.; Davies, K.J. The Oxidative Inactivation of Mitochondrial Electron Transport Chain Components and ATPase. *J. Biol. Chem.* **1990**, *265*, 16330–16336. [[CrossRef](#)]
325. Chen, J.; Schenker, S.; Frosto, T.A.; Henderson, G.I. Inhibition of Cytochrome c Oxidase Activity by 4-Hydroxynonenal (HNE). Role of HNE Adduct Formation with the Enzyme Subunits. *Biochim. Biophys. Acta* **1998**, *1380*, 336–344. [[CrossRef](#)] [[PubMed](#)]
326. Karu, T.I.; Pyatibrat, L.V.; Kolyakov, S.F.; Afanasyeva, N.I. Absorption Measurements of a Cell Monolayer Relevant to Phototherapy: Reduction of Cytochrome c Oxidase under near IR Radiation. *J. Photochem. Photobiol. B* **2005**, *81*, 98–106. [[CrossRef](#)]
327. Sommer, A.P.; Haddad, M.K.; Fecht, H.-J. Light Effect on Water Viscosity: Implication for ATP Biosynthesis. *Sci. Rep.* **2015**, *5*, 12029. [[CrossRef](#)] [[PubMed](#)]
328. Sommer, A.P. Mitochondrial Cytochrome c Oxidase Is Not the Primary Acceptor for near Infrared Light-It Is Mitochondrial Bound Water: The Principles of Low-Level Light Therapy. *Ann. Transl. Med.* **2019**, *7* (Suppl. 1), S13. [[CrossRef](#)] [[PubMed](#)]
329. Sommer, A.P.; Schemmer, P.; Pavláth, A.E.; Försterling, H.-D.; Mester, Á.R.; Trelles, M.A. Quantum Biology in Low Level Light Therapy: Death of a Dogma. *Ann. Transl. Med.* **2020**, *8*, 440. [[CrossRef](#)] [[PubMed](#)]
330. Hasinoff, B.B.; Davey, J.P. The Kinetics of the Aerobic Oxidation of Ferrocycytochrome c by Cytochrome c Oxidase in Solvents of Increased Viscosity Are Partially Diffusion Controlled. *Biochim. Biophys. Acta* **1987**, *892*, 1–9. [[CrossRef](#)] [[PubMed](#)]
331. Feng, C.; Kedia, R.V.; Hazzard, J.T.; Hurley, J.K.; Tollin, G.; Enemark, J.H. Effect of Solution Viscosity on Intramolecular Electron Transfer in Sulfite Oxidase. *Biochemistry* **2002**, *41*, 5816–5821. [[CrossRef](#)]
332. Passarella, S.; Ostuni, A.; Atlante, A.; Quagliariello, E. Increase in the ADP/ATP Exchange in Rat Liver Mitochondria Irradiated in Vitro by Helium-Neon Laser. *Biochem. Biophys. Res. Commun.* **1988**, *156*, 978–986. [[CrossRef](#)]
333. Karu, T.; Pyatibrat, L.; Kalendo, G. Irradiation with He Ne Laser Increases ATP Level in Cells Cultivated in Vitro. *J. Photochem. Photobiol. B* **1995**, *27*, 219–223. [[CrossRef](#)]
334. Sommer, A.P.; Bieschke, J.; Friedrich, R.P.; Zhu, D.; Wanker, E.E.; Fecht, H.J.; Mereles, D.; Hunstein, W. 670 Nm Laser Light and EGCG Complementarily Reduce Amyloid- β Aggregates in Human Neuroblastoma Cells: Basis for Treatment of Alzheimer's Disease? *Photomed. Laser Surg.* **2012**, *30*, 54–60. [[CrossRef](#)]
335. Castellano-González, G.; Pichaud, N.; Ballard, J.W.O.; Bessedé, A.; Marcal, H.; Guillemin, G.J. Epigallocatechin-3-Gallate Induces Oxidative Phosphorylation by Activating Cytochrome c Oxidase in Human Cultured Neurons and Astrocytes. *Oncotarget* **2016**, *7*, 7426–7440. [[CrossRef](#)]
336. Reiter, R.J.; Rosales-Corral, S.; Tan, D.X.; Jou, M.J.; Galano, A.; Xu, B. Melatonin as a Mitochondria-Targeted Antioxidant: One of Evolution's Best Ideas. *Cell. Mol. Life Sci.* **2017**, *74*, 3863–3881. [[CrossRef](#)] [[PubMed](#)]
337. Petrosillo, G.; De Benedictis, V.; Ruggiero, F.M.; Paradies, G. Decline in Cytochrome c Oxidase Activity in Rat-Brain Mitochondria with Aging. Role of Peroxidized Cardiolipin and Beneficial Effect of Melatonin. *J. Bioenerg. Biomembr.* **2013**, *45*, 431–440. [[CrossRef](#)] [[PubMed](#)]
338. Agil, A.; Chayah, M.; Visiedo, L.; Navarro-Alarcon, M.; Rodríguez Ferrer, J.M.; Tassi, M.; Reiter, R.J.; Fernández-Vázquez, G. Melatonin Improves Mitochondrial Dynamics and Function in the Kidney of Zucker Diabetic Fatty Rats. *J. Clin. Med. Res.* **2020**, *9*, 2916. [[CrossRef](#)] [[PubMed](#)]
339. Fernández Vázquez, G.; Reiter, R.J.; Agil, A. Melatonin Increases Brown Adipose Tissue Mass and Function in Zucker Diabetic Fatty Rats: Implications for Obesity Control. *J. Pineal Res.* **2018**, *64*, e12472. [[CrossRef](#)]
340. Randi, E.B.; Zuhra, K.; Pecze, L.; Panagaki, T.; Szabo, C. Physiological Concentrations of Cyanide Stimulate Mitochondrial Complex IV and Enhance Cellular Bioenergetics. *Proc. Natl. Acad. Sci. USA* **2021**, *118*, e2026245118. [[CrossRef](#)]
341. Pacher, P. Cyanide Emerges as an Endogenous Mammalian Gasotransmitter. *Proc. Natl. Acad. Sci. USA* **2021**, *118*, e2108040118. [[CrossRef](#)]
342. Zuhra, K.; Szabo, C. The Two Faces of Cyanide: An Environmental Toxin and a Potential Novel Mammalian Gasotransmitter. *FEBS J.* **2022**, *289*, 2481–2515. [[CrossRef](#)]
343. Nelson, L. Acute Cyanide Toxicity: Mechanisms and Manifestations. *J. Emerg. Nurs.* **2006**, *32* (Suppl. 4), S8–S11. [[CrossRef](#)]

344. Leavesley, H.B.; Li, L.; Prabhakaran, K.; Borowitz, J.L.; Isom, G.E. Interaction of Cyanide and Nitric Oxide with Cytochrome c Oxidase: Implications for Acute Cyanide Toxicity. *Toxicol. Sci.* **2008**, *101*, 101–111. [[CrossRef](#)]
345. Gunasekar, P.G.; Borowitz, J.L.; Isom, G.E. Cyanide-Induced Generation of Oxidative Species: Involvement of Nitric Oxide Synthase and Cyclooxygenase-2. *J. Pharmacol. Exp. Ther.* **1998**, *285*, 236–241. [[PubMed](#)]
346. Zhang, W.; Xu, K.; Yue, L.; Shao, Z.; Feng, Y.; Fang, M. Two-Dimensional Carbazole-Based Derivatives as Versatile Chemosensors for Colorimetric Detection of Cyanide and Two-Photon Fluorescence Imaging of Viscosity in Vitro. *Dyes Pigments* **2017**, *137*, 560–568. [[CrossRef](#)]
347. Martín, M.; Macías, M.; León, J.; Escames, G.; Khaldy, H.; Acuña-Castroviejo, D. Melatonin Increases the Activity of the Oxidative Phosphorylation Enzymes and the Production of ATP in Rat Brain and Liver Mitochondria. *Int. J. Biochem. Cell Biol.* **2002**, *34*, 348–357. [[CrossRef](#)]
348. Martín, M.; Macías, M.; Escames, G.; Reiter, R.J.; Agapito, M.T.; Ortiz, G.G.; Acuña-Castroviejo, D. Melatonin-Induced Increased Activity of the Respiratory Chain Complexes I and IV Can Prevent Mitochondrial Damage Induced by Ruthenium Red in Vivo. *J. Pineal Res.* **2000**, *28*, 242–248. [[CrossRef](#)]
349. Jiang, G.-B.; Zheng, X.; Yao, J.-H.; Han, B.-J.; Li, W.; Wang, J.; Huang, H.-L.; Liu, Y.-J. Ruthenium(II) Polypyridyl Complexes Induce BEL-7402 Cell Apoptosis by ROS-Mediated Mitochondrial Pathway. *J. Inorg. Biochem.* **2014**, *141*, 170–179. [[CrossRef](#)] [[PubMed](#)]
350. Li, W.; Jiang, G.-B.; Yao, J.-H.; Wang, X.-Z.; Wang, J.; Han, B.-J.; Xie, Y.-Y.; Lin, G.-J.; Huang, H.-L.; Liu, Y.-J. Ruthenium(II) Complexes: DNA-Binding, Cytotoxicity, Apoptosis, Cellular Localization, Cell Cycle Arrest, Reactive Oxygen Species, Mitochondrial Membrane Potential and Western Blot Analysis. *J. Photochem. Photobiol. B* **2014**, *140*, 94–104. [[CrossRef](#)]
351. Li, Y.; Zhang, J.; Wan, J.; Liu, A.; Sun, J. Melatonin Regulates A β Production/clearance Balance and A β Neurotoxicity: A Potential Therapeutic Molecule for Alzheimer's Disease. *Biomed. Pharmacother.* **2020**, *132*, 110887. [[CrossRef](#)] [[PubMed](#)]
352. Cardinali, D.P. Melatonin: Clinical Perspectives in Neurodegeneration. *Front. Endocrinol.* **2019**, *10*, 480. [[CrossRef](#)]
353. Vincent, B. Protective Roles of Melatonin against the Amyloid-Dependent Development of Alzheimer's Disease: A Critical Review. *Pharmacol. Res.* **2018**, *134*, 223–237. [[CrossRef](#)]
354. Wang, J.-Z.; Wang, Z.-F. Role of Melatonin in Alzheimer-like Neurodegeneration. *Acta Pharmacol. Sin.* **2006**, *27*, 41–49. [[CrossRef](#)]
355. Srinivasan, V.; Pandi-Perumal, S.R.; Maestroni, G.J.; Esquifino, A.I.; Hardeland, R.; Cardinali, D.P. Role of Melatonin in Neurodegenerative Diseases. *Neurotox. Res.* **2005**, *7*, 293–318. [[CrossRef](#)] [[PubMed](#)]
356. Ono, K.; Mochizuki, H.; Ikeda, T.; Nihira, T.; Takasaki, J.-I.; Teplow, D.B.; Yamada, M. Effect of Melatonin on α -Synuclein Self-Assembly and Cytotoxicity. *Neurobiol. Aging* **2012**, *33*, 2172–2185. [[CrossRef](#)]
357. Lin, A.M.Y.; Fang, S.F.; Chao, P.L.; Yang, C.H. Melatonin Attenuates Arsenite-Induced Apoptosis in Rat Brain: Involvement of Mitochondrial and Endoplasmic Reticulum Pathways and Aggregation of Alpha-Synuclein. *J. Pineal Res.* **2007**, *43*, 163–171. [[CrossRef](#)]
358. Pappolla, M.; Bozner, P.; Soto, C.; Shao, H.; Robakis, N.K.; Zagorski, M.; Frangione, B.; Ghiso, J. Inhibition of Alzheimer Beta-Fibrillogenesis by Melatonin. *J. Biol. Chem.* **1998**, *273*, 7185–7188. [[CrossRef](#)] [[PubMed](#)]
359. Skribanek, Z.; Balásperi, L.; Mák, M. Interaction between Synthetic Amyloid-Beta-Peptide (1-40) and Its Aggregation Inhibitors Studied by Electrospray Ionization Mass Spectrometry. *J. Mass Spectrom.* **2001**, *36*, 1226–1229. [[CrossRef](#)] [[PubMed](#)]
360. Poeggeler, B.; Miravalle, L.; Zagorski, M.G.; Wisniewski, T.; Chyan, Y.J.; Zhang, Y.; Shao, H.; Bryant-Thomas, T.; Vidal, R.; Frangione, B.; et al. Melatonin Reverses the Profibrillogenic Activity of Apolipoprotein E4 on the Alzheimer Amyloid Abeta Peptide. *Biochemistry* **2001**, *40*, 14995–15001. [[CrossRef](#)]
361. Pappolla, M.A.; Matsubara, E.; Vidal, R.; Pacheco-Quinto, J.; Poeggeler, B.; Zagorski, M.; Sambamurti, K. Melatonin Treatment Enhances A β Lymphatic Clearance in a Transgenic Mouse Model of Amyloidosis. *Curr. Alzheimer Res.* **2018**, *15*, 637–642. [[CrossRef](#)]
362. Matsubara, E.; Bryant-Thomas, T.; Pacheco Quinto, J.; Henry, T.L.; Poeggeler, B.; Herbert, D.; Cruz-Sanchez, F.; Chyan, Y.-J.; Smith, M.A.; Perry, G.; et al. Melatonin Increases Survival and Inhibits Oxidative and Amyloid Pathology in a Transgenic Model of Alzheimer's Disease. *J. Neurochem.* **2003**, *85*, 1101–1108. [[CrossRef](#)]
363. Quinn, J.; Kulhanek, D.; Nowlin, J.; Jones, R.; Praticò, D.; Rokach, J.; Stackman, R. Chronic Melatonin Therapy Fails to Alter Amyloid Burden or Oxidative Damage in Old Tg2576 Mice: Implications for Clinical Trials. *Brain Res.* **2005**, *1037*, 209–213. [[CrossRef](#)]
364. Lahiri, D.K.; Chen, D.; Ge, Y.-W.; Bondy, S.C.; Sharman, E.H. Dietary Supplementation with Melatonin Reduces Levels of Amyloid Beta-Peptides in the Murine Cerebral Cortex. *J. Pineal Res.* **2004**, *36*, 224–231. [[CrossRef](#)]
365. Ali, T.; Kim, M.O. Melatonin Ameliorates Amyloid Beta-Induced Memory Deficits, Tau Hyperphosphorylation and Neurodegeneration via PI3/Akt/GSk3 β Pathway in the Mouse Hippocampus. *J. Pineal Res.* **2015**, *59*, 47–59. [[CrossRef](#)] [[PubMed](#)]
366. Luengo, E.; Buendia, I.; Fernández-Mendivil, C.; Trigo-Alonso, P.; Negredo, P.; Michalska, P.; Hernández-García, B.; Sánchez-Ramos, C.; Bernal, J.A.; Ikezu, T.; et al. Pharmacological Doses of Melatonin Impede Cognitive Decline in Tau-Related Alzheimer Models, Once Tauopathy Is Initiated, by Restoring the Autophagic Flux. *J. Pineal Res.* **2019**, *67*, e12578. [[CrossRef](#)]
367. Balmik, A.A.; Das, R.; Dangi, A.; Gorantla, N.V.; Marelli, U.K.; Chinnathambi, S. Melatonin Interacts with Repeat Domain of Tau to Mediate Disaggregation of Paired Helical Filaments. *Biochim. Biophys. Acta Gen. Subj.* **2020**, *1864*, 129467. [[CrossRef](#)]
368. Das, R.; Balmik, A.A.; Chinnathambi, S. Effect of Melatonin on Tau Aggregation and Tau-Mediated Cell Surface Morphology. *Int. J. Biol. Macromol.* **2020**, *152*, 30–39. [[CrossRef](#)] [[PubMed](#)]

369. Kumar, S.; Nussinov, R. Salt Bridge Stability in Monomeric Proteins. *J. Mol. Biol.* **1999**, *293*, 1241–1255. [[CrossRef](#)]
370. Xu, D.; Tsai, C.J.; Nussinov, R. Hydrogen Bonds and Salt Bridges across Protein-Protein Interfaces. *Protein Eng.* **1997**, *10*, 999–1012. [[CrossRef](#)]
371. Musafia, B.; Buchner, V.; Arad, D. Complex Salt Bridges in Proteins: Statistical Analysis of Structure and Function. *J. Mol. Biol.* **1995**, *254*, 761–770. [[CrossRef](#)] [[PubMed](#)]
372. Tarus, B.; Straub, J.E.; Thirumalai, D. Dynamics of Asp23-Lys28 Salt-Bridge Formation in Abeta10-35 Monomers. *J. Am. Chem. Soc.* **2006**, *128*, 16159–16168. [[CrossRef](#)]
373. Zwier, T.S. The spectroscopy of solvation in hydrogen-bonded aromatic clusters. *Annu. Rev. Phys. Chem.* **1996**, *47*, 205–241. [[CrossRef](#)]
374. Zhu, L.; Gong, Y.; Lju, H.; Sun, G.; Zhang, Q.; Qian, Z. Mechanisms of Melatonin Binding and Destabilizing the Protofilament and Filament of Tau R3–R4 Domains Revealed by Molecular Dynamics Simulation. *Phys. Chem. Chem. Phys.* **2021**, *23*, 20615–20626. [[CrossRef](#)]
375. Köpke, E.; Tung, Y.C.; Shaikh, S.; Alonso, A.C.; Iqbal, K.; Grundke-Iqbal, I. Microtubule-Associated Protein Tau. Abnormal Phosphorylation of a Non-Paired Helical Filament Pool in Alzheimer Disease. *J. Biol. Chem.* **1993**, *268*, 24374–24384. [[CrossRef](#)] [[PubMed](#)]
376. Wang, J.Z.; Gong, C.X.; Zaidi, T.; Grundke-Iqbal, I.; Iqbal, K. Dephosphorylation of Alzheimer Paired Helical Filaments by Protein Phosphatase-2A and -2B. *J. Biol. Chem.* **1995**, *270*, 4854–4860. [[CrossRef](#)] [[PubMed](#)]
377. Wang, J.Z.; Grundke-Iqbal, I.; Iqbal, K. Restoration of Biological Activity of Alzheimer Abnormally Phosphorylated Tau by Dephosphorylation with Protein Phosphatase-2A, -2B and -1. *Brain Res. Mol. Brain Res.* **1996**, *38*, 200–208. [[CrossRef](#)] [[PubMed](#)]
378. Poppek, D.; Keck, S.; Ermak, G.; Jung, T.; Stolzing, A.; Ullrich, O.; Davies, K.J.A.; Grune, T. Phosphorylation Inhibits Turnover of the Tau Protein by the Proteasome: Influence of RCAN1 and Oxidative Stress. *Biochem. J* **2006**, *400*, 511–520. [[CrossRef](#)]
379. Bloom, G.S. Amyloid- β and Tau: The Trigger and Bullet in Alzheimer Disease Pathogenesis. *JAMA Neurol.* **2014**, *71*, 505–508. [[CrossRef](#)]
380. Cline, E.N.; Bicca, M.A.; Viola, K.L.; Klein, W.L. The Amyloid- β Oligomer Hypothesis: Beginning of the Third Decade. *J. Alzheimer's Dis.* **2018**, *64*, S567–S610. [[CrossRef](#)]
381. Kametani, F.; Hasegawa, M. Reconsideration of Amyloid Hypothesis and Tau Hypothesis in Alzheimer's Disease. *Front. Neurosci.* **2018**, *12*, 25. [[CrossRef](#)]
382. Chen, X.-Q.; Mobley, W.C. Alzheimer Disease Pathogenesis: Insights From Molecular and Cellular Biology Studies of Oligomeric A β and Tau Species. *Front. Neurosci.* **2019**, *13*, 659. [[CrossRef](#)]
383. Chen, X.; Chen, M.; Schafer, N.P.; Wolynes, P.G. Exploring the Interplay between Fibrillization and Amorphous Aggregation Channels on the Energy Landscapes of Tau Repeat Isoforms. *Proc. Natl. Acad. Sci. USA* **2020**, *117*, 4125–4130. [[CrossRef](#)] [[PubMed](#)]
384. Ruben, G.C.; Ciardelli, T.L.; Grundke-Iqbal, I.; Iqbal, K. Alzheimer Disease Hyperphosphorylated Tau Aggregates Hydrophobically. *Synapse* **1997**, *27*, 208–229. [[CrossRef](#)]
385. Wegmann, S.; Eftekhazadeh, B.; Tepper, K.; Zoltowska, K.M.; Bennett, R.E.; Dujardin, S.; Laskowski, P.R.; MacKenzie, D.; Kamath, T.; Commins, C.; et al. Tau Protein Liquid-Liquid Phase Separation Can Initiate Tau Aggregation. *EMBO J.* **2018**, *37*, e98049. [[CrossRef](#)] [[PubMed](#)]
386. Mandl, I.; Grauer, A.; Neuberger, C. Solubilization of Insoluble Matter in Nature; I. The Part Played by Salts of Adenosinetriphosphate. *Biochim. Biophys. Acta* **1952**, *8*, 654–663. [[CrossRef](#)] [[PubMed](#)]
387. Hayes, M.H.; Peuchen, E.H.; Dovichi, N.J.; Weeks, D.L. Dual Roles for ATP in the Regulation of Phase Separated Protein Aggregates in Xenopus Oocyte Nucleoli. *Elife* **2018**, *7*, e35224. [[CrossRef](#)]
388. Patel, A.; Malinowska, L.; Saha, S.; Wang, J.; Alberti, S.; Krishnan, Y.; Hyman, A.A. ATP as a Biological Hydrotrope. *Science* **2017**, *356*, 753–756. [[CrossRef](#)]
389. Kurisaki, I.; Tanaka, S. ATP Converts A β 42 Oligomer into Off-Pathway Species by Making Contact with Its Backbone Atoms Using Hydrophobic Adenosine. *J. Phys. Chem. B* **2019**, *123*, 9922–9933. [[CrossRef](#)] [[PubMed](#)]
390. Mehringer, J.; Do, T.-M.; Touraud, D.; Hohenschutz, M.; Khoshsim, A.; Horinek, D.; Kunz, W. Hofmeister versus Neuberger: Is ATP Really a Biological Hydrotrope? *Cell Rep. Phys. Sci.* **2021**, *2*, 100343. [[CrossRef](#)]
391. Zhang, C.; Rissman, R.A.; Feng, J. Characterization of ATP Alternations in an Alzheimer's Disease Transgenic Mouse Model. *J. Alzheimer's Dis.* **2015**, *44*, 375–378. [[CrossRef](#)]
392. Pal, S.; Paul, S. ATP Controls the Aggregation of A β 16-22 Peptides. *J. Phys. Chem. B* **2020**, *124*, 210–223. [[CrossRef](#)]
393. Oro, J. Mechanism of Synthesis of Adenine from Hydrogen Cyanide under Possible Primitive Earth Conditions. *Nature* **1961**, *191*, 1193–1194. [[CrossRef](#)]
394. Newby, A.C. Adenosine and the Concept of "retaliatory Metabolites". *Trends Biochem. Sci.* **1984**, *9*, 42–44. [[CrossRef](#)]
395. Cate, J.H.; Gooding, A.R.; Podell, E.; Zhou, K.; Golden, B.L.; Szewczak, A.A.; Kundrot, C.E.; Cech, T.R.; Doudna, J.A. RNA Tertiary Structure Mediation by Adenosine Platforms. *Science* **1996**, *273*, 1696–1699. [[CrossRef](#)]
396. Ren, C.-L.; Shan, Y.; Zhang, P.; Ding, H.-M.; Ma, Y.-Q. Uncovering the Molecular Mechanism for Dual Effect of ATP on Phase Separation in FUS Solution. *Sci. Adv.* **2022**, *8*, eabo7885. [[CrossRef](#)]
397. Kang, J.; Lim, L.; Song, J. ATP Enhances at Low Concentrations but Dissolves at High Concentrations Liquid-Liquid Phase Separation (LLPS) of ALS/FTD-Causing FUS. *Biochem. Biophys. Res. Commun.* **2018**, *504*, 545–551. [[CrossRef](#)]

398. Henninger, J.E.; Oksuz, O.; Shrinivas, K.; Sagi, I.; LeRoy, G.; Zheng, M.M.; Andrews, J.O.; Zamudio, A.V.; Lazaris, C.; Hannett, N.M.; et al. RNA-Mediated Feedback Control of Transcriptional Condensates. *Cell* **2021**, *184*, 207–225.e24. [[CrossRef](#)] [[PubMed](#)]
399. Maharana, S.; Wang, J.; Papadopoulos, D.K.; Richter, D.; Pozniakovsky, A.; Poser, I.; Bickle, M.; Rizk, S.; Guillén-Boixet, J.; Franzmann, T.M.; et al. RNA Buffers the Phase Separation Behavior of Prion-like RNA Binding Proteins. *Science* **2018**, *360*, 918–921. [[CrossRef](#)] [[PubMed](#)]
400. Aida, H.; Shigeta, Y.; Harada, R. The Role of ATP in Solubilizing RNA-Binding Protein Fused in Sarcoma. *Proteins* **2022**, *90*, 1606–1612. [[CrossRef](#)]
401. Coskuner, O.; Murray, I.V.J. Adenosine Triphosphate (ATP) Reduces Amyloid- β Protein Misfolding in Vitro. *J. Alzheimer's Dis.* **2014**, *41*, 561–574. [[CrossRef](#)] [[PubMed](#)]
402. Cohen, T.; Frydman-Marom, A.; Rechter, M.; Gazit, E. Inhibition of Amyloid Fibril Formation and Cytotoxicity by Hydroxyindole Derivatives. *Biochemistry* **2006**, *45*, 4727–4735. [[CrossRef](#)] [[PubMed](#)]
403. Morshedi, D.; Rezaei-Ghaleh, N.; Ebrahim-Habibi, A.; Ahmadian, S.; Nemat-Gorgani, M. Inhibition of Amyloid Fibrillation of Lysozyme by Indole Derivatives—Possible Mechanism of Action. *FEBS J.* **2007**, *274*, 6415–6425. [[CrossRef](#)]
404. Swan, I.D. The Inhibition of Hen Egg-White Lysozyme by Imidazole and Indole Derivatives. *J. Mol. Biol.* **1972**, *65*, 59–62. [[CrossRef](#)] [[PubMed](#)]
405. Di Bella, G.; Mascia, F.; Gualano, L.; Di Bella, L. Melatonin Anticancer Effects: Review. *Int. J. Mol. Sci.* **2013**, *14*, 2410–2430. [[CrossRef](#)]
406. Di Bella, G.; Gualano, L.; Di Bella, L. Melatonin with Adenosine Solubilized in Water and Stabilized with Glycine for Oncological Treatment—Technical Preparation, Effectivity and Clinical Findings. *Neuro Endocrinol. Lett.* **2017**, *38*, 465–474.
407. Todisco, M. Effectiveness of a Treatment Based on Melatonin in Five Patients with Systemic Sclerosis. *Am. J. Ther.* **2006**, *13*, 84–87. [[CrossRef](#)]
408. Todisco, M.; Rossi, N. Melatonin for Refractory Idiopathic Thrombocytopenic Purpura: A Report of 3 Cases. *Am. J. Ther.* **2002**, *9*, 524–526. [[CrossRef](#)] [[PubMed](#)]
409. Pattanayak, G.K.; Liao, Y.; Wallace, E.W.J.; Budnik, B.; Drummond, D.A.; Rust, M.J. Daily Cycles of Reversible Protein Condensation in Cyanobacteria. *Cell Rep.* **2020**, *32*, 108032. [[CrossRef](#)] [[PubMed](#)]
410. Borea, P.A.; Gessi, S.; Merighi, S.; Vincenzi, F.; Varani, K. Pathological Overproduction: The Bad Side of Adenosine. *Br. J. Pharmacol.* **2017**, *174*, 1945–1960. [[CrossRef](#)] [[PubMed](#)]
411. Zimmermann, H. Extracellular Metabolism of ATP and Other Nucleotides. *Naunyn-Schmiedeberg's Arch. Pharmacol.* **2000**, *362*, 299–309. [[CrossRef](#)]
412. Fredholm, B.B. Physiological and Pathophysiological Roles of Adenosine. *Sleep Biol. Rhythms* **2011**, *9*, 24–28. [[CrossRef](#)]
413. Chang, C.-P.; Wu, K.-C.; Lin, C.-Y.; Chern, Y. Emerging Roles of Dysregulated Adenosine Homeostasis in Brain Disorders with a Specific Focus on Neurodegenerative Diseases. *J. Biomed. Sci.* **2021**, *28*, 70. [[CrossRef](#)]
414. Antonioli, L.; Blandizzi, C.; Pacher, P.; Haskó, G. Immunity, Inflammation and Cancer: A Leading Role for Adenosine. *Nat. Rev. Cancer* **2013**, *13*, 842–857. [[CrossRef](#)]
415. Morandi, F.; Horenstein, A.L.; Rizzo, R.; Malavasi, F. The Role of Extracellular Adenosine Generation in the Development of Autoimmune Diseases. *Mediat. Inflamm.* **2018**, *2018*, 7019398. [[CrossRef](#)] [[PubMed](#)]
416. Blay, J.; White, T.D.; Hoskin, D.W. The Extracellular Fluid of Solid Carcinomas Contains Immunosuppressive Concentrations of Adenosine. *Cancer Res.* **1997**, *57*, 2602–2605.
417. Rudolphi, K.A.; Schubert, P. Adenosine and Brain Ischemia. In *Adenosine and Adenine Nucleotides: From Molecular Biology to Integrative Physiology*; Belardinelli, L., Pelleg, A., Eds.; Springer: Boston, MA, USA, 1995; pp. 391–397. [[CrossRef](#)]
418. Tan, D.-X.; Hardeland, R. The Reserve/Maximum Capacity of Melatonin's Synthetic Function for the Potential Dimorphism of Melatonin Production and Its Biological Significance in Mammals. *Molecules* **2021**, *26*, 7302. [[CrossRef](#)] [[PubMed](#)]
419. Löfgren, L.; Pehrsson, S.; Hägglund, G.; Tjellström, H.; Nylander, S. Accurate Measurement of Endogenous Adenosine in Human Blood. *PLoS ONE* **2018**, *13*, e0205707. [[CrossRef](#)]
420. Waldhauser, F.; Weiszenbacher, G.; Tatzer, E.; Gisinger, B.; Waldhauser, M.; Schemper, M.; Frisch, H. Alterations in Nocturnal Serum Melatonin Levels in Humans with Growth and Aging. *J. Clin. Endocrinol. Metab.* **1988**, *66*, 648–652. [[CrossRef](#)] [[PubMed](#)]
421. Kennaway, D.J.; Lushington, K.; Dawson, D.; Lack, L.; van den Heuvel, C.; Rogers, N. Urinary 6-Sulfatoxymelatonin Excretion and Aging: New Results and a Critical Review of the Literature. *J. Pineal Res.* **1999**, *27*, 210–220. [[CrossRef](#)]
422. Waldhauser, F.; Kovács, J.; Reiter, E. Age-Related Changes in Melatonin Levels in Humans and Its Potential Consequences for Sleep Disorders. *Exp. Gerontol.* **1998**, *33*, 759–772. [[CrossRef](#)]
423. Waldhauser, F.; Weiszenbacher, G.; Frisch, H.; Zeitlhuber, U.; Waldhauser, M.; Wurtman, R.J. Fall in Nocturnal Serum Melatonin during Prepuberty and Pubescence. *Lancet* **1984**, *1*, 362–365. [[CrossRef](#)]
424. Burch, J.B.; Reif, J.S.; Yost, M.G.; Keefe, T.J.; Pitrat, C.A. Reduced Excretion of a Melatonin Metabolite in Workers Exposed to 60 Hz Magnetic Fields. *Am. J. Epidemiol.* **1999**, *150*, 27–36. [[CrossRef](#)]
425. Prayag, A.S.; Najjar, R.P.; Gronfier, C. Melatonin Suppression Is Exquisitely Sensitive to Light and Primarily Driven by Melanopsin in Humans. *J. Pineal Res.* **2019**, *66*, e12562. [[CrossRef](#)]
426. Bojkowski, C.J.; Aldhous, M.E.; English, J.; Franey, C.; Poulton, A.L.; Skene, D.J.; Arendt, J. Suppression of Nocturnal Plasma Melatonin and 6-Sulphatoxymelatonin by Bright and Dim Light in Man. *Horm. Metab. Res.* **1987**, *19*, 437–440. [[CrossRef](#)]

427. Tan, D.-X.; Reiter, R.J.; Manchester, L.C.; Yan, M.-T.; El-Sawi, M.; Sainz, R.M.; Mayo, J.C.; Kohen, R.; Allegra, M.; Hardeland, R. Chemical and Physical Properties and Potential Mechanisms: Melatonin as a Broad Spectrum Antioxidant and Free Radical Scavenger. *Curr. Top. Med. Chem.* **2002**, *2*, 181–197. [CrossRef]
428. National Center for Biotechnology Information. *PubChem Compound Summary for CID 5957, Adenosine-5'-Triphosphate*; National Center for Biotechnology Information: Bethesda, MD, USA, 2023. Available online: https://pubchem.ncbi.nlm.nih.gov/compound/Adenosine-5_-triphosphate (accessed on 5 January 2023).
429. National Center for Biotechnology Information. *PubChem Compound Summary for CID 896, Melatonin*; National Center for Biotechnology Information: Bethesda, MD, USA, 2023. Available online: <https://pubchem.ncbi.nlm.nih.gov/compound/Melatonin> (accessed on 7 January 2023).
430. Ishii, M.; Wang, G.; Racchumi, G.; Dyke, J.P.; Iadecola, C. Transgenic Mice Overexpressing Amyloid Precursor Protein Exhibit Early Metabolic Deficits and a Pathologically Low Leptin State Associated with Hypothalamic Dysfunction in Arcuate Neuropeptide Y Neurons. *J. Neurosci.* **2014**, *34*, 9096–9106. [CrossRef]
431. Feng, Z.; Qin, C.; Chang, Y.; Zhang, J.-T. Early Melatonin Supplementation Alleviates Oxidative Stress in a Transgenic Mouse Model of Alzheimer's Disease. *Free. Radic. Biol. Med.* **2006**, *40*, 101–109. [CrossRef] [PubMed]
432. Bachmanov, A.A.; Reed, D.R.; Beauchamp, G.K.; Tordoff, M.G. Food Intake, Water Intake, and Drinking Spout Side Preference of 28 Mouse Strains. *Behav. Genet.* **2002**, *32*, 435–443. [CrossRef] [PubMed]
433. Gould, S.J. Allometry in Primates, with Emphasis on Scaling and the Evolution of the Brain. *Contrib. Primatol.* **1975**, *5*, 244–292. [PubMed]
434. Mirth, C.K.; Frankino, W.A.; Shingleton, A.W. Allometry and Size Control: What Can Studies of Body Size Regulation Teach Us about the Evolution of Morphological Scaling Relationships? *Curr. Opin. Insect Sci.* **2016**, *13*, 93–98. [CrossRef]
435. Galilei, G. *Dialogues Concerning Two New Sciences, 1637*; Crew, H.; De Salvio, A., Translators; Macmillan: New York, NY, USA, 1914.
436. Boxenbaum, H. Interspecies Scaling, Allometry, Physiological Time, and the Ground Plan of Pharmacokinetics. *J. Pharmacokinet. Pharmacodyn.* **1982**, *10*, 201–227. [CrossRef] [PubMed]
437. Boxenbaum, H.; Fertig, J.B. Scaling of Antipyrine Intrinsic Clearance of Unbound Drug in 15 Mammalian Species. *Eur. J. Drug Metab. Pharmacokinet.* **1984**, *9*, 177–183. [CrossRef]
438. Boxenbaum, H. Interspecies Pharmacokinetic Scaling and the Evolutionary-Comparative Paradigm. *Drug Metab. Rev.* **1984**, *15*, 1071–1121. [CrossRef]
439. Ritschel, W.A.; Vachharajani, N.N.; Johnson, R.D.; Hussain, A.S. The Allometric Approach for Interspecies Scaling of Pharmacokinetic Parameters. *Comp. Biochem. Physiol. Part C* **1992**, *103*, 249–253. [CrossRef] [PubMed]
440. Boxenbaum, H.; DiLea, C. First-Time-in-Human Dose Selection: Allometric Thoughts and Perspectives. *J. Clin. Pharmacol.* **1995**, *35*, 957–966. [CrossRef] [PubMed]
441. Hu, T.M.; Hayton, W.L. Allometric Scaling of Xenobiotic Clearance: Uncertainty versus Universality. *AAPS PharmSci* **2001**, *3*, E29. [CrossRef] [PubMed]
442. Gibson, S.; Numa, A. The Importance of Metabolic Rate and the Folly of Body Surface Area Calculations. *Anaesthesia* **2003**, *58*, 50–55. [CrossRef] [PubMed]
443. Savage, V.M.; Gillooly, J.F.; Woodruff, W.H.; West, G.B.; Allen, A.P.; Enquist, B.J.; Brown, J.H. The Predominance of Quarter-Power Scaling in Biology. *Funct. Ecol.* **2004**, *18*, 257–282. [CrossRef]
444. Glazier, D.S. Beyond the “3/4-Power Law”: Variation in the Intra- and Interspecific Scaling of Metabolic Rate in Animals. *Biol. Rev. Camb. Philos. Soc.* **2005**, *80*, 611–662. [CrossRef]
445. West, G.B.; Brown, J.H. The Origin of Allometric Scaling Laws in Biology from Genomes to Ecosystems: Towards a Quantitative Unifying Theory of Biological Structure and Organization. *J. Exp. Biol.* **2005**, *208 Pt 9*, 1575–1592. [CrossRef]
446. Rhomberg, L.R.; Lewandowski, T.A. Methods for Identifying a Default Cross-Species Scaling Factor. *Hum. Ecol. Risk Assess. Int. J.* **2006**, *12*, 1094–1127. [CrossRef]
447. Reagan-Shaw, S.; Nihal, M.; Ahmad, N. Dose Translation from Animal to Human Studies Revisited. *FASEB J.* **2008**, *22*, 659–661. [CrossRef]
448. White, C.R.; Kearney, M.R. Metabolic Scaling in Animals: Methods, Empirical Results, and Theoretical Explanations. *Compr. Physiol.* **2014**, *4*, 231–256. [CrossRef]
449. Glazier, D.S. Effects of Contingency versus Constraints on the Body-Mass Scaling of Metabolic Rate. *Challenges* **2018**, *9*, 4. [CrossRef]
450. Li, X.-X.; He, J.-H. Along the evolution process kleiber's 3/4 law makes way for rubner's surface law: A fractal approach. *Fractals* **2019**, *27*, 1950015. [CrossRef]
451. Dodds, P.S.; Rothman, D.H.; Weitz, J.S. Re-Examination of the “3/4-Law” of Metabolism. *J. Theor. Biol.* **2001**, *209*, 9–27. [CrossRef] [PubMed]
452. White, C.R.; Seymour, R.S. Mammalian Basal Metabolic Rate Is Proportional to Body mass^{2/3}. *Proc. Natl. Acad. Sci. USA* **2003**, *100*, 4046–4049. [CrossRef]
453. White, C.R.; Cassey, P.; Blackburn, T.M. Allometric Exponents Do Not Support a Universal Metabolic Allometry. *Ecology* **2007**, *88*, 315–323. [CrossRef]
454. Banavar, J.R.; Moses, M.E.; Brown, J.H.; Damuth, J.; Rinaldo, A.; Sibly, R.M.; Maritan, A. A General Basis for Quarter-Power Scaling in Animals. *Proc. Natl. Acad. Sci. USA* **2010**, *107*, 15816–15820. [CrossRef]

455. Dreyer, G. The normal basal metabolism in man: And its relation to the size of the body and age, expressed in simple formulæ. *Lancet* **1920**, *196*, 289–291. [[CrossRef](#)]
456. Kleiber, M. Body Size and Metabolism. *Hilgardia* **1932**, *6*, 315–353. [[CrossRef](#)]
457. Nair, A.B.; Jacob, S. A Simple Practice Guide for Dose Conversion between Animals and Human. *J. Basic Clin. Pharm.* **2016**, *7*, 27–31. [[CrossRef](#)] [[PubMed](#)]
458. Reading, B.D.; Freeman, B. Simple Formula for the Surface Area of the Body and a Simple Model for Anthropometry. *Clin. Anat.* **2005**, *18*, 126–130. [[CrossRef](#)]
459. Cheung, M.C.; Spalding, P.B.; Gutierrez, J.C.; Balkan, W.; Namias, N.; Koniari, L.G.; Zimmers, T.A. Body Surface Area Prediction in Normal, Hypermuscular, and Obese Mice. *J. Surg. Res.* **2009**, *153*, 326–331. [[CrossRef](#)]
460. Gouma, E.; Simos, Y.; Verginadis, I.; Lykoudis, E.; Evangelou, A.; Karkabounas, S. A Simple Procedure for Estimation of Total Body Surface Area and Determination of a New Value of Meeh’s Constant in Rats. *Lab. Anim.* **2012**, *46*, 40–45. [[CrossRef](#)]
461. Toutain, P.L.; Bousquet-Mélou, A. Bioavailability and Its Assessment. *J. Vet. Pharmacol. Ther.* **2004**, *27*, 455–466. [[CrossRef](#)] [[PubMed](#)]
462. Waldhauser, F.; Waldhauser, M.; Lieberman, H.R.; Deng, M.H.; Lynch, H.J.; Wurtman, R.J. Bioavailability of Oral Melatonin in Humans. *Neuroendocrinology* **1984**, *39*, 307–313. [[CrossRef](#)]
463. Zetner, D.; Andersen, L.P.K.; Alder, R.; Jessen, M.L.; Tolstrup, A.; Rosenberg, J. Pharmacokinetics and Safety of Intravenous, Intravesical, Rectal, Transdermal, and Vaginal Melatonin in Healthy Female Volunteers: A Cross-Over Study. *Pharmacology* **2021**, *106*, 169–176. [[CrossRef](#)] [[PubMed](#)]
464. Lane, E.A.; Moss, H.B. Pharmacokinetics of Melatonin in Man: First Pass Hepatic Metabolism. *J. Clin. Endocrinol. Metab.* **1985**, *61*, 1214–1216. [[CrossRef](#)]
465. DeMuro, R.L.; Nafziger, A.N.; Blask, D.E.; Menhinick, A.M.; Bertino, J.S., Jr. The Absolute Bioavailability of Oral Melatonin. *J. Clin. Pharmacol.* **2000**, *40*, 781–784. [[CrossRef](#)] [[PubMed](#)]
466. Harpsøe, N.G.; Andersen, L.P.H.; Gögenur, I.; Rosenberg, J. Clinical Pharmacokinetics of Melatonin: A Systematic Review. *Eur. J. Clin. Pharmacol.* **2015**, *71*, 901–909. [[CrossRef](#)]
467. Andersen, L.P.H.; Werner, M.U.; Rosenkilde, M.M.; Harpsøe, N.G.; Fuglsang, H.; Rosenberg, J.; Gögenur, I. Pharmacokinetics of Oral and Intravenous Melatonin in Healthy Volunteers. *BMC Pharmacol. Toxicol.* **2016**, *17*, 8. [[CrossRef](#)]
468. Di, W.L.; Kadva, A.; Johnston, A.; Silman, R. Variable Bioavailability of Oral Melatonin. *N. Engl. J. Med.* **1997**, *336*, 1028–1029. [[CrossRef](#)]
469. Bagci, S.; Horoz, Ö.Ö.; Yildizdas, D.; Reinsberg, J.; Bartmann, P.; Müller, A. Melatonin Status in Pediatric Intensive Care Patients with Sepsis. *Pediatr. Crit. Care Med.* **2012**, *13*, e120–e123. [[CrossRef](#)]
470. Tordjman, S.; Anderson, G.M.; Pichard, N.; Charbuy, H.; Touitou, Y. Nocturnal Excretion of 6-Sulphatoxymelatonin in Children and Adolescents with Autistic Disorder. *Biol. Psychiatry* **2005**, *57*, 134–138. [[CrossRef](#)] [[PubMed](#)]
471. Tordjman, S.; Anderson, G.M.; Bellissant, E.; Botbol, M.; Charbuy, H.; Camus, F.; Graignic, R.; Kermarrec, S.; Fougerou, C.; Cohen, D.; et al. Day and Nighttime Excretion of 6-Sulphatoxymelatonin in Adolescents and Young Adults with Autistic Disorder. *Psychoneuroendocrinology* **2012**, *37*, 1990–1997. [[CrossRef](#)]
472. Kennaway, D.J.; Flanagan, D.E.; Moore, V.M.; Cockington, R.A.; Robinson, J.S.; Phillips, D.I. The Impact of Fetal Size and Length of Gestation on 6-Sulphatoxymelatonin Excretion in Adult Life. *J. Pineal Res.* **2001**, *30*, 188–192. [[CrossRef](#)]
473. Girotti, L.; Lago, M.; Ianovsky, O.; Carbajales, J.; Elizari, M.V.; Brusco, L.I.; Cardinali, D.P. Low Urinary 6-Sulphatoxymelatonin Levels in Patients with Coronary Artery Disease. *J. Pineal Res.* **2000**, *29*, 138–142. [[CrossRef](#)]
474. Yeleswaram, K.; McLaughlin, L.G.; Knipe, J.O.; Schabdach, D. Pharmacokinetics and Oral Bioavailability of Exogenous Melatonin in Preclinical Animal Models and Clinical Implications. *J. Pineal Res.* **1997**, *22*, 45–51. [[CrossRef](#)] [[PubMed](#)]
475. Kopin, I.J.; Pare, C.M.; Axelrod, J.; Weissbach, H. The Fate of Melatonin in Animals. *J. Biol. Chem.* **1961**, *236*, 3072–3075. [[CrossRef](#)]
476. Raynaud, F.; Mauviard, F.; Geoffriau, M.; Claustrat, B.; Pevet, P. Plasma 6-Hydroxymelatonin, 6-Sulfatoxymelatonin and Melatonin Kinetics after Melatonin Administration to Rats. *Biol. Signals* **1993**, *2*, 358–366. [[CrossRef](#)] [[PubMed](#)]
477. Choudhary, S.; Kumar, A.; Saha, N.; Chaudhury, N.K. PK-PD Based Optimal Dose and Time for Orally Administered Supra-Pharmacological Dose of Melatonin to Prevent Radiation Induced Mortality in Mice. *Life Sci.* **2019**, *219*, 31–39. [[CrossRef](#)] [[PubMed](#)]
478. Galley, H.F.; Allen, L.; Colin, P.J.; Galt, S.P.; Webster, N.R. Dose Assessment of Melatonin in Sepsis (DAMSEL2) Study: Pharmacokinetics of Two Doses of Oral Melatonin in Patients with Sepsis. *J. Pineal Res.* **2022**, *73*, e12830. [[CrossRef](#)]
479. Mao, S.; Chen, J.; Wei, Z.; Liu, H.; Bi, D. Intranasal Administration of Melatonin Starch Microspheres. *Int. J. Pharm.* **2004**, *272*, 37–43. [[CrossRef](#)]
480. Priprem, A.; Johns, J.R.; Limsitthichaikoon, S.; Limphirat, W.; Mahakunakorn, P.; Johns, N.P. Intranasal Melatonin Nanoniosomes: Pharmacokinetic, Pharmacodynamics and Toxicity Studies. *Ther. Deliv.* **2017**, *8*, 373–390. [[CrossRef](#)]
481. Maeda, H.; Ogawa, Y.; Nakayama, H. Inclusion Complexes of Melatonin with Modified Cyclodextrins. *J. Incl. Phenom. Macrocycl. Chem.* **2014**, *78*, 217–224. [[CrossRef](#)]
482. Sakellaropoulou, A.; Siamidi, A.; Vlachou, M. Melatonin/Cyclodextrin Inclusion Complexes: A Review. *Molecules* **2022**, *27*, 445. [[CrossRef](#)]
483. Barchas, J.; DaCosta, F.; Spector, S. Acute Pharmacology of Melatonin. *Nature* **1967**, *214*, 919–920. [[CrossRef](#)]
484. Boutin, J.A.; Jockers, R. Melatonin Controversies, an Update. *J. Pineal Res.* **2021**, *70*, e12702. [[CrossRef](#)] [[PubMed](#)]

485. Cai, R.; Yang, H.; He, J.; Zhu, W. The Effects of Magnetic Fields on Water Molecular Hydrogen Bonds. *J. Mol. Struct.* **2009**, *938*, 15–19. [[CrossRef](#)]
486. Menczel Schrire, Z.; Gordon, C.J.; Palmer, J.R.; Murray, J.; Hickie, I.; Rogers, N.L.; Lewis, S.J.; Terpening, Z.; Pye, J.E.; Naismith, S.L.; et al. Actigraphic and Melatonin Alignment in Older Adults with Varying Dementia Risk. *Chronobiol. Int.* **2022**, 1–12. [[CrossRef](#)]
487. Glacet, R.; Reynaud, E.; Robin-Choteau, L.; Reix, N.; Hugueny, L.; Ruppert, E.; Geoffroy, P.A.; Kilic-Huck, Ü.; Comtet, H.; Bourgin, P. A Comparison of Four Methods to Estimate Dim Light Melatonin Onset: A Repeatability and Agreement Study. *Chronobiol. Int.* **2022**, 1–9. [[CrossRef](#)] [[PubMed](#)]
488. Irwin, M.R.; Vitiello, M.V. Implications of Sleep Disturbance and Inflammation for Alzheimer’s Disease Dementia. *Lancet Neurol.* **2019**, *18*, 296–306. [[CrossRef](#)] [[PubMed](#)]

Disclaimer/Publisher’s Note: The statements, opinions and data contained in all publications are solely those of the individual author(s) and contributor(s) and not of MDPI and/or the editor(s). MDPI and/or the editor(s) disclaim responsibility for any injury to people or property resulting from any ideas, methods, instructions or products referred to in the content.